Using Vibrational Spectroscopy to understand the catalytic behaviour of iron carbonyl catalysts

Connor Matthew Bowes

Master of Science by Research

University of York
Chemistry

September 2025

Abstract

Detailed understanding of the mechanistic pathways underpinning metal-catalysed reactions permit for rational development of complexes with efficiency and enhanced activity. Observing the bonding and formation events that underpin a catalytic reaction is necessary to truly be able to design better catalytic systems as it would be understood which species are short lived or if they are observable at low concentrations. The aim of this project is to investigate the mechanistic pathways controlling the behaviour of iron carbonyl complexes used as catalysts for transfer dehydrogenation on fast time scales. Ultrafast TRIR was performed, observations were made on timescales ranging from 1 ps to 1 ms using a pump wavelength of 330 nm on [1a] and [3a] in seven solvents. In all solvents, initial formation (< 1 ps) and relaxation (< 200 ps) of an excited state was observed. Followed (200 ps) by the observation of the photodissociation of a CO ligand and a rapid solvent coordination to the vacant site [$2a_{Solvents}$] and [$4a_{Solvents}$]. In five of the seven the aqua complex [$2a_{OH2}$] and [$4a_{OH2}$] formed and persisted for the rest of the experiment. In the case of isopropyl alcohol, transfer dehydrogenation occurs.

[1a] was also studied using IR_{PUMP}-IR_{PROBE} in three solvents to examine the vibrational dynamics and solvent interactions of the carbonyl ligand stretching modes. Ultrafast vibrational energy dissipation occurred in two solvent dependent relaxation pathways, rapid intramolecular vibrational redistribution (IVR ~ 0.2-7.6 ps) and relaxation to the ground vibrational state (T_1 ~ 1.7-44.2 ps) different solvents affected the rate of the two pathways with THF having the quickest IVR and heptane the largest range of the T_1. This study has provided a better understanding into the mechanistic pathways that underpin catalysis by iron carbonyl complexes, specifically, the fundamental processes underpinning CO-photodissociation and the nature of the activated iron catalyst.

List of Contents

List of Figures

List of Schemes

List of Tables

Acknowledgements

I would like to take this opportunity to thank my supervisor Professor Jason Lynam for his continuous support and guidance throughout my two years at the University of York I am incredibly grateful to him for this amazing opportunity he has given me. I would also like to thank Dr Charlotte Willans for her guidance as my thesis advisory panel (TAP) member. I would also like to thank all the staff at the ULTRA facility (in particular Dr Ian Clark and Marta Szynkiewicz) for their help and support with the TRIR experiments. I would also like to thank Dr Danny Shaw for all his help and guidance with the IR_{PUMP}-IR_{PROBE} experiments. I would like to thank all past and present members of the SLUGS group who have made my time at York really really enjoyable and offered advice when I most needed it. I would also like to thank Matthew McRobie who synthesised and purified the iron compounds used in this thesis. At last, I would like to thank my family for their continuous support through the last two years, I am incredibly grateful to you all.

Author's Declaration

I declare that this thesis is a presentation of original work and I am the sole author. This work has not previously been presented for an award at this, or any other, University. All sources are acknowledged as References.

Connor Matthew Bowes

University of York, September 2025

Abbreviations and Symbols

α	Alpha
AgF	Silver(I) Fluoride
BH	Borrowing Hydrogen
β	Beta
BBO	Beta Barium Borate
CaF_3	Calcium Trifluoride
CF_3	Trifluormethyl Group
C-H	Carbon-Hydrogen Bond
CLF	Central Laser Facility
cm^{-1}	Wavenumber
CPME	Cyclopentyl Methyl Ether
CO	Carbon Monoxide
COOMe	Methoxycarbonyl Group
$CuCl_2$	Copper(II) Chloride
DCE	1,2-Dichloroethane
$FeBr_3$	Iron(III) Bromide
$Fe(CO)_5$	Iron Pentacarbonyl
$Fe_2(CO)_9$	Diiron Nonacarbonyl
$Fe_3(CO)_{12}$	Triiron Dodecacarbonyl
fs	Femtosecond
FTIR	Fourier Transform Infrared Spectroscopy
H	Hydrogen
H_2	Di-hydrogen
H_2O	Water
HAT	Hydrogen Auto-Transfer
h_ν	Wavenumber
Hz	Hertz
IPA	Isopropyl Alcohol
IR	Infrared
Ir	Iridium
IVR	Intramolecular Vibrational Energy Redistribution
K_2CO_3	Potassium Carbonate
kHz	Kilohertz
Kg	Kilogram
KTA	Potassium Titanyl Arsenate
LED	Light-Emitting Diode
Mol%	Mole Percent
Me_3NO	Trimethylamine N-oxide
mg	Milligrams
MLCT	Metal ligand to charge transfer
mM	Millimeter
NCMe	Acetonitrile

$Ni(acac)_2$	Nickel(II) Bis(acetylacetonate)
nm	Nanometer
NMR	Nuclear Magnetic Resonance
n-pr	Normal-Propyl Group
ns	Nanosecond
OMe	Methoxy Group
OPA	Optical Parametric Amplifier
ps	Picosecond
PTFE	Polytetrafluoroethylene
Rh	Rhodium
Ru	Ruthenium
STFC	Science and Technology Facilities Council
T_1	Relaxation to the Ground Vibrational State
^{t}BuOK	Potassium tert-butoxide
THF	Tetrahydrofuran
TRIR	Time-Resolved Infrared Spectroscopy
$TR^{M}PS$	Time-Resolved Multiple Probe Spectroscopy
µM	Micrometer
µs	Microsecond
UV	Ultraviolet
V_{CO}	Vibrational Circular Dichroism
W	Watt
Yb:KGW	Ytterbium-Doped Potassium Gadolinium Tungstate

1 Introduction

These reactions were chosen as iron is an earth-abundant metal and many complexes are inexpensive and readily available. As mentioned in section 1.1 HAT, with rhodium and ruthenium are often used for this method however they are expensive. To replace these precious metals improvements to reactions of catalysed earth-abundant metals must be studied. Research into manganese carbonyl complexes has been carried out by Professor Jason Lynam using TRIR and IR_{PUMP}-IR_{PROBE}, for these reasons iron is a great alternative and an in-depth study using both TRIR and IR_{PUMP}-IR_{PROBE} would be beneficial to achieve this outcome.

1.1 Hydrogen Auto-transfer (HAT)

The hydrogen auto-transfer (HAT) reaction also known as borrowing hydrogen (BH), is a powerful method that combines with transfer hydrogenation (avoiding the direct use of molecular hydrogen). In this reaction dihydrogen previously from a donor molecule is stored by a catalytic metal fragment and is subsequently released in a final hydrogenation step. The development of catalytic systems in HAT reactions involves the use of metal complexes or stabilised metal particles meaning that H_2 dissociation and recombination is straightforward, ideally without needing harsh reaction conditions. Unfortunately, the majority of the metal hydrides that form during hydrogen activation processes are too stable to easily return the activated hydrogen, resulting in them being inactive in HAT reactions. For example, iridium (Ir),[1] rhodium (Rh),[2] and ruthenium (Ru),[3] complexes are some of the homogenous complexes that have been previously reported for these types of reactions. One notable example is Shov's catalyst, a bi-ruthenium $[(\eta^5\text{-}C_4Ph_4CO)]RuH(CO)_2]_2$ complex developed by Shov and co-workers in 1986.[4]

HAT reactions start with a metal-catalysed dehydrogenation in which a less reactive donor molecule is temporarily converted into a reactive substrate: (an alkane converts into an alkene, an alcohol converts into either an aldehyde, or a ketone and an amine converts into an imine). The more activated intermediate can go through additional transformations to produce an unsaturated compound that will be reduced with the help of the metal hydrides produced during the first dehydrogenation step. The general scheme for the HAT method is shown in Scheme 1.

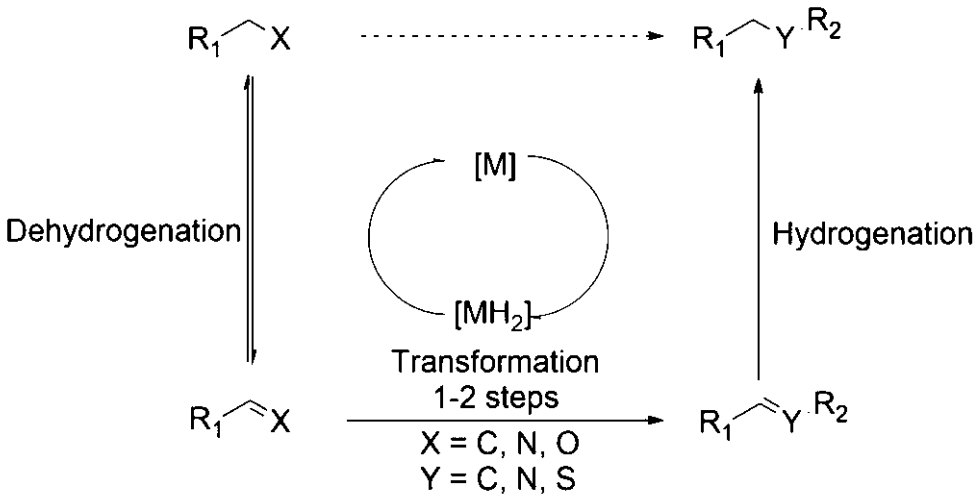

Scheme 1. General scheme for Hydrogen Auto-transfer.

Following Scheme 1, this reaction follows three steps: 1) dehydrogenation, 2) intermediate reaction, 3) hydrogenation.

Taking into consideration that the intermediate reaction step is a common organic reaction that involves the dehydrogenated substrate (example, an aldehyde), the involvement of the metal is not essential at this point, however this assumption may not be the case because an electrophilic metal component of the catalyst can, increase the electrophilic nature of the C=O bond, meaning there is an increase in the reactivity.

One notable detail of this reaction is that the hydrogenation step is often thermodynamically favoured, because of this the global processes moves completely to the products, resulting in an efficient, sustainable and low-waste process. The irreversibility of the third step in Scheme 1 pushes the first dehydrogenation step to near completion. For this situation, the same function can catalyse the dehydrogenation of the reactant and the hydrogenation of the intermediate product with the metal hydrides that are formed in the first step. On this basis HAT is an exceptional method from an economic, environmental, and synthetic viewpoint. Based on all the positive attributes, there has been a growing interest in the HAT method.[5]

1.2 Iron Carbonyl Complexes

There has been a lot of research focused on the use of iron catalysts in HAT (see sections 1.3, 1.4 and 1.5), iron carbonyl complexes are the building blocks of high-performance iron catalysis. It is necessary to fully understand their synthesis to control Fe-H intermediates which pushes the latest developments in HAT.

The synthesis of tricarbonyl(tetraphenylcyclopentadienone)iron complex (**iron complex 1**) was first reported by Schrauzer in 1959,[6] from the reaction between $Fe(CO)_5$ with tolane **1** (Scheme 2).

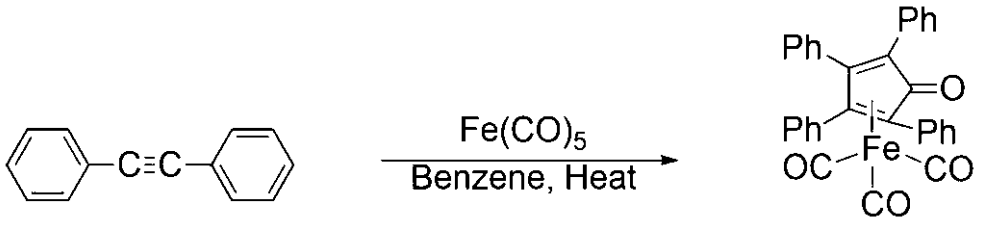

1 **Iron Complex 1**

Scheme 2. Synthesis of Tricarbonyl(tetraphenylcyclopentadienone)iron.
The products formed were stable, crystalline and diamagnetic under normal conditions. Two other complexes could be isolated, and their structures are shown in Figure 1.

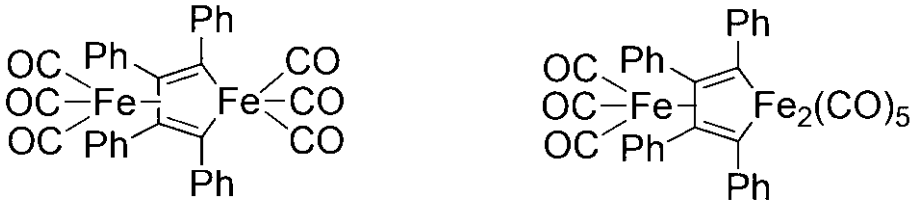

2 **3**

Figure 1: Structures of isolated complexes.
Small quantities of hexaphenylbenzene (a trimerization product of tolane) and tetraphenylcyclopentadienone were isolated from the reaction mixture. This research also revealed the conversion proceeded through the generation of diiron and triiron complexes which, when heated can decompose into lower nuclearity iron-containing species.

In 1992.[7] Pearson employed the cyclisation of dialkynes such as **4** with $Fe(CO)_5$ to produce **iron complex 2** (Scheme 3). This involved carrying out the reaction in a high-pressure vessel to have high pressures of CO gas produced. This synthetic method was then used on a variety of different dialkynes to produce multiple iron complexes. With different substitution patterns.

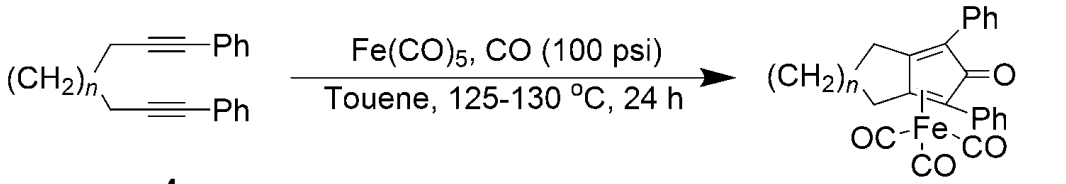

4 **Iron Complex 2**
81%

Scheme 3. Synthesis of Iron Complex 2.

In 1994 the Pearson group reported the synthesis of additional derivates of the iron complexes,[8] building on the use of previous research to the preparation of chiral (racemic) iron complexes (**iron complex 3**) was reported by incorporating an alcohol group into the starting racemic diyne **5** (Scheme 4).

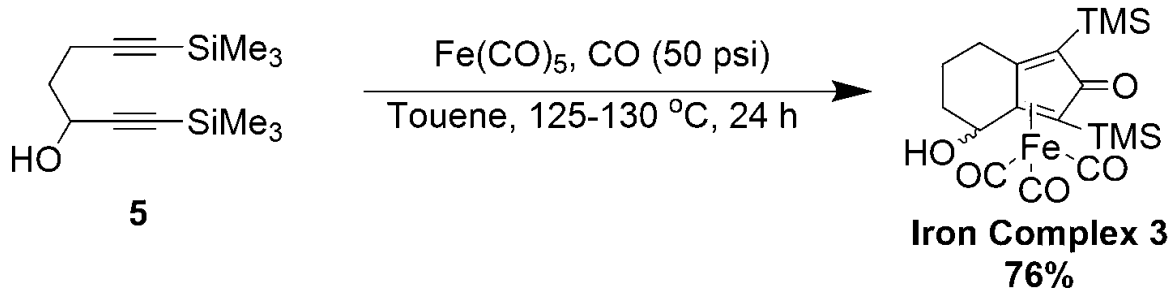

Scheme 4. Synthesis of Iron Complex 3.

In 2002 the synthesis of this type of iron complex was described in another publication by Pearson *et al*,[9] this publication focused on research into the synthesis of $Fe(CO)_5$-promoted cyclocarbonylation derivatives as part of the synthetic method to create cyclopentadienones through complex decomposition. This method required the combination of two 3-trimethyl-2-propyn-1-ol, **6,** molecules to give the substrate **7** that contains a silyl ether moiety (Scheme 5).

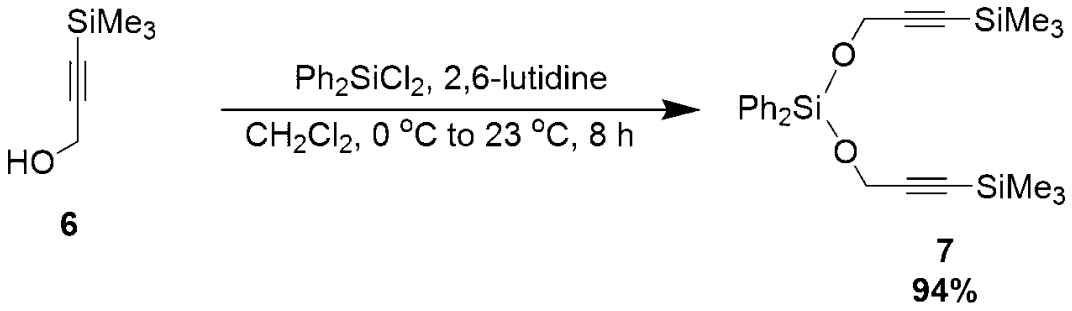

Scheme 5. Synthetic Route of Dialkyne Derivative 7.

Reaction of iron pentacarbonyl under an atmosphere of CO, produced **iron complex 6** with a yield of 65% (Scheme 6).

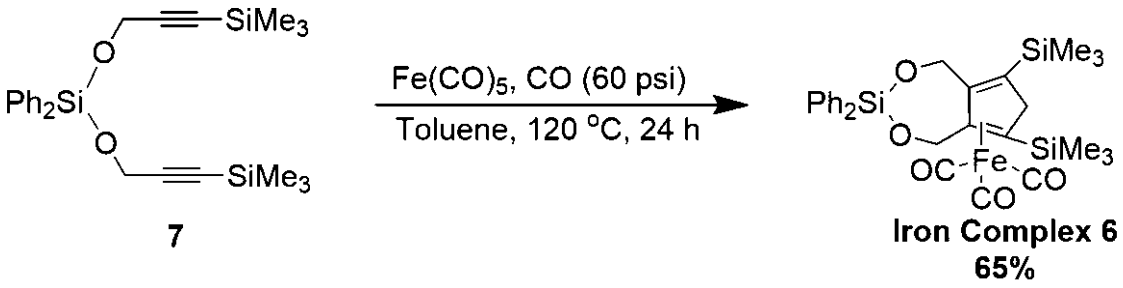

Scheme 6. Synthesis of Iron Complex 4 Using Dialkyne 7.

This research showed that the synthesis of (cyclopentadienone)iron tricarbonyl complexes can be used for synthesising cyclopentadienone derivatives effectively (following decomplexation). The chemistry of cyclopentadienones is an area that has been thoroughly documented and includes oxidation, reduction, Grignard reagents, and employed to a type of Diels Alder reaction.[10]

In 1992, Knölker *et al* published[11] the synthesis of **iron complex 5**, from a reaction between iron pentacarbonyl and trimethylsilyacetylene heated at 140 °C in a sealed tube. This, provided the 2,5-bistrimethylsilyl-substitued (R = H) iron complex as a single regioisomer in 69% yield (Scheme 7, Table 1).

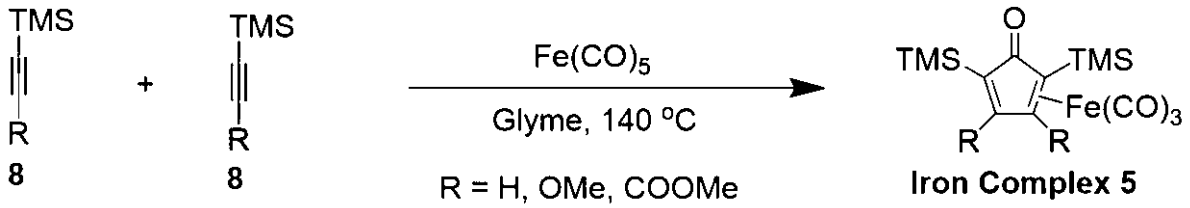

Scheme 7. Synthesis of Iron Complex 5.

R	Yield %
H	69
OMe	42
COOMe	28

Table 1. Results of [2+2+1] Cycloaddition of two Alkynes and CO.

Even though iron carbonyl complexes have shown to have lower toxicity levels when compared to other metal-based catalysts, using iron carbonyl reagents such as $Fe(CO)_5$, $Fe_2(CO)_9$ or $Fe_3(CO)_{12}$, still provide major drawbacks regarding health and safety. The synthesis of these iron complexes produces high levels and pressures of CO gas, which when used in large quantities can pose a significant risk to health and safety. However, even with this knowledge the use of these iron complexes to oxidation and reduction reactions has become an area of interest for research into iron catalysis.[12]

1.3 Iron Carbonyl Complexes used for the Oxidation of Alcohol Functional Groups.

In 2010 Coleman *et al*[13] employed **iron complex 6** for the oxidation of a variety of alcohols achieving exceptional yields ranging from 73 to 91%. This iron complex was used as a hydrogen transfer catalyst for the conversion of an aryl alcohol into the corresponding ketone. Coleman discovered that the most appropriate method for these reactions was to use the conditions shown in Scheme 8.

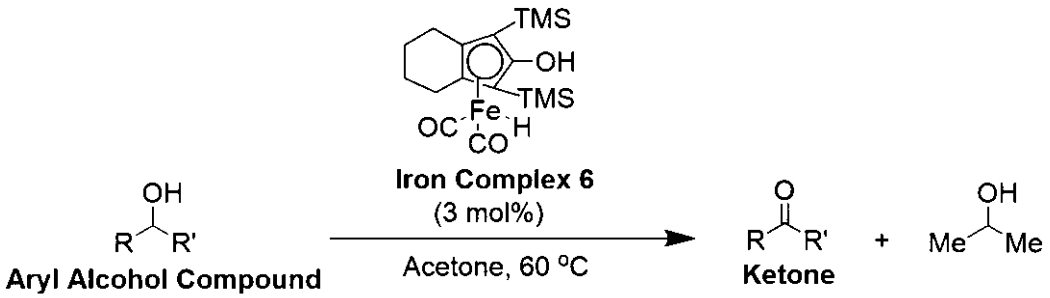

Scheme 8. Oxidation Method Using Iron Complex 6.

The oxidation reaction utilises acetone for both the reaction solvent and the hydrogen acceptor compound. Previous research suggests that the hydrogen transfer process happens following the pathway shown in Scheme 9.

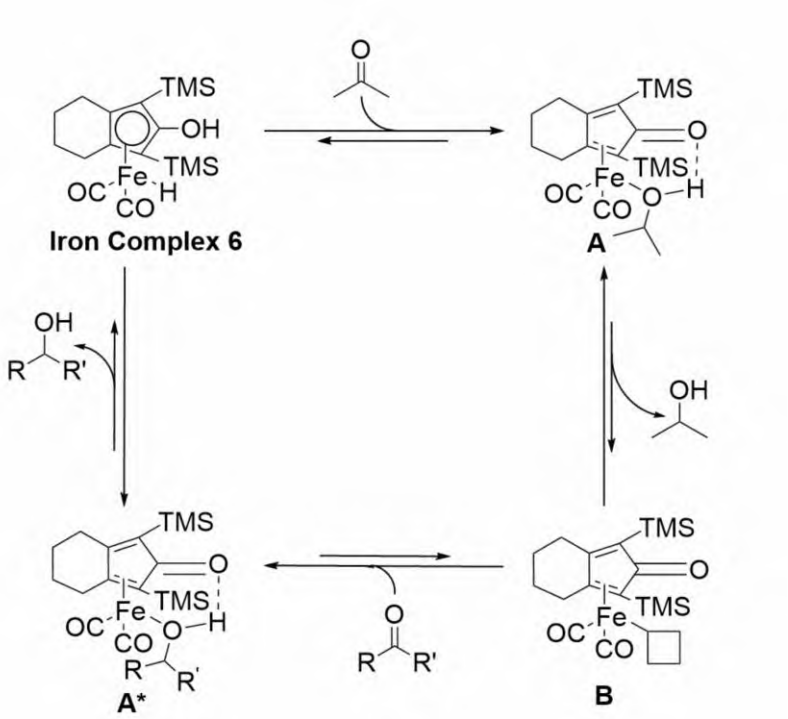

Scheme 9. Proposed catalytic pathway for the iron-catalysed oxidation of alcohols.

The study by Coleman *et al*, revealed that these types of catalysts can carry out the oxidation of alcohols using a variety of different functional groups such as alkene, alkoxide, CF_3 or halogens without these extra functional groups producing any unnecessary difficulties under the employed reaction conditions.

Research using **iron complex 6** with acetone acting as a hydrogen acceptor using similar derivates was carried out in 2010 by Funk *et al*,[14] using the catalyst to carry out the oxidation of alcohol, for this research, trimethylamine N-oxide was used to perform *in situ* activation of the catalyst be removing a carbon monoxide ligand from the iron carbonyl complex, thus producing the active species B (Scheme 9).

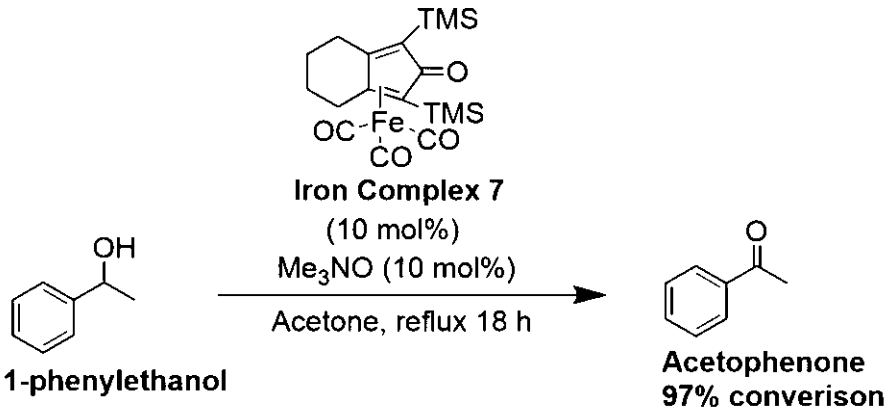

Scheme 10. Oxidation Reaction Method Used by Funk *et al*.[14]

Oxidation of 1-phenylethanol to acetophenone was used to analyse the applicability of the reaction and it was discovered that this reaction can achieve an exceptionally high (97%) conversion (Scheme 10). This oxidation method has been used on a variety of secondary alcohols and percentage yields ranging from 40 to 94% were obtained. Different alcohols were oxidised to the respective ketones using a variety of functional groups.

In 2011 Wills *et al*[15] demonstrated the use of iron carbonyl complexes as hydrogen transfer catalysts where the oxidation of 1-phenylethanol to acetophenone was used to examine the use of iron complexes 1, 7 and 8.

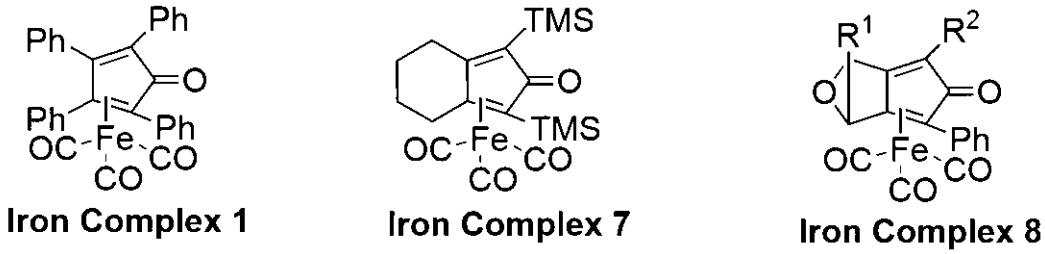

Figure 2. Iron Carbonyl Complexes Employed by Wills *et al*.[15]

The synthesis of the iron complexes was employed to show the easy acquirement of these iron complexes, because these iron complexes were all synthesised through a cyclisation reaction using $Fe(CO)_5$ and the respective diynes.

These iron carbonyl complexes were analysed for catalytic activity, at various catalyst loadings. Studies of H_2O addition were carried out, as well as using various times and temperatures, Iron complex 1 showed the most catalytic activity, achieving a 95% conversion to ketone using the conditions shown in Scheme 11 for the oxidation of 1-phenylethanol to acetophenone. When **iron complex 7** was used the reaction was unsuccessful, however an impure iron hydride complex was observed using ^{1}H NMR.

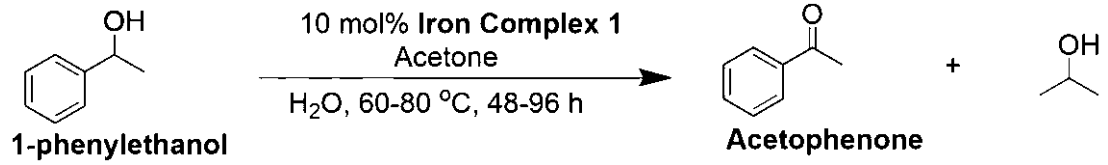

Scheme 11. Method Used by Wills *et al.*[15]

Use of the hydrogen acceptor compound **9** and the substrate shown in Scheme 12 was examined. Yields of up to 99% were achieved using iron complex 1 and iron complexes 7 and 8 produced ketone conversions of up to 61% and 63%. Using the alcohol substrate, where R^1 refers to the use of para-methoxy groups, causes a notable increase of the oxidation process and produces yields of up to 100% within a shorter period (6 hours). When R^1 refers to the employment of a para-chloro group, yields were reduced to 27-48%. Using aldehyde and ketone derivates of **9**, there was no observed improvement to the yields through the use of choices to acetone.

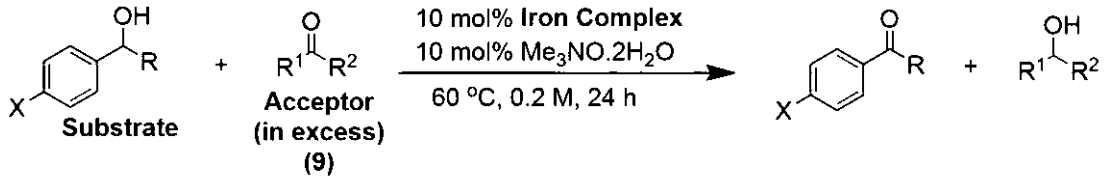

X = Cl, H, OMe R = H, Me R^1 = Et, Me, n-pr R^2 = H, Me

Scheme 12. Oxidation of 1-Phenylethanol and Derivatives Catalysed by Iron Complexes Activated in Situ by TMANO.

When the complexes were analysed with paraformaldehyde acting as an acceptor with toluene as the solvent system, an interesting observation occurred: the formation of acetophenone was obtained however the major product of the reaction in most situations was 1-phenyl-ethyl formate (**10**). One noteworthy observation the authors made was that to the best of their knowledge the paraformaldehyde-formate conversion had not previously been reported using any type of iron-based catalyst and has the potential to be a “green” transformation because of the low toxicity of iron when comparing to the more often used precious-metal catalysts.

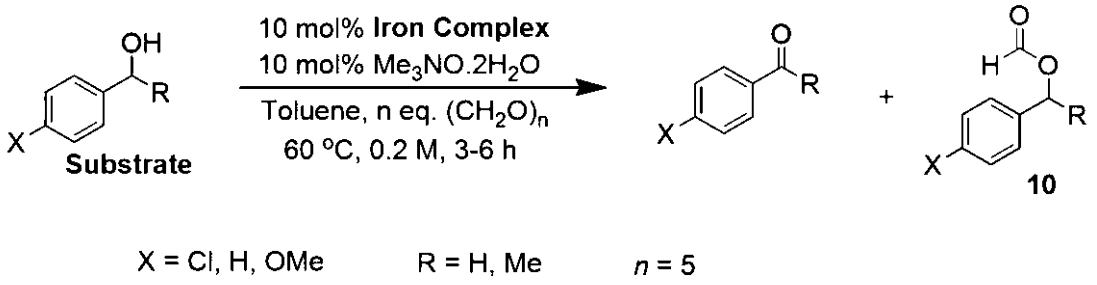

Scheme 13. Reaction of 1-Phenylethanol in the Presence of Paraformaldehyde Using Iron Complexes.

1.4 Iron Carbonyl Complexes used for the Reduction of Carbonyl Functional Groups

In 2007 Casey *et al*[16] demonstrated the use of iron complexes for the reduction of carbonyl groups, this publication described the use of the activated **iron complex 6** for the reduction of acetophenone to 1-phenylethanol. This was accomplished obtaining an excellent yield of 83% (Scheme 14).

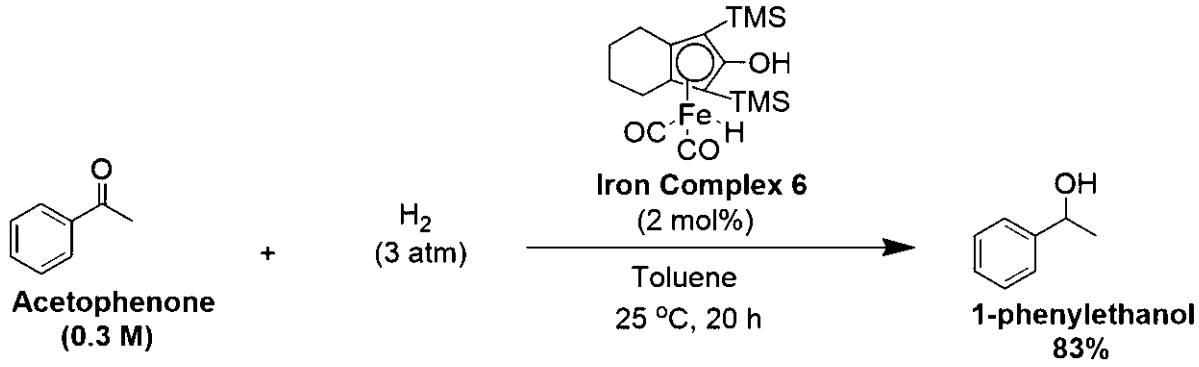

Scheme 14. Catalysed Iron Reduction Reaction.

The extent of the use of iron complex 6 was further examined through the reduction of a variety of aryl and unsaturated imines and ketones, this was done successfully obtaining yields of 46% and 91%.

Using this method with different hydrogen donor methods was also explored, with the reduction of acetophenone being carried out through using transfer hydrogenation using isopropanol as the reducing agent. An alcohol was successfully produced with a yield of 87% (Scheme 15).

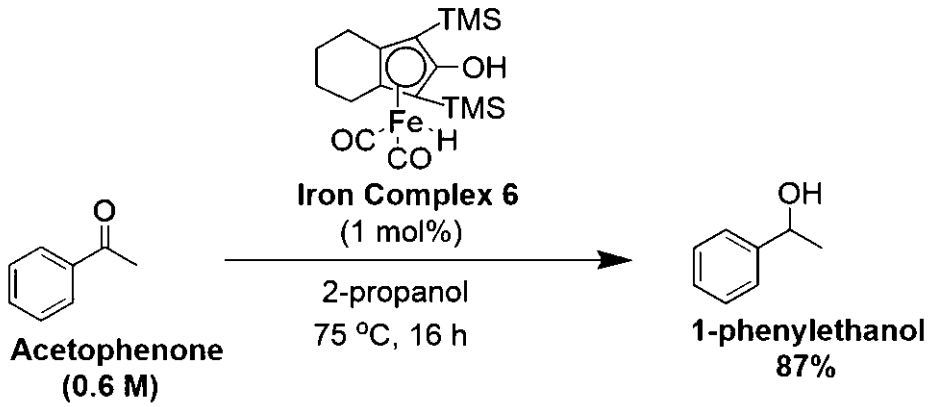

Scheme 15. Isopropanol used for Hydrogen Donation.

Casey *et* al[17] produced a detailed paper, in this paper they attempted to produce a detailed understanding of the steps of the catalytic mechanism for the reduction processes and the reaction mechanism from Figure 3 was presented. The description of the pathway of the mechanism agreed with other published assumptions on the mechanism pathways of iron-catalysed reactions.

They demonstrated that the reduction reaction obeyed a second order rate reaction, being first order, the aldehyde and the iron hydride species. The other results demonstrated the highly labile nature of the alcohol-iron species. Further supporting the likelihood of the proposed mechanism.

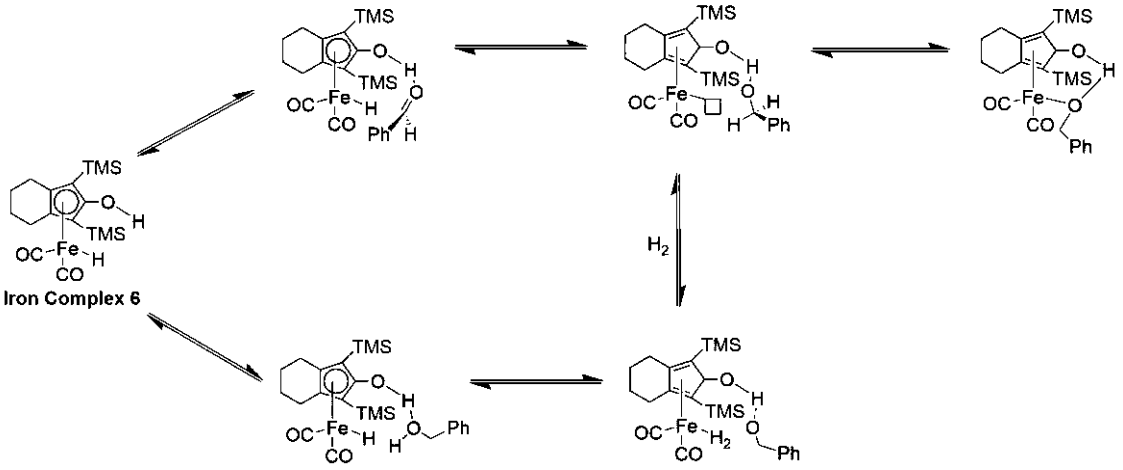

Figure 3. Mechanistic Study Proposed by Casey *et al*.[17]

The use of dihydrogen being used to activate the iron catalyst was utilised instead of using a hydrogen donor compound. This is done through the coordination of H_2 onto the iron centre, this creates a stable η^2-H_2 complex. The heterocyclic cleave of the H_2, takes place between the centre of the iron and the oxygen that is attached to the cyclopentadienone, this creates the desired iron-hydride species.

This method for the activation of the iron complex was demonstrated by Beller *et al*.[18] This paper gave a description of the reduction of aldehydes, α,β-unsaturated aldehydes and ketones. **Iron complexes 9 and 10** with an ether or carbon chain moieties, were synthesised from the similar silated dialkynes through a cyclisation using $Fe(CO)_5$, this method has been established to be an effective synthetic route.

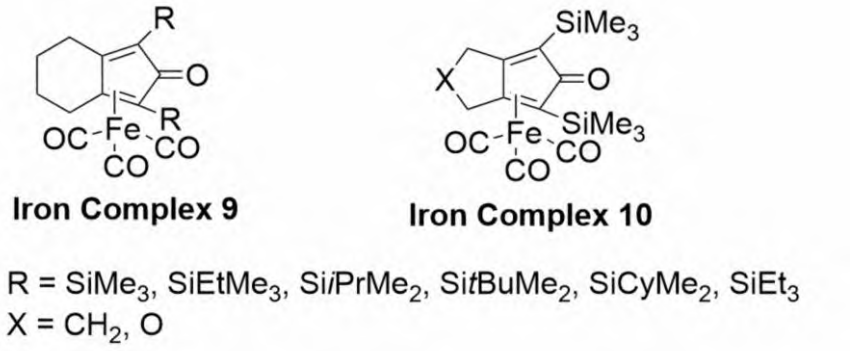

Iron Complex 9 **Iron Complex 10**

R = $SiMe_3$, $SiEtMe_3$, Si*i*$PrMe_2$, Si*t*$BuMe_2$, $SiCyMe_2$, $SiEt_3$
X = CH_2, O

Figure 4. Iron Complexes Used by Beller *et al*.[18]

Reduction of acetophenone to 1-phenylethanol was used as a trial reaction to analyse the activity of various iron complexes used for the reduction reaction. Iron complex 11 showed an exceptional catalytic activity for the reduction of acetophenone.

Upon further study into the optimisation of the reaction conditions to be carried out with **iron complex 11**, regarding catalyst loading, pressure of hydrogen gas, temperature of the reaction and solvent system, they found that a catalyst loading could be as low as 0.05 mol% and able to maintain a percentage yield of >99% (Scheme 16). This catalyst loading was considerably lower than the amounts used in other publications focusing on the use of iron carbonyl complexes as oxidation or reduction catalysts. The standard catalyst loadings used in other publications is between 2-10 mol%, showing a notable development in the use of this type of catalysis to be used as a hydrogen transfer catalyst for pressure hydrogen reaction.

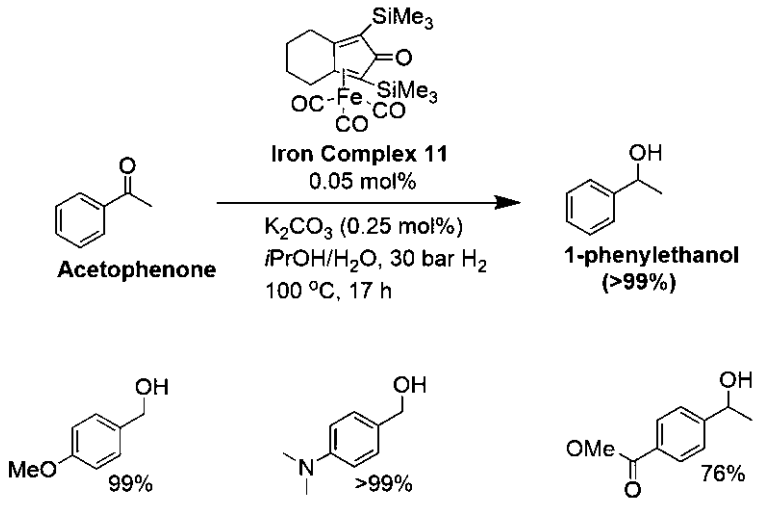

Scheme 16. Altered Method Used By Beller *et al*.[18]

Using these improved reactions conditions, the full extent of the set of catalytic conditions was analysed by carrying out the reduction of a variety of aryl ketones, this was achieved obtaining exceptional yields 76% to >99%. These conditions were then used for the reduction of alkyl ketones, aldehydes and α,β-unsaturated aldehydes with exceptional yields 82% to >99%.

In 2012 Beller *et al*[19] published a research paper focusing on the use of **iron complex 7**, the K_2CO_3 catalytic system was employed and the conditions of the water-gas shifting using both CO and water in the reaction for the source of H_2 for the hydrogenation reactions.

The reduction of benzaldehyde to benzyl alcohol was employed to enhance the reaction conditions (Scheme 17). By using these enhanced conditions, exceptional yields of 99% were obtained and this synthetic method was used for a variety of aldehydes and aryl aldehydes with furan, indole or thiophene functional groups.

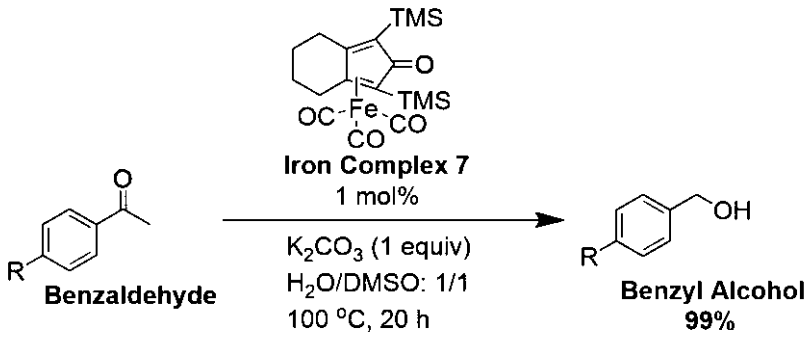

R = aloxide, alkyl, H, halogen, nitrile

Scheme 17. Enhanced Reaction Conditions Used by Beller *et al*.[19]

These reduction reactions achieved yields > 76%. Applying the same conditions for a variety of aliphatic and α,β-unsaturated aldehydes achieved yields > 62% while reduction of aldehydes with a furan group reduced yields to 59%.

1.5 The Use of Iron Complexes for Hydrogen Auto-transfer Reactions

There have been numerous publications in the past decade focusing on the use of iron carbonyl complexes as hydrogen transfer catalysts for oxidation and reduction reactions in alcohols, carbonyl and imine groups. The foundations of both these processes were combined, and this permitted a series of publications to be produced regarding the use of iron carbonyl complexes for hydrogen auto-transfer reactions.

The majority of the research that has been published regarding oxidation and reduction reactions, the use of **iron complex 7** has been proven to be a useful catalyst in hydrogen auto-transfer reactions.

The first publication was in 2014 by Feringa *et al*,[20] this was then followed be a further publication in 2016.[21] The 2014 publication produced a detailed overview of the possible uses of an innovative method, starting by investigating into the *N*-alkylation of aniline based reagents (**11**), with 1-pentanol (**12**), this produces a variety of example compounds i.e. **13** (Scheme 18).

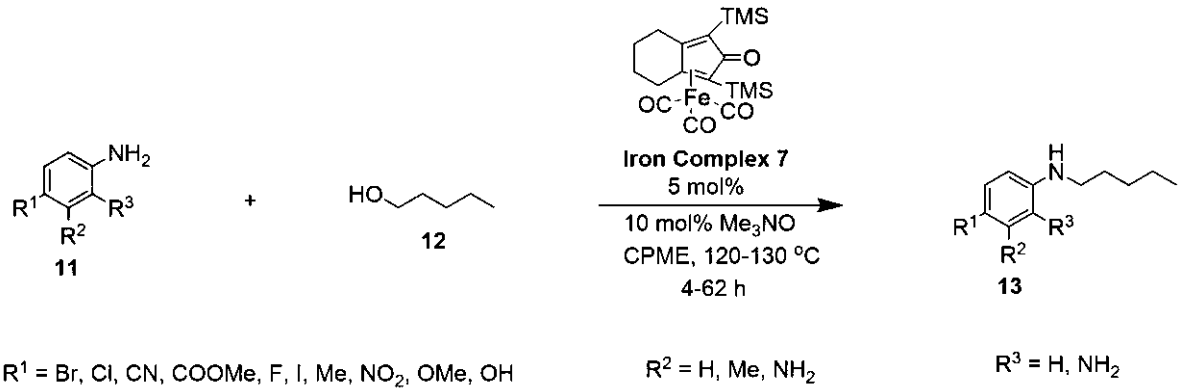

Scheme 18. The Reaction Conditions Employed by Feringa *et al*.[20]

This detailed introduction to the use of this type of catalysis was subsequently followed by the *N*-alkylation of a variety of benzylamine **14** (Scheme 19) and piperidine-based amines **15** (Scheme 20) with primary alcohols such as, 1-pentanol,**12**, and diols such as butane-1,4-diol, pentane-1,5-diol or hexane-1,6-diol. Analysis into the utilisation of benzylamines that contain halogenated substituents i.e. chloro, fluoro or trifluoromethyl groups located at the 3- or 5- phenyl ring positions, producing some interesting outcomes, this includes the observation that the presence of the electron-withdrawing group found at the benzylic ring, increases the reactivity of the amine towards the hydrogen auto-transfer method, when compared to the reactivity of benzylamine. This produced higher reaction yields going from 62% to 80%-95%. Using *p*-methyl substituted benzylamine revealed that

an electron-donating group reduces the reactivity of the amine and causes the reaction yield to drop to 30%.

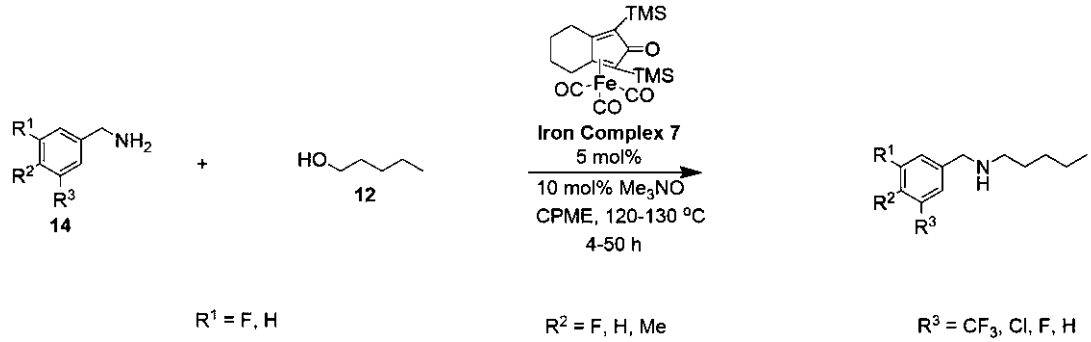

Scheme 19. Use of Benzylamine Derivatives for Hydrogen Auto-transfer.

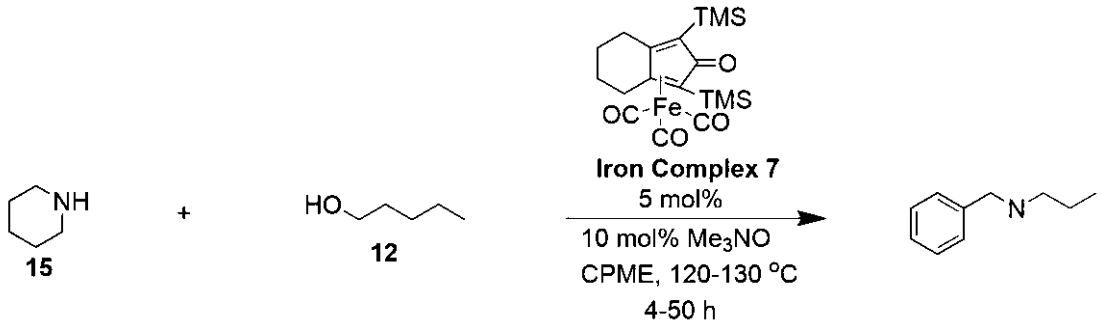

Scheme 20. Use of Piperidine for Hydrogen Auto-transfer.

The publication releveled the use of a newly developed method for the use of dialcohols for the synthesis of tertiary cyclic amines, using halogenated benzylamine derivatives **16** (Scheme 21).

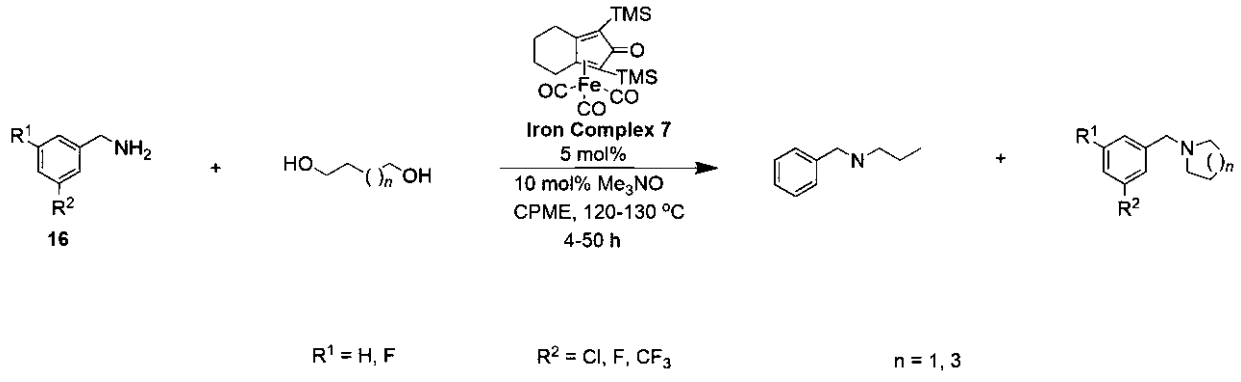

Scheme 21. Synthesis of Cyclic Tertiary Amines.

In 2016 another publication, gave a more thorough analysis into the use of the hydrogen auto-trasnfer method for the *N*-alkylation of aliphatic amines (piperazine, piperidine or morpholine).[21] This work started with an examination into the most favourable temperature and solvent conditions for the use of HAT reactions using morpholine (Scheme 22). The results from this study revelaed that when using 135 ^{o}C and using a different solvent system (toluene or DCE), it was found that the converison of this reaction could be increased from 39% to a yield of >95%.

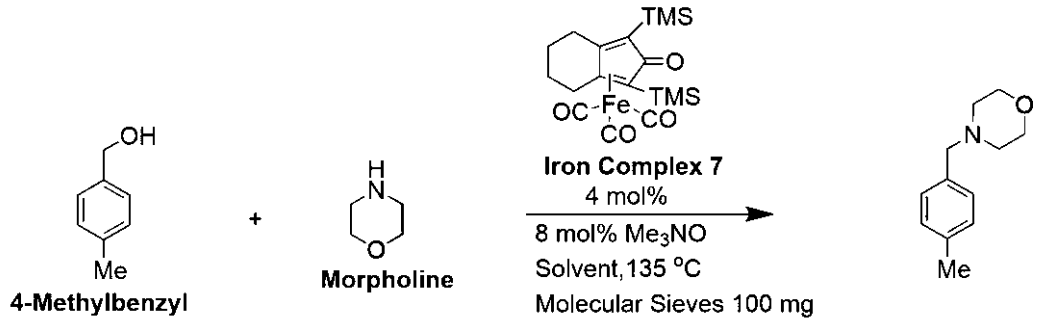

Scheme 22. *N*-alkylation of morpholine.

This improved method was used for the *N*-alkylation a wide variety morpholine, piperidine, piperazine and other aliphatic-based amines with benzylic alcohol-based derivatives.

The results described in both publications employ the use of electron-withdrawing groups in either alcohol or amine starting reagents, using the electron-withdrawing groups in amines produced a positive effect upon the reactivity of the associated reagent. Although, the reactivity of the alcohol reagents which contained an electron-withdrawing group were adversely affected. One possible reason that was suggested in the publication was that behind these investigations was the reactivity of the imine intermediate, produced during the HAT reaction, towards the reduction reaction to produce the sought-after amine product.

In 2014 Wills *et al* produced a publication,[22] which focused on the use of **iron complex 1** for HAT. This employed aniline as the amine of interest and a variety of benzyl alcohol derivatives and aliphatic alcohols in (Scheme 23).

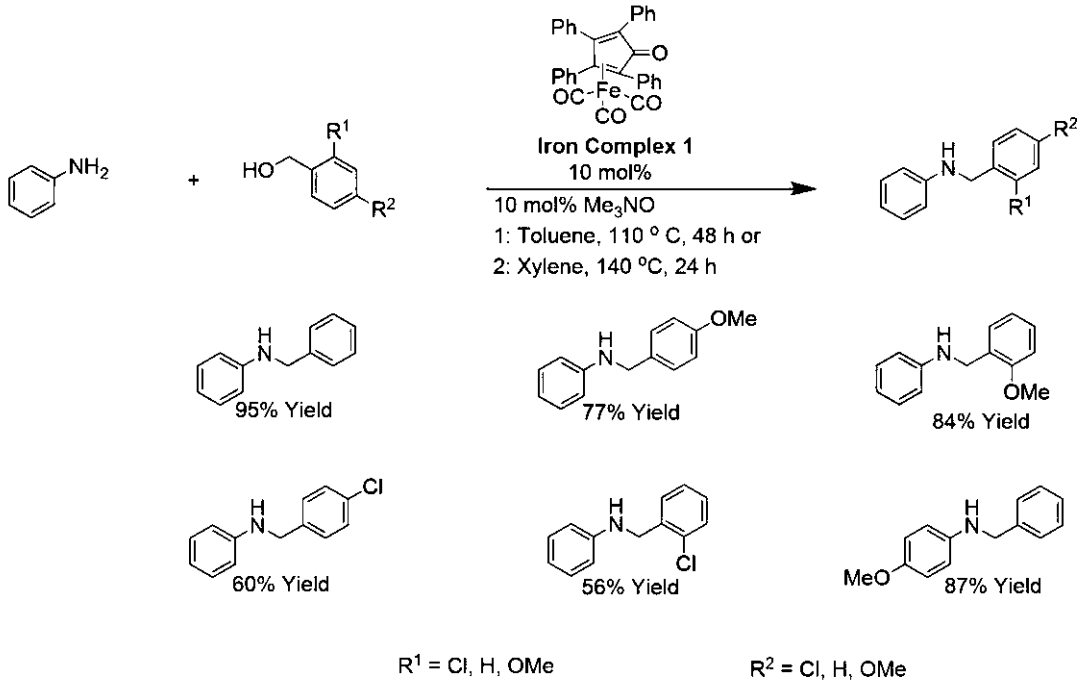

Scheme 23. Use of Complex 1 For Hydrogen Auto-transfer.

The publication discussed how the use *N*-alkylation of aniline produced both the secondary and tertiary amine derivatives, using a variety of benzyl alcohol derivatives creating secondary alcohols and the aliphatic alcohols creating both secondary and tertiary alcohols. The method to do this is set out in (Scheme 23) it can be used in the use of benzyl alcohols, at 110 °C and a reaction time of 48 hours. Reaction conditions (Scheme 23) were used for the rest of the duration of the published examples, employing a different reaction solvent system, a shorter reaction time of as well as a higher reaction temperature of 140 °C. These reaction conditions within the publication align with the reaction conditions set out in previous literature within this area of research and further publications.

When this method was used on aliphatic alcohols (Scheme 24) it was revealed that using a primary aliphatic alcohol (1-pentanol) produced a mixture of tertiary and secondary amine products, obtaining a yield of up to 72% for the secondary amine product and the tertiary amine had a conversion of 28%. These results are in conjunction with other observed results in other published literature.

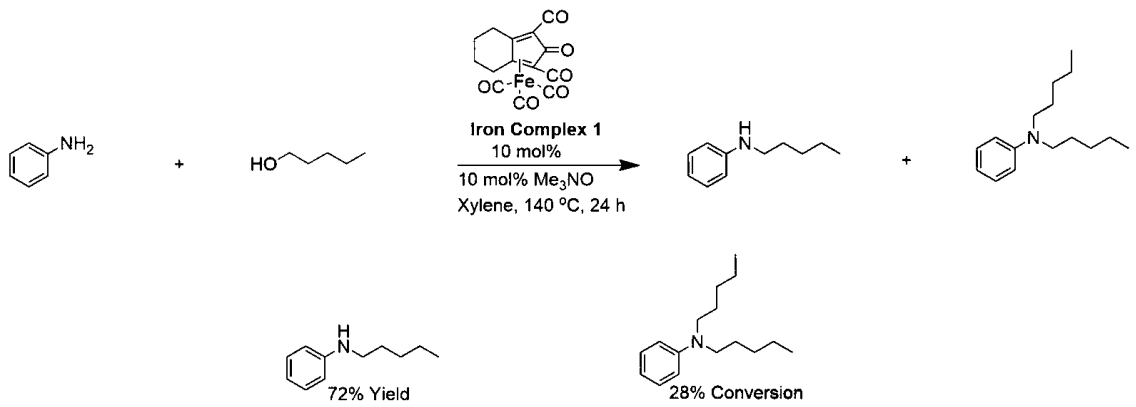

Scheme 24. Use of Aliphatic Alcohols for Hydrogen Auto-transfer.

In 2015 Zhao *et al* reported,[23] a different route to using iron carbonyl complexes (Scheme 25) this was done by using a Lewis acid to allow the use of secondary alcohols with this method.

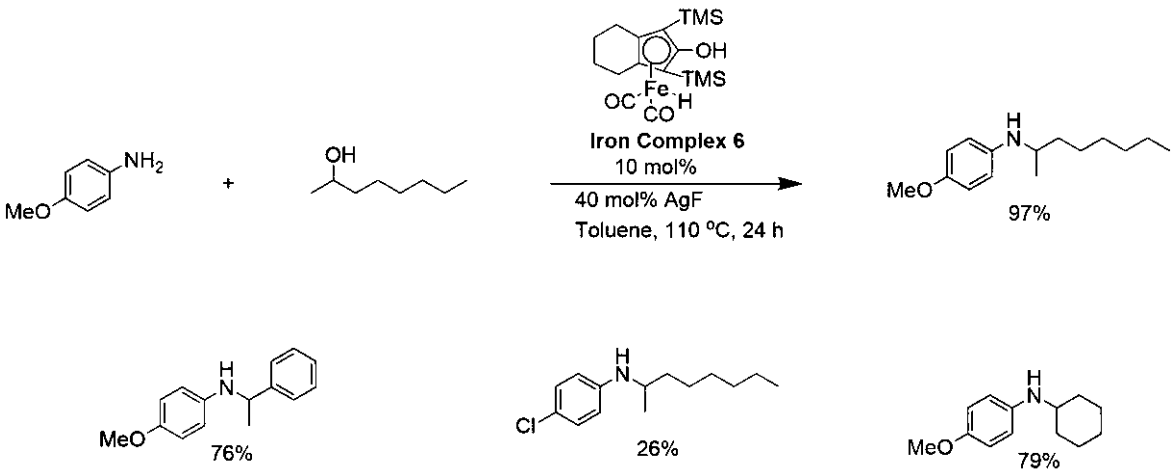

Scheme 25. Use of Lewis Acid for Hydrogen Auto-transfer.

After rigorous experimentation using a variety of different organic acids (such as *p*-Toluenesulfonic acid, phosphoric acid or formic acid) and metal salts (such as $Ni(acac)_2$, $FeBr_3$, $CuCl_2$, AgF), the conditions shown in Scheme 25 were shown to give the product in 97% yield. These reaction conditions allowed for the use of the HAT method to a variety of unsymmetrical secondary alcohols, that at one point were challenging targets within the previously reported methods.

In 2018 Morrill reported,[24] the use of methanol as a methylating reagent as well as the solvent to methylate numerous nucleophiles. Acetophenone derivatives were shown to be useful nucleophiles in this publication (Scheme 26).

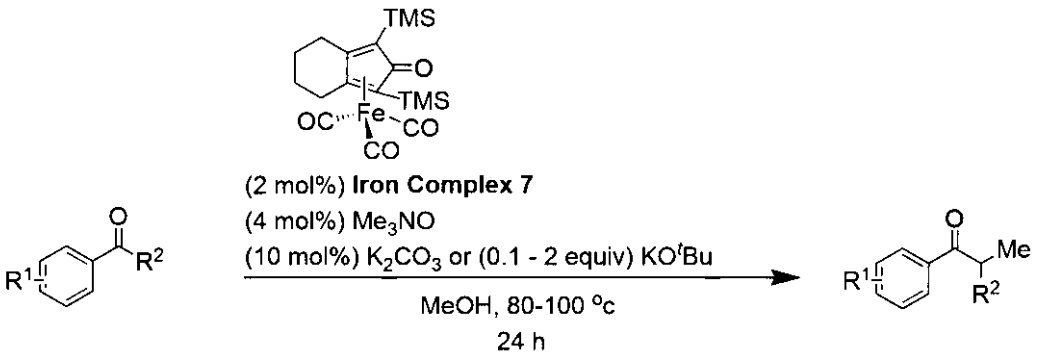

Scheme 26. Iron Catalysed Methylation of Ketones.

A total of 27 examples were reported, including substrates with heteroatoms, and electron-withdrawing groups moietes obtaining an 80% average yield. When R^2 = H exclusive dimethylation was observed. In addition, the methylation of butyrophenone was carried out on a scale of 10 mmol, producing an isolated yield of 99% and revealing the scalability of this method.

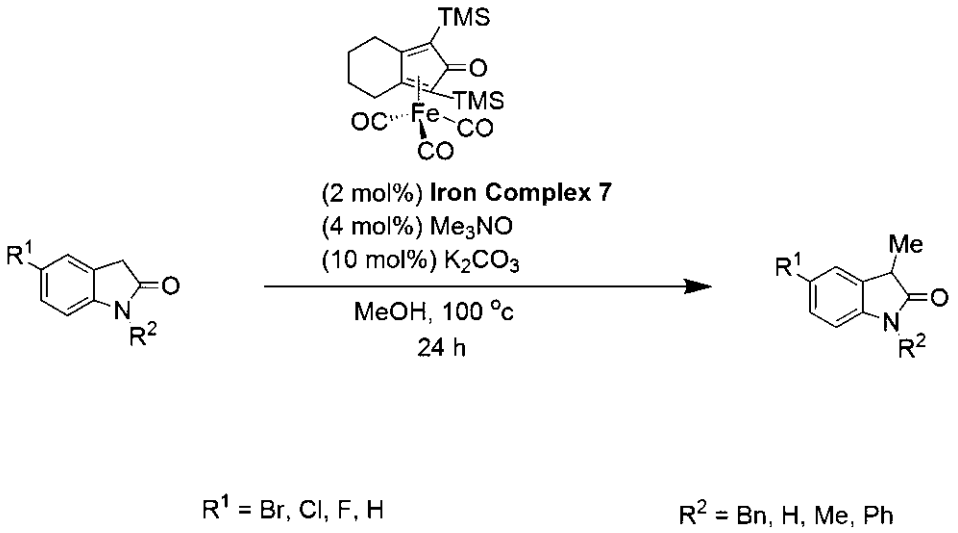

Scheme 27. Iron Catalysed Methylation of Oxindoles.

In addition, 7 examples of oxindoles were reported as nucleophiles (Scheme 27), producing the 3-methyloxindoles with an average yield of 77%. Tolerance of a variety of substrates bearing halogens was reported, and there no *N*-methylation even where R^2 = H, revealing the selectivity of this transformation towards *C*-alkylation.

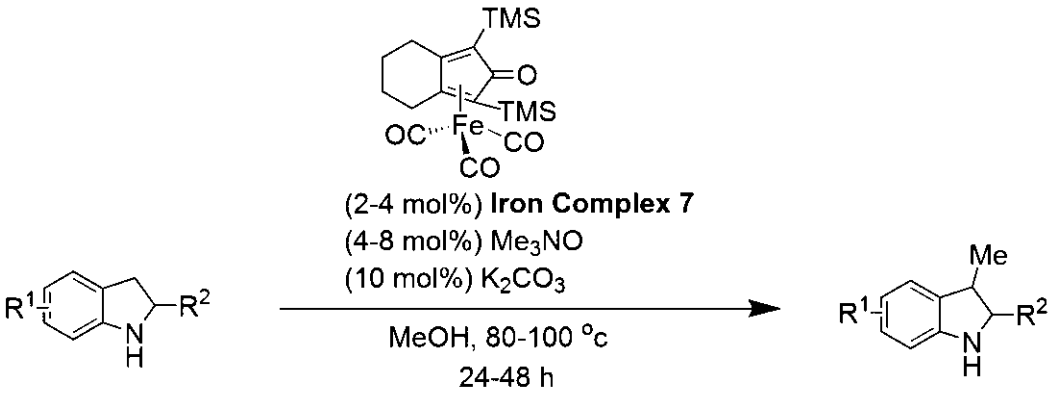

R^1 = Br, Cl, F, H R^2 = H, Me

Scheme 28. Iron Catalysed Methylation of Indoles.

Seven examples of Indoles were reported as nucleophiles (Scheme 28), achieving an average yield of 76%. This demonstrated the selectivity for the *C*-methylation at the 3-position, with no reported methylation or *N*-methylation in the 2-position. It was shown that the remaining 2-functionalisation did not hinder the alkylation, even with the increased steric bulk of the nucleophile.

There were various *N*-methylation procedures that were shown in this transformation (Scheme 29).

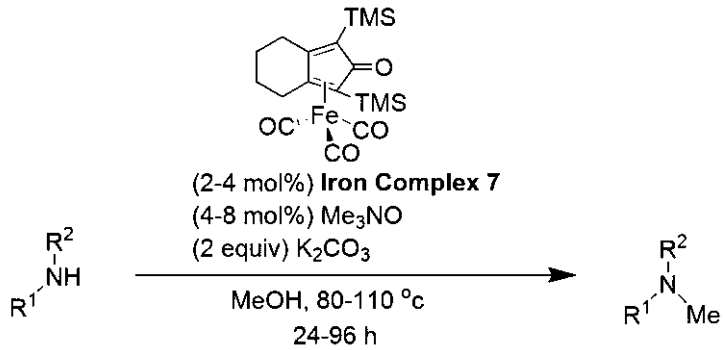

R^1 = Ar, Bn, Heteroaryl, Ph R^2 = Bn, H, Me $R^1 = R^2$ = Cycloalkyl

Scheme 29. Primary and Secondary Amine Methylation.

A variety of amines were employed in this method, 11 examples for methylation were reported, achieving an average yield of 76%. Both primary and secondary alcohols were tolerated, although primary aliphatic amines were not reported as nucleophiles. This method was expanded for sulfonamide methylation. Although, because of the lower nucleophilicity of sulfonamides, adjustments to the reaction conditions were carried out using iron complex 12 (Scheme 30).

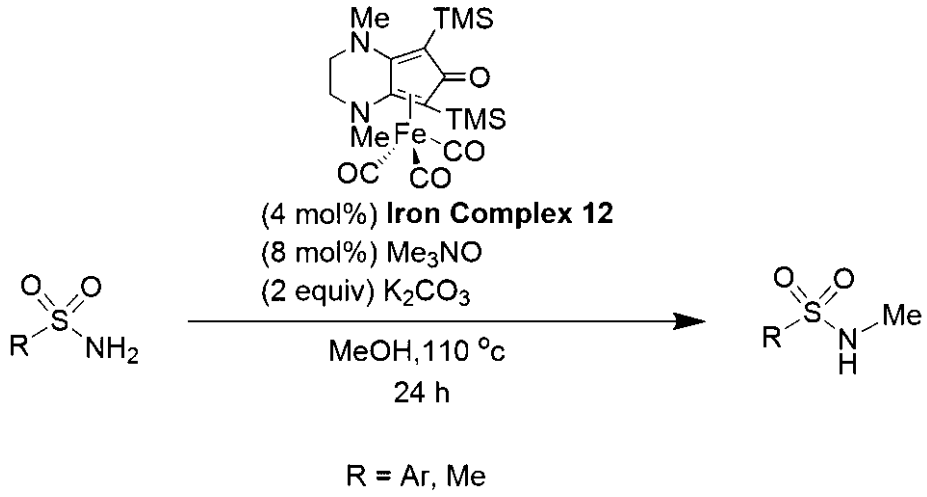

Scheme 30. Iron Catalysed Methylation of Sulfonamides with methanol.

1.6 Light Induced reactions of Iron carbonyl complexes.

Light-induced reactions of metal carbonyls often involve photoinduced CO dissociation or CO release from the metal complex. These photochemical reactions are fast and can occur on the picosecond timescale of light absorption, and the ligand-deficient fragment have the potential to bind with solvents or other molecules such as H_2O.[25]

In 1999 Knölker and co-workers[26] showed that photoirradiation with a 150 W medium-pressure mercury, can cause the exchange of a CO ligand for an acetonitrile using **iron complex 11** (Scheme 31). This observation has motivated further studies into using photoirradiation using iron carbonyl complexes for the HAT alkylation reactions.

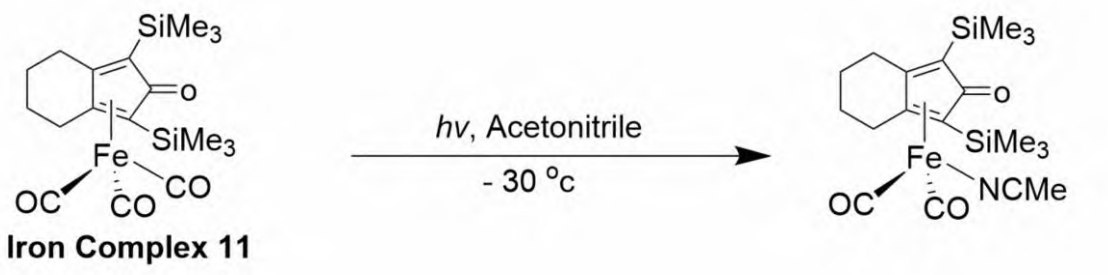

Scheme 31. Photolytically induced exchange reaction of iron complex 11 in acetonitrile.

In 2022 Sundaraju *et al* reported an iron-catalysed methylation of ketones using light irradiation.[27] This publication reported a variety of acetophenone derivatives were produced in the presence of **iron complex 11** (4 mol%) and ^{t}BuOK (2 equiv) in methanol. The reaction mixture was irradiated using four 7 W LED bulb lamps in a light chamber for a period of 24 hours. Because of the light irradiation, the temperature within the chamber reached 42 °C. Using these reaction conditions α-methylated ketones were isolated obtaining yields between 37 to 99%, Scheme 32) Di-methylation of *p*-methyl acetophenone gave a yield of 41%. 1-Tetralone produced the methylated ketones with a yield of 44%. The methylation of ethisterone did not provide the saturated product however the tetrasubstituted olefin derivative that came from the isomerisation of the *exo* methylene to the more stable *endo* alkene.

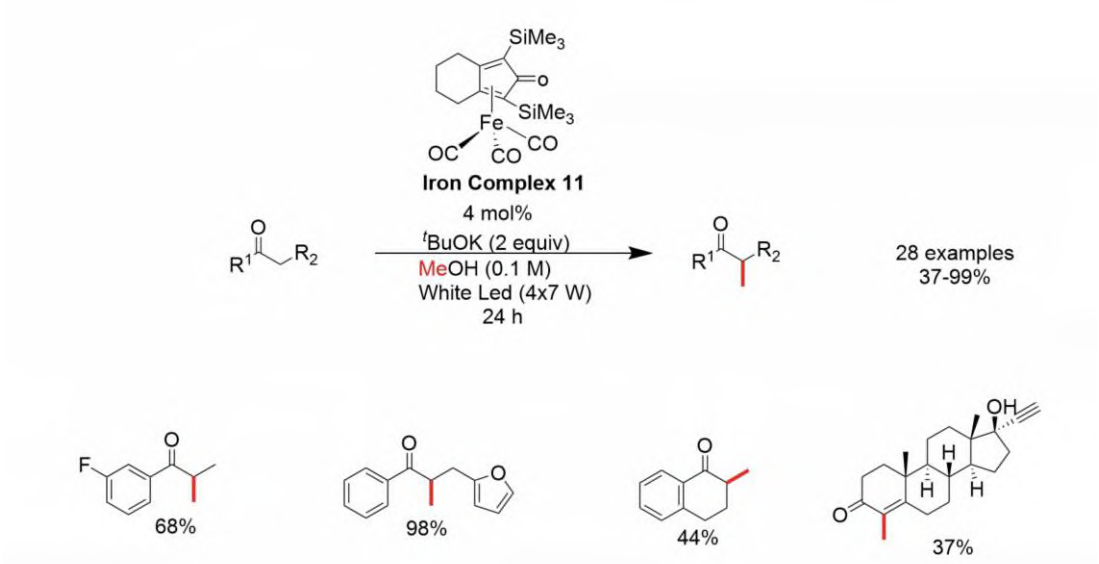

Scheme 32. Methylation of Ketones using irradiation of light demonstrated by Sundaraju *et al*.[27]

Deuterated methanol was used as a pro-electrophile (Scheme 33), the deuterated product was acquired with a yield of 93% with 72-87% deuterium incorporation, demonstrating that methanol was the source of methyl group.

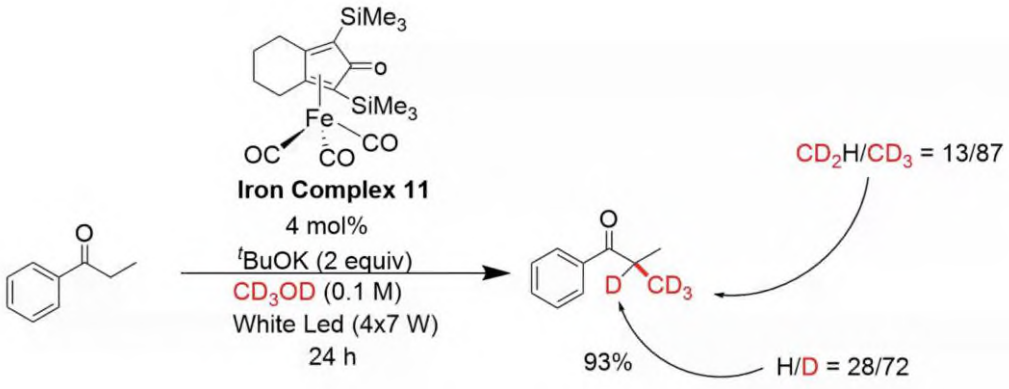

Scheme 33. First Controlled Experiment Carried out by Sundaraju *et al*.[27]

When a second experiment was carried out, an enone derivative was involved in the reaction conditions and provided the reduced product with a yield of 90%, suggesting that the enone is an intermediate with the alkylation reaction (Scheme 34).

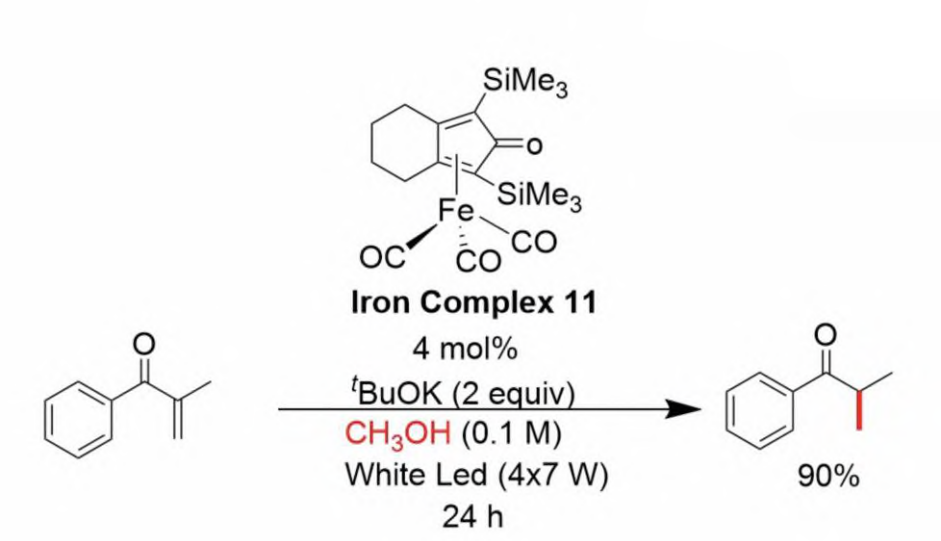

Scheme 34. Second Controlled Experiment Carried out by Sundaraju *et al*.[27]

This experiment was carried out again using the deuterated methanol as the solvent (Scheme 35). The reduced product was obtained with a yield of 81% with 94% deuterium incorporation, confirming that methanol is the hydride source.

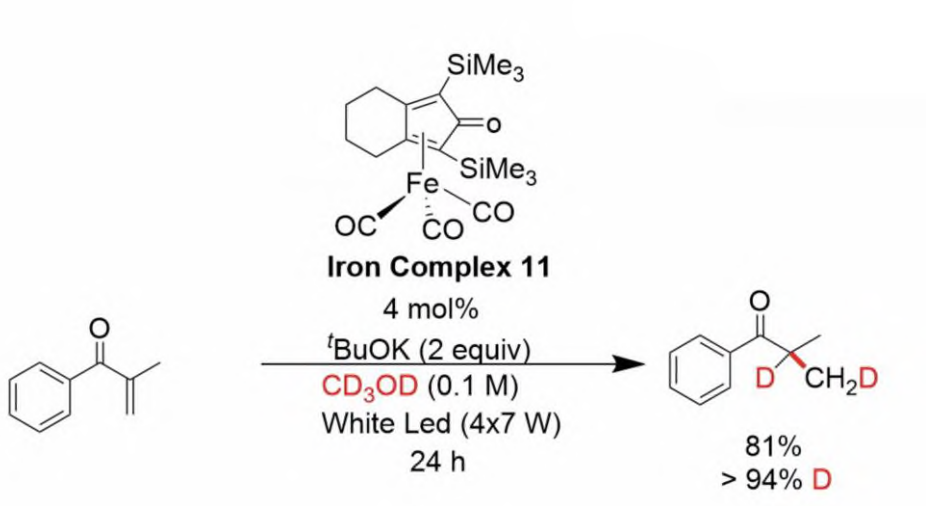

Scheme 35. Third and Final Controlled Experiment Carried out by Sundaraju *et al*.[27]

Additional analysis was carried out, UV-vis spectrum of iron complex 11 exhibited a maximum absorbance at 319 nm. After irradiation, the absorption underwent a red shift, with an isosbestic point located at 332 nm. Carrying out the reaction using thermal conditions did not produce any alkylated product at 40 ^{o}C, however the α-methylated ketone was obtained with 18 and 32% yield at temperatures of 50 and 60 ^{o}C. Confirming the necessity of light in this alkylation reaction.

1.7 Project Outline

As previously highlighted iron carbonyl complexes can be used in HAT reactions often obtaining high yields. However, these reactions require the use of additives such as Me_3NO, high reaction temperatures (110-140 ^oC) and high catalyst loadings and are major drawbacks. It is essential to find strategies to either reduce or eliminate these issues if they are to be used more frequently. One suggested method is to carry out an in-depth study into their mechanisms; this would provide an insight that is necessary to design more appropriate catalyst systems.

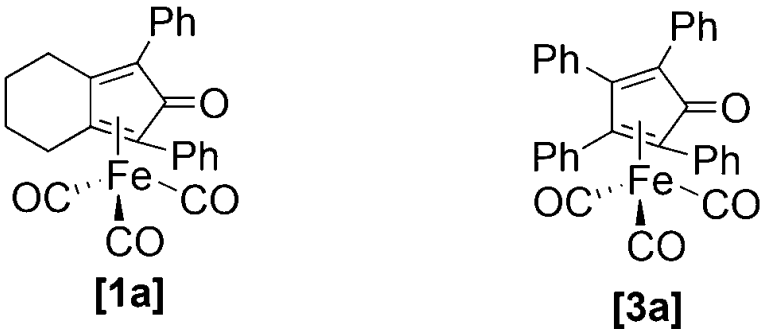

Figure 5. The Two Iron Carbonyl Complexes Studied in this Research Project.

This research project focuses on two iron carbonyl complexes (Figure 5), a group of catalysts that have been of growing interest. This is because of the presence of both the metal and the organic carbonyl. This allows for the reaction to be observed using infrared spectroscopy.

Previous research carried out by the Lynam group using manganese carbonyl complexes using Time-Resolved Infrared Spectroscopy. [28] The research using TRIR allowed for the observation of essential pathways in manganese catalysed C-H functionlisation reactions, observing an alkyne binding to the metal, this was followed by C-C bond formation occurring. Something noteworthy within the findings that was indicated that solvents such as THF will at first bind to the metal through the two electrons of a C-H bond before isomerisating to the more thermodynamically favoured O-bound form. This allows for the reaction to be observed using infrared spectroscopy. These iron carbonyl complexes are an ideal candidate for similar investigation.

In particular, Knölker has previously demonstrated that photolysis of **[3a]** results in CO-dissociation and formation of the corresponding acetonitrile complex. It was anticipated that this would be the key step in the catalytic reaction as it would provide a vacant coordination site at the metal, enable substrate binding. If this substrate were an alcohol, for example, the hydrogen transfer reaction would occur, as predicated in Scheme 36.

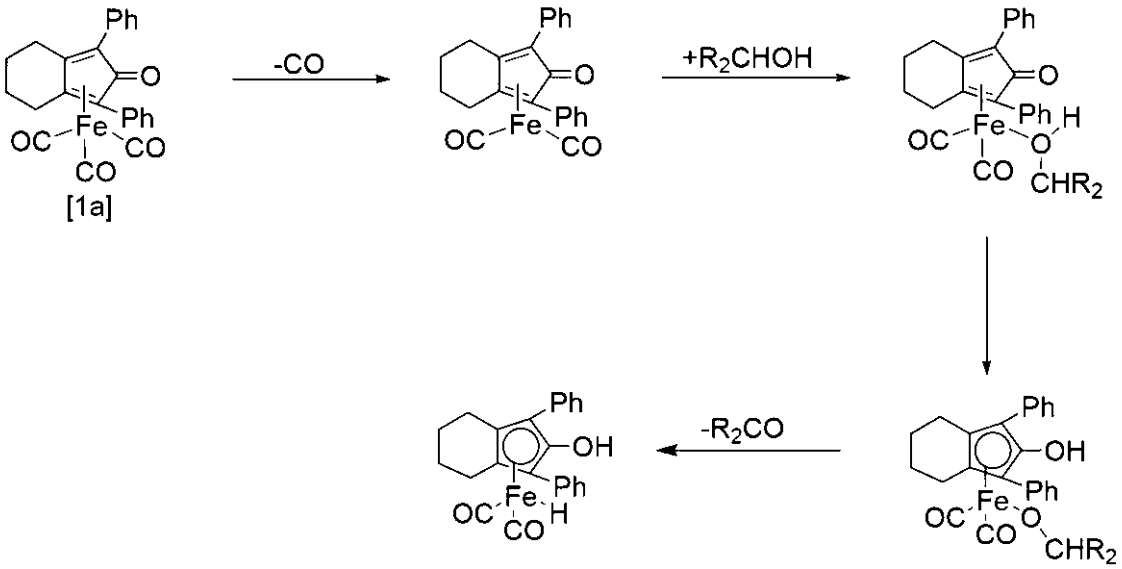

Scheme 36. Proposed mechanism for transfer dehydrogenation.

Time-resolved spectroscopy therefore provides a key method to explore these processes – in this pump-probe methods, the UV pump light would trigger the dissociation of the CO ligand (similar to that observed on longer timescales by Knölker) and then the fate of the activated iron complex would be observed by an IR probe pulse in the mid-IR. The vibrational mode of the remaining CO-ligands and the carbonyl group of the organic ligand would report on the nature of the resulting photoproducts.

These experiments use the time-resolved multiple-probe (TR^{M}PS) spectroscopic method. Which allows for the observation of events occurring over 9 orders of magnitude (1 ps – 1 ms) in time. This spectroscopic method is located at the Central Laser Facility (CLF) at Didcot UK and was used to produce the data shown in this thesis.

The main aim of this research project is to investigate the mechanistic pathways that occur over 9 orders of magnitude; by identifying these pathways rational decisions can be made to improve these reactions. In this project the behaviour of [1a] and [3a] were studied in 7 solvent systems (acetone, acetonitrile, cyclopentyl methyl ether, heptane, isopropyl alcohol, tetrahydrofuran and toluene). These solvents were chosen as they have been used in studies involving TRIR and they are readily available.

Results & Discussion

2 Time-Resolved Infrared Spectroscopy

The aim of this project is to gain a better understanding of the mechanistic pathways that iron carbonyl complexes undergo. However, these pathways are extremely difficult to observe because they happen at rapid timescales often (ps to μs). Time-Resolved Infrared (TRIR) spectroscopy is a pump-probe method that permits the observation of these timescales as it measures from 1 ps to 988.5 μs. Another reason is that this technique has been used in the past to investigate manganese carbonyl complexes and has achieved good results making it an appropriate technique to investigate these iron complexes.

2.1 Background

The majority of modern Fourier Transform IR (FTIR) instruments have a spectral resolution of approximately 0.5 cm^{-1}, which is suitable for the majority of purposes for 'static' or slowly changing systems, however a variety of methods are necessary for systems in which intermediate species have a lifetime of < 0.1 s. In order to observe rapid photochemical changes, Time-Resolved Infrared Spectroscopy (TRIR) is needed.

Time-resolved infrared spectroscopy is a prominent analytical method that permits the observation of biological, chemical and physical processes that take place a timescale as low as a sub-picosecond.[29] Infrared spectroscopy is ideal for ultra-fast measurements because of its high temporal resolution (femtosecond to minutes depending on the technique used), which is far greater than a technique like NMR spectroscopy (milliseconds to seconds). Metal carbonyls are extremely useful at acquiring data from because of their high intensity and discrete vibrational transitions observed often within the region of 2100-1850 cm^{-1}.

There are some major challenges when using ultra-fast time-resolved infrared spectroscopy, one notable issue is the accuracy in determining time and the starting of the process to be observed. This technique uses a pump pulse that produces a photochemical reaction, and a second laser pulse is used to spectrally probe the progress of the reaction after a known controllable time delay (< 200 fs).[30] Irradiation generates a variety of processes because of the reactivity of the generated excited state (i.e. ligand dissociation or non-dissociative fluorescence and phosphoresce to allow additional reactivity). The pump pulse (typically UV/Vis) is used to either activate or excite the sample to be analysed and the pulse observes the changes within the Infrared spectrum. By differing the delay between the two beams, observation of the changes of the sample over various timescales is permitted.

The quantity of pump-probe delays that can be observed in an experiment is another challenge within TRIR.Time-delays that are above nanoseconds are attained using electronic delays,[30] shorter time need high-precision optical delay lines.[31] There are a variety of examples of instrumental setups that can attain both of these types of delays within a single experiment,[32-35] the most relevant example presented in this thesis is known as Time-Resolved Multiple Probe Spectroscopy ($TR^{M}PS$).[36,37] The procedure of $TR^{M}PS$ acts through a "pump-probe-probe-probe" arrangement, where the first pump beam is followed by several probe beams (with defined time-delays

between them) before the next pump beam takes place. This means that an optical delay can adapt and makes it possible to attain data from short timescales, whilst obtaining the data from longer timescales using electronic delay.

Time-resolved multiple probe spectroscopy is versatile as it enables events occurring over nine orders of magnitude in time to be observed, greater than any other time-resolved infrared spectroscopy techniques.[36]

2.2 Instrumentation

Time-Resolved Infrared Spectroscopy (TRIR) can be used in various experimental setups. In this project, Time-Resolved Multiple Probe Spectroscopy ($TR^{M}PS$) is used on the LIFEtime spectrometer at the ULTRA facility (Rutherford Appleton Laboratory) to achieve pump-probe delays between picoseconds and a millisecond. For this project a pump wavelength of 330 nm was chosen (a UV-vis spectrum of [1a] in heptane was carried out and exhibited a broad absorption band at 330 nm). The tuning of the laser pulse is carried out by using an optical parametric amplifier (OPA). Within the probe beam infrared light is used,- to,- produce *in situ* IR spectra of the solution containing the metal carbonyl compound at desired delays. The infrared beam gets split into two, one beam is the reference beam that permits correction for any variations in the laser pulse intensity between different datapoints. (**Figure 6).**

To ensure photolysis of photoproducts does not occur, the concentration of the iron complexes must be low, while still being concentrated enough to produce an intense spectrum with a good signal-to-noise ratio. Because of this, the reaction mixture was flowed through the IR cell, that is constantly rastered. The flow is produced by a peristaltic pump, and the solution is reused from the solution reservoir to the Harrick cell and back. Every reaction is carried out under an inert atmosphere (in the case of this study argon was chosen).

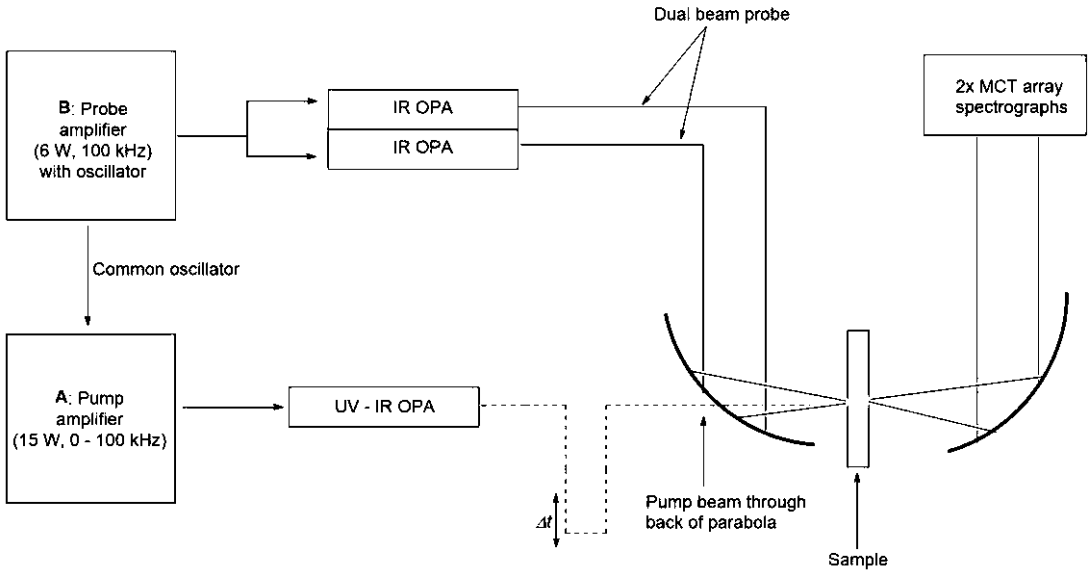

Figure 6. Schematic of the dual-amplifier laser system, with OPA and experimental layout.

The timing of the pump and probe beams are controlled by electronic and optical delays, where the optical delays are responsible for the sub-nanosecond timescales and the electronic delays accomplish the microsecond timescales. Both the electronic and optical delays are used to obtain the nanosecond timescales.

In the setup of the LIFEtime instrument, the repetition rate is 100 kHz, this causes repeated probe delays every 10 microseconds. This repetition creates clusters of datapoints that are observed within kinetic traces at longer durations. An artifact is frequently observed within the clustered points, that is caused by a timing issue with the optical delay line between each probe beam ("pump-probe-probe-probe"). The artifact is greater relative to the signal when analysing weak IR bands because those bonds create a smaller direct transient IR signal. If the sample's vibrational signal is weak, the broad thermal artifact dominates the resulting spectrum.[38] The artifact is a constant size so it appears larger when the peaks are weak. The reported infrared spectrum are difference spectra that are acquired by subtracting the recorded background spectrum from the transient signal, this leads to lost species exhibiting negative peaks and any newly formed species being positive.

2.2.1 Ground state IR spectrum of [1a]

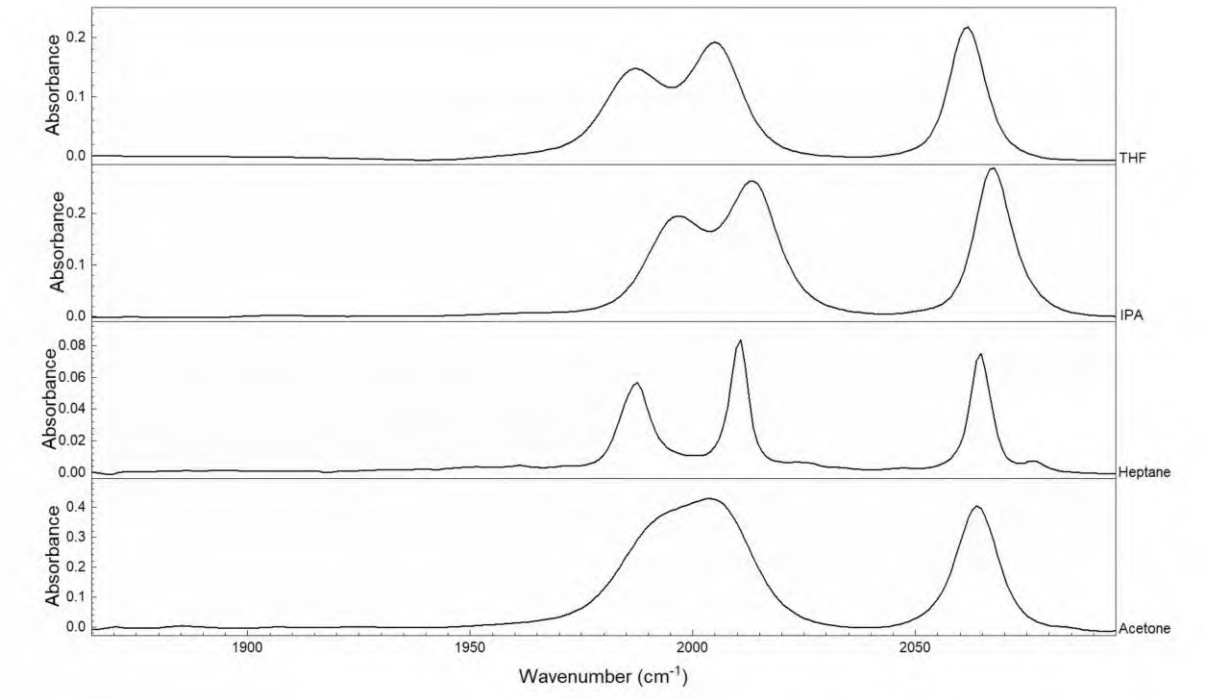

Figure 7. Stacked FTIR spectrum of [1a] in four different solvent systems, resolution of 1 cm^{-1}.

Solvent	Wavenumber (cm^{-1})
Acetone	2004 and 2064
Heptane	1987, 2010 and 2064
IPA	1997, 2013 and 2067
THF	1987, 2004 and 2061

Table 2. List of four solvents of the stacked spectrum and the wavenumbers of the observable peaks.

The ground state IR spectrum of [1a] was recorded in a variety of solvents. The carbonyl stretches (2095-1865 cm^{-1}) exhibited distinct shifts based on solvent polarity and coordinating ability. As shown in table 2, the three peaks are assigned to the symmetric stretch and two asymmetric stretches that are associated with the three metal-coordinated carbonyl ligands. Both [1a] and [3a] are members of the C_s group. The C_s group has two irreducible representations: *A*' and *A*", both are IR active (*A*' in both the x and y planes, *A*" in the z plane). When reduced, the stretching vibrations of metal-coordinated carbonyl ligands reduce to *A*' and 2*A*". These three IR active modes give rise to three observed bands. When comparing the IR spectra what is observed is that heptane, IPA and THF have three identifiable peaks that is because acetone is a polar solvent that has a carbonyl group (C=O). The carbon of the acetone interacts with the carbonyl oxygen atoms. Changing the π-backbonding from the iron to the carbonyl ligand, thus broadens the peaks. Heptane is a non-polar and non-coordinating, meaning sharp and resolved peaks. While IPA is a polar solvent, acetone has the potential to produce stronger dipolar interactions. THF is coordinating however doesn't exhibit the same intense broadening effect in the iron carbonyl complex as acetone does because of the different strength interactions.[39,40,41]

2.2.2 UV-Vis Spectrum

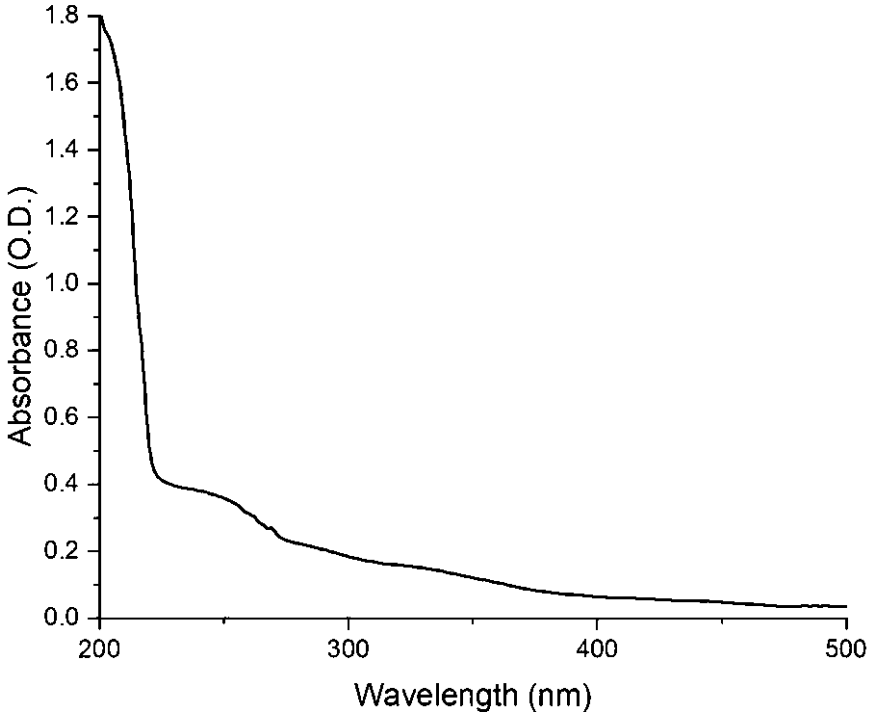

Figure 8 UV-Vis absorption spectrum of [1a] in heptane.

A UV-Vis analysis was carried out to determine the appropriate wavelength for the TRIR experiments. A pump wavelength of 330 nm was chosen as there is an observed band.

2.3 Time-resolved Infra-Red Spectra for [1] from 2 ps to 200 ps.

2.3.1 Acetone

Acetone was chosen as a solvent system as it is readily available in most laboratories and is a fairly cheap solvent. Acetone was also the solvent used in the oxidation reactions by Funk *et al*[14] and Wills *et al*[15] (Schemes 10 and 11).

Photolysis of a solution of the metal carbonyl region of [1a] at 330 nm in the polar coordinating solvent acetone was examined using (TR^{M}PS). The resulting difference spectra are shown in Figure 9 with the ground state spectrum of [1a] as a reference.

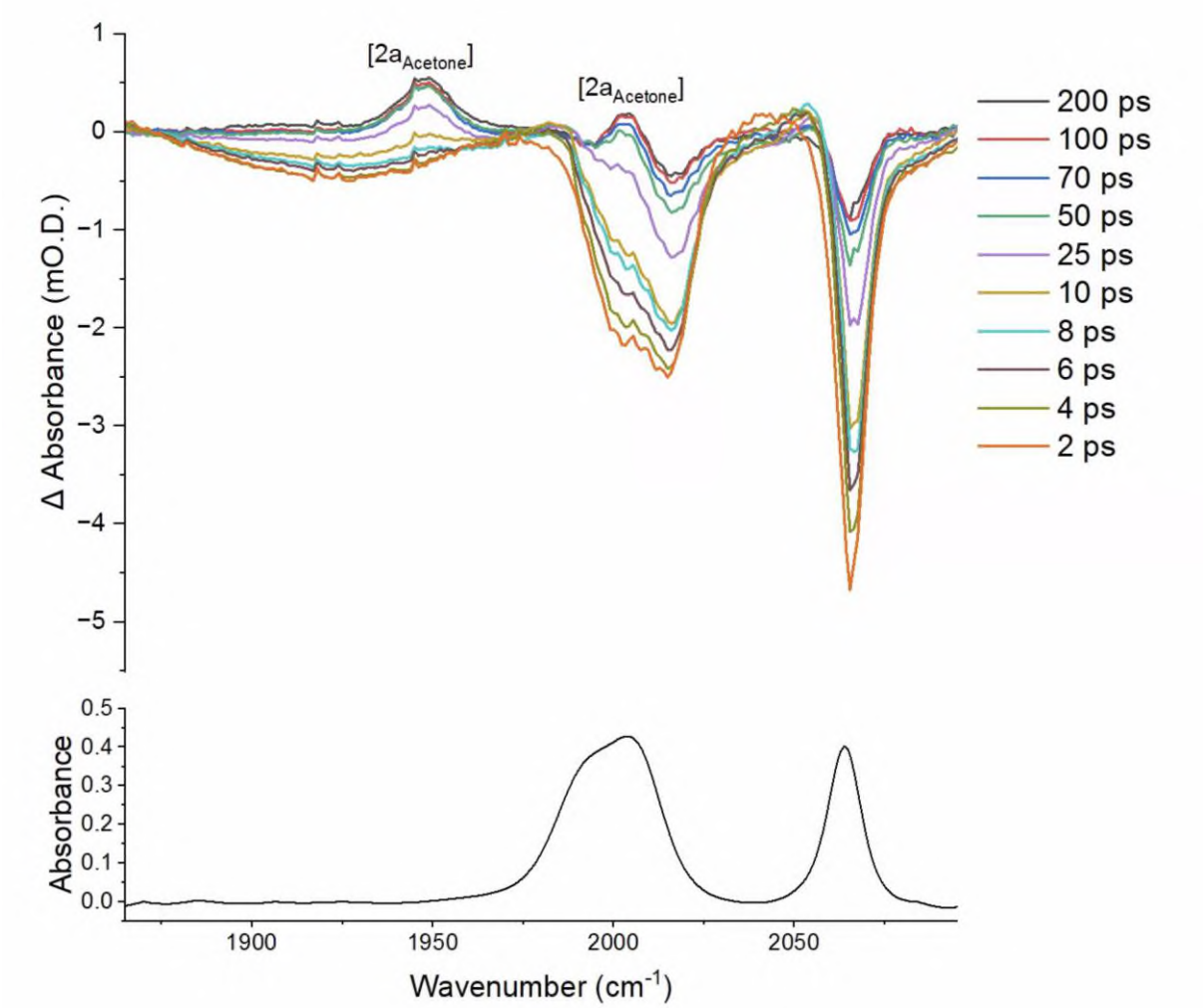

Figure 9. (Top) TRIR spectra of the 330 nm photolysis of the metal carbonyl region of [1a] at selected early pump-probe delays in acetone. The positive bands of [2a$_{acetone}$] represents the solvent coordinated complex. (Bottom) Ground state IR spectrum of [1a] in acetone.

The difference spectra show a variety of negative bands that closely resemble the position profile of the ground state spectrum of [1a]. This demonstrates that the ground state of [1a] is used up during the experiment.

Within a couple of ps two positive bands were observed at 1970 cm^{-1} and a band located at 2043 cm^{-1}. Within 6 ps these bands shift to just above 1980 cm^{-1} and just above 2050 cm^{-1}. From 25 ps bands observed at 1945 cm^{-1} and the other band located just above 2000 cm^{-1} start to grow in intensity and at 100 ps become the dominate observed positive bands. These bands had the largest growth in intensity and were therefore assigned to the solvent coordinated complex [$2a_{acetone}$]. The justification for this assignment was that there are two observed bands that have an equal intensity indicating a CO ligand is lost. Therefore a 16 electron complex, a strong Lewis acid which the solvent coordinates.[42,43] There is an observable broad decrease in the spectrum, this is suspected to be caused by a baseline correction issue.

Over the course of the first 200 picoseconds of the experiment, the three negative bleach bands for (2002, 2014 and 2065 cm^{-1}) decrease in intensity. This is consistent with the ground state being regenerated on this timescale. As shown in Figure 10, the kinetics of this ground state bleach recovery were modelled using the negative bleach peak at 2065 cm^{-1}. This was effectively fitted to a bi-exponential model with time constants of (8.1 $\pm$ 1.1) ps and (37.3 $\pm$ 8.6) ps (the errors reported are at 95% confidence intervals). The bands also recovers to 19.0% of its original height. This demonstrates that on these time scales the primary fate of the light-activated complex is regeneration of the ground state. The organic carbonyl region has a bleach peak at approximately 1645 cm^{-1}, meaning an accurate spectrum couldn't be obtained as the bleach peak interfered with the spectrum.

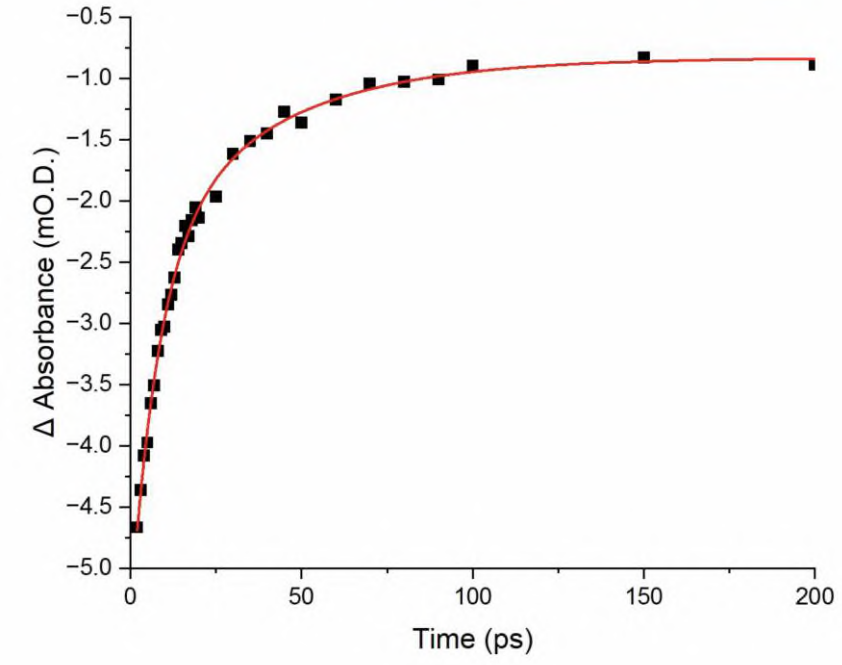

Figure 10. The change in absorbance of the bleach recovery at 2065 cm^{-1} from 2 to 200 ps. The solid red line represents a bi-exponential fit with lifetimes of 8.1 $\pm$ 1.1 ps and 37.3 $\pm$ 8.6 ps.

2.3.2 IR_{PUMP}-IR_{PROBE} spectroscopic analysis of the metal carbonyl region of [1a] in acetone.

The UV_{PUMP}-IR_{PROBE} data demonstrated that over 75% of the initially formed photoproducts regenerate ground state of the complex over the course of 200 ps.

One possible reason for this is known as geminate recombination, following CO-loss there are two outcomes that can happen following rapid loss of a CO ligand (1): the solvent binds to the vacant site[25] or (2): the dissociate CO does not escape from the local sphere of the complex and then rebinds to the iron. As the energy of the photon used to excite the complex is greater than the Fe-CO bond dissociation energy, the recombination of the CO results in a complex in an excited vibrational state (e.g. v_1). The energy of the $v_0 \rightarrow v_1$ transitions are at higher wavenumber than the corresponding $v_1 \rightarrow v_2$ that would be observed if the vibrationally exited states are present.[44]

To determine the position of these "hot bands" and IR_{PUMP}-IR_{PROBE} experiment was performed. Here a fs pulse is used to populate vibrational excited states of the sample, the nature of which are then interrogated with a second IR pulse these excited vibrational modes can be observed and their subsequent dynamics gives insight to intramolecular vibrational redistribution (IVR) and relaxation to the ground vibrational state (T_1).[45] These experiments were carried out using (acetone, heptane and THF). The anharmonic constant from 2004 cm^{-1} to 1971 cm^{-1} is 33 cm^{-1} and from 2064 cm^{-1} to 2047 cm^{-1} is 17 cm^{-1}.

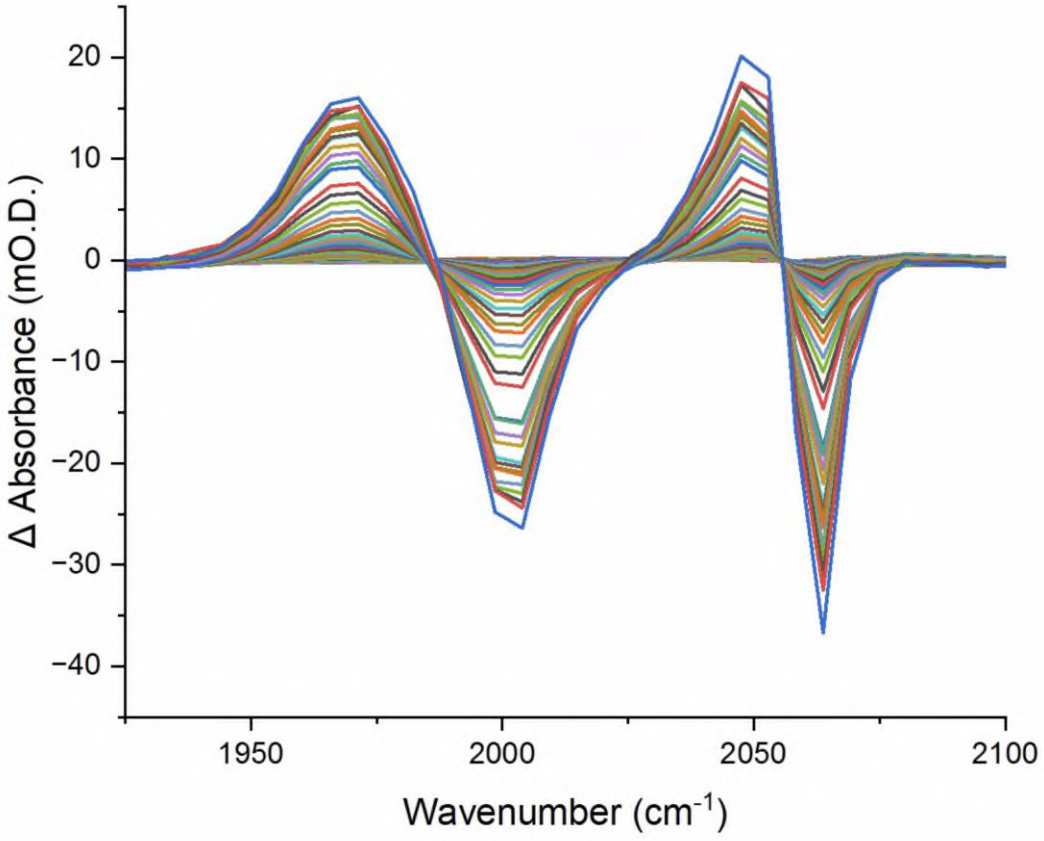

Figure 11. The IR_{PUMP}-IR_{PROBE} spectrum of [1a] in acetone.

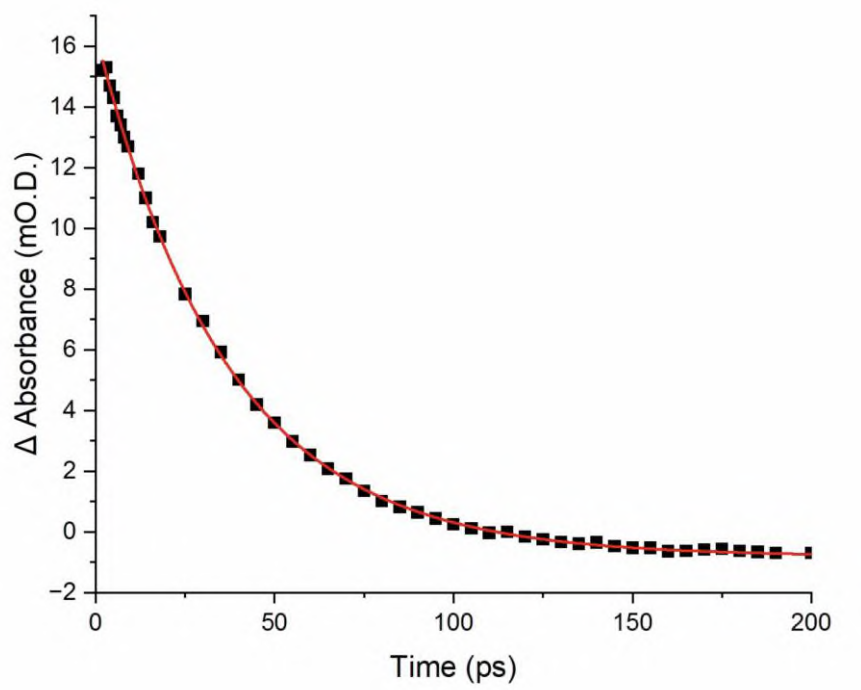

Figure 12. Change in absorbance of the vibrationally excited state at 1966 cm^{-1} from 2 to 200 ps. The solid red line represents a single exponential fit with a lifetime of 36.6 ± 0.3 ps.

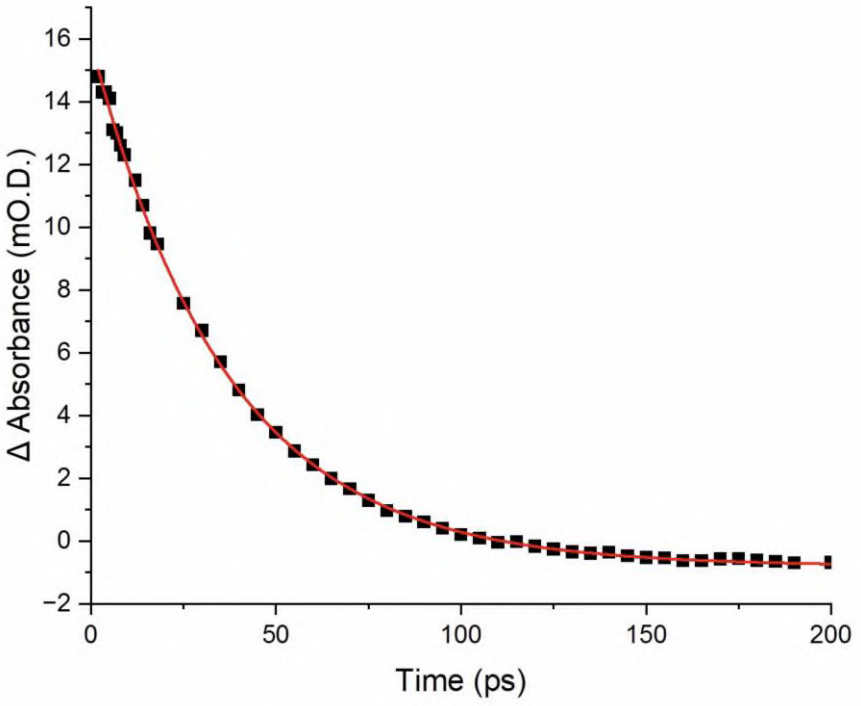

Figure 13. Change in absorbance of the vibrationally excited state at 1971 cm^{-1} from 2 to 200 ps. The solid red line represents a single exponential fit with a lifetime of 36.5 ± 0.3 ps.

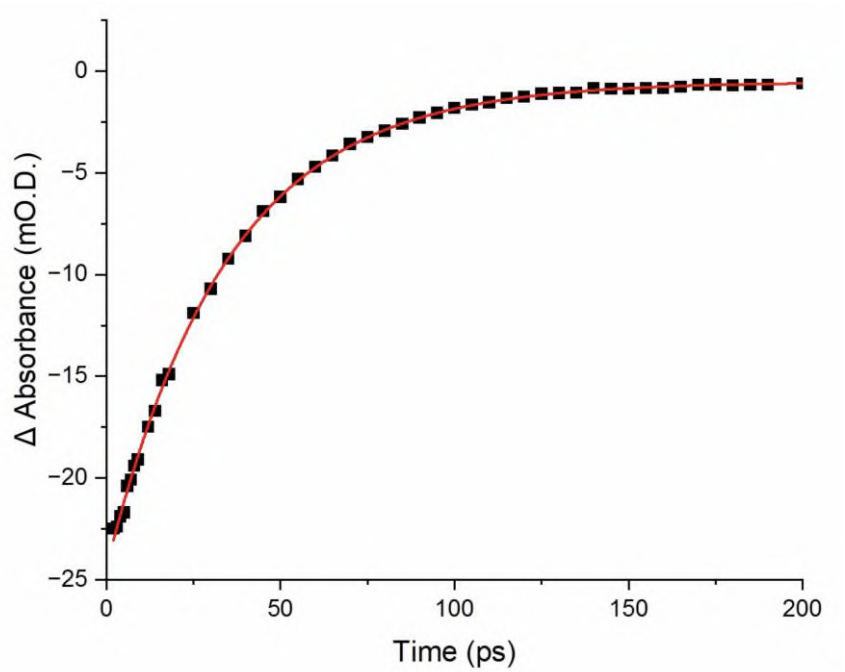

Figure 14. The change in absorbance of the bleach recovery at 1999 cm^{-1} from 2 to 200 ps. The solid red line represents a single exponential fit with a lifetime of 34.6 ± 0.3 ps.

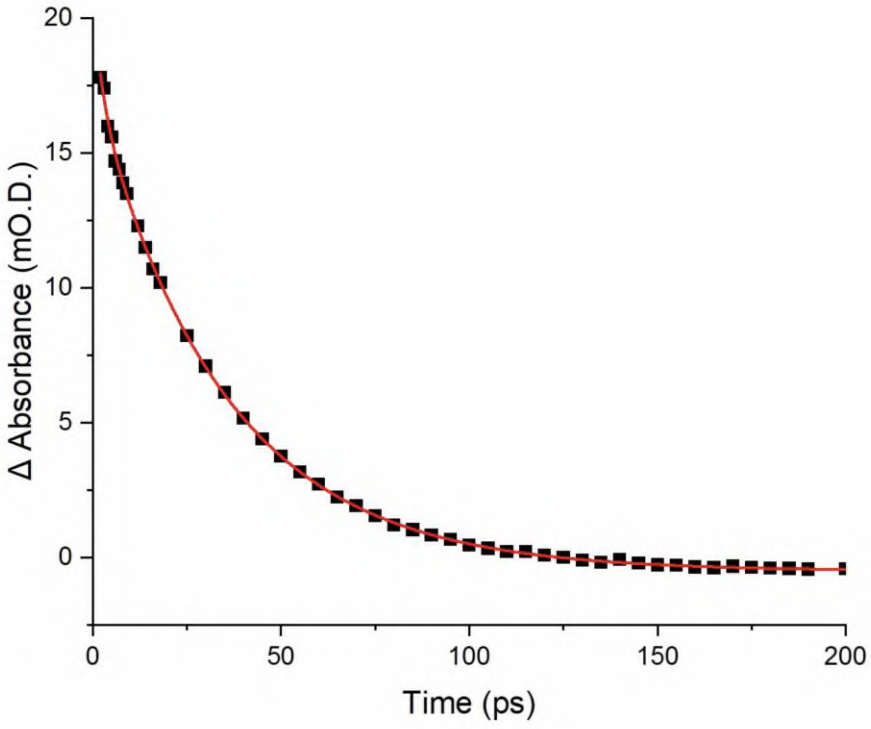

Figure 15. Change in absorbance at the vibrationally excited state at 2047 cm^{-1} from 2 to 200 ps. The solid red line represents a bi-exponential fit with lifetimes of 2.7 ± 0.4 ps and 34.8 ± 0.3 ps.

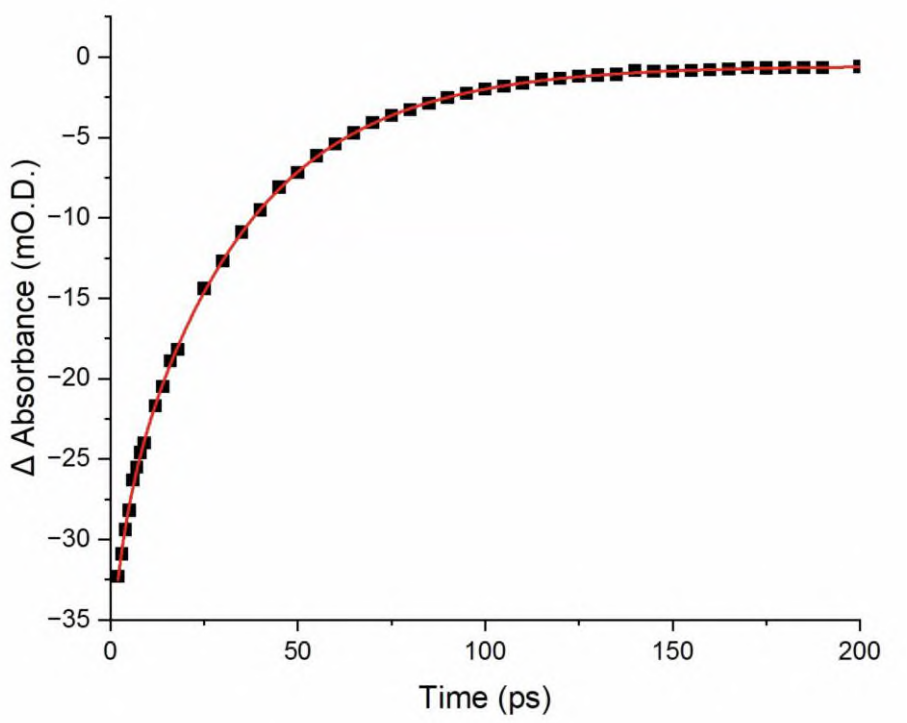

Figure 16. The change in absorbance of the bleach recovery at 2064 cm^{-1} from 2 to 200 ps. The solid red line represents a bi-exponential fit with lifetimes of 3.5 ± 0.4 ps and 33.0 ± 0.3 ps.

	Vibrational lifetime (T_1) (ps)					IVR	
Solvent	1966 cm^{-1}	1971 cm^{-1}	1999 cm^{-1}	2047 cm^{-1}	2064 cm^{-1}	2047 cm^{-1}	2064 cm^{-1}
Acetone	36.6 ± 0.3	36.5 ± 0.3	34.6 ± 0.3	34.8 ± 0.3	33.0 ± 0.3	2.7 ± 0.4	3.5 ± 0.4

Table 3. Vibrational dynamics of the metal carbonyl region of [1a] in acetone obtained from fitting IR_{PUMP}-IR_{PROBE} data to exponential functions.

At early times (2-20 ps), the TRIR data of [1a] in acetone, there are positive bands positioned between (1970-1980 and 2040-2050 cm^{-1}). For the IR_{PUMP}-IR_{PROBE} there are three positive bands (1966, 1971 and 2047 cm^{-1}). What is observed, is that the positive bands from the TRIR and the positive bands from the IR_{PUMP}-IR_{PROBE} data occur at the same band position. This supports their assignment to the $v_1 \rightarrow v_2$ transition of a vibrationally excited state. As shown in table 3, the T_1 values of the relaxation to the ground state occurs between 33-37 ps and IVR occurs between 2.7-3.5 ps. The formation of this vibrationally excited state in the TRIR data is possibly a consequence of a geminate recombination of a photodissociated CO. This occurs on fs timescale so it's consequences can be observed. The observation of two bands (at different positions to those in the IR_{PUMP}-IR_{PROBE} spectra) is consistent with the formation of a dicarbonyl complex.
The positive peaks exhibit a $v_1 \rightarrow v_2$ transition and the negative bleach peaks exhibit a $v_0 \rightarrow v_1$ transition.

2.3.3 Acetonitrile

Acetonitrile was chosen as a solvent system because it was the solvent system used by Knölker in 1999 for the photoirradiation of the CO ligand[26] and more recently has been used to study the mechanistic pathways that the manganese complex [Mn(ppy)(CO)$_4$] undergoes in a thermal reaction[42], making it an appropriate solvent system for the iron catalyst.

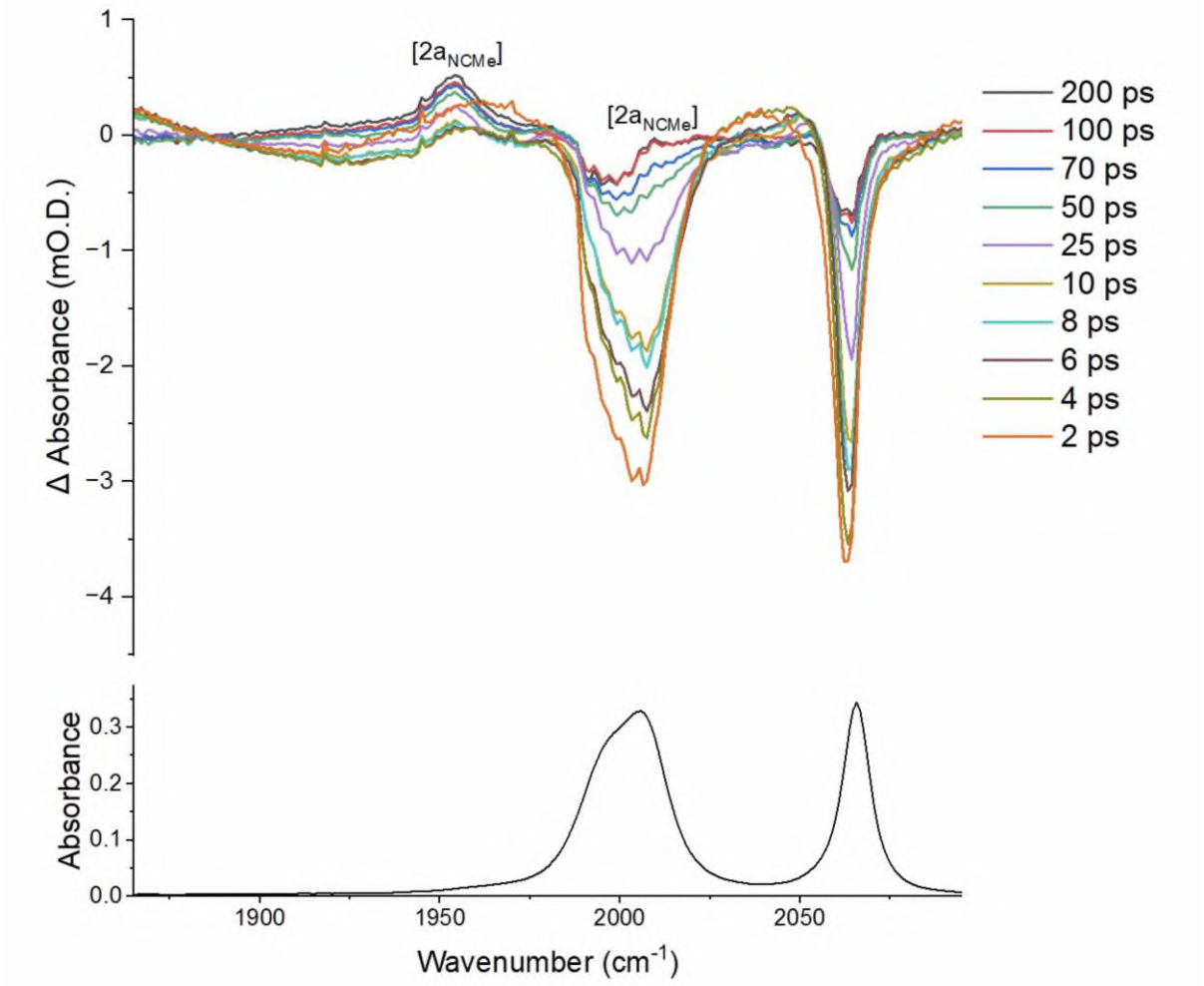

Figure 17. (Top) TRIR spectra of the 330 nm photolysis of the metal carbonyl region of [1a] at selected early pump-probe delays in NCMe. The positive bands of [2a$_{NCMe}$] represents the solvent coordinated complex. (Bottom) Ground state IR spectrum of [1a] in NCMe.

In a couple of ps two positive bands are observed near 1960 cm^{-1} and 2040 cm^{-1}. From 4 to 50 ps these bands shift near to 1955 cm^{-1} and 2050 cm^{-1}. From 70 ps bands observed at 1955 cm^{-1} and 2010 cm^{-1} and continue to grow in positive intensity until 200 ps. Knölker did not analyse the metal carbonyl region of the photoirradiated therefore the TRIR results could not be compared, however the observation of two positive peaks indicated a loss of a CO ligand and therefore assigned to the solvent coordinated complex [2a$_{NCMe}$].

Over the course of the first 200 picoseconds of the experiment, the three negative bleach bands for (2003, 2006 and 2062 cm^{-1}) decrease in intensity. This is

consistent with the ground state being regenerated on this timescale. As shown in Figure 18, the kinetics of this ground state bleach recovery were modelled using the negative bleach peak at 2062 cm^{-1}. This was effectively fitted to a bi-exponential model with time constants of (7.6 ± 1.7) ps and (29.8 ± 6.7) ps (the errors reported are at 95% confidence intervals). The bands also recovers to 17.4% of its original height. This demonstrates that on these time scales the primary fate of the light-activated complex is regeneration of the ground state. The organic carbonyl region was measured however the data had a systematic error.

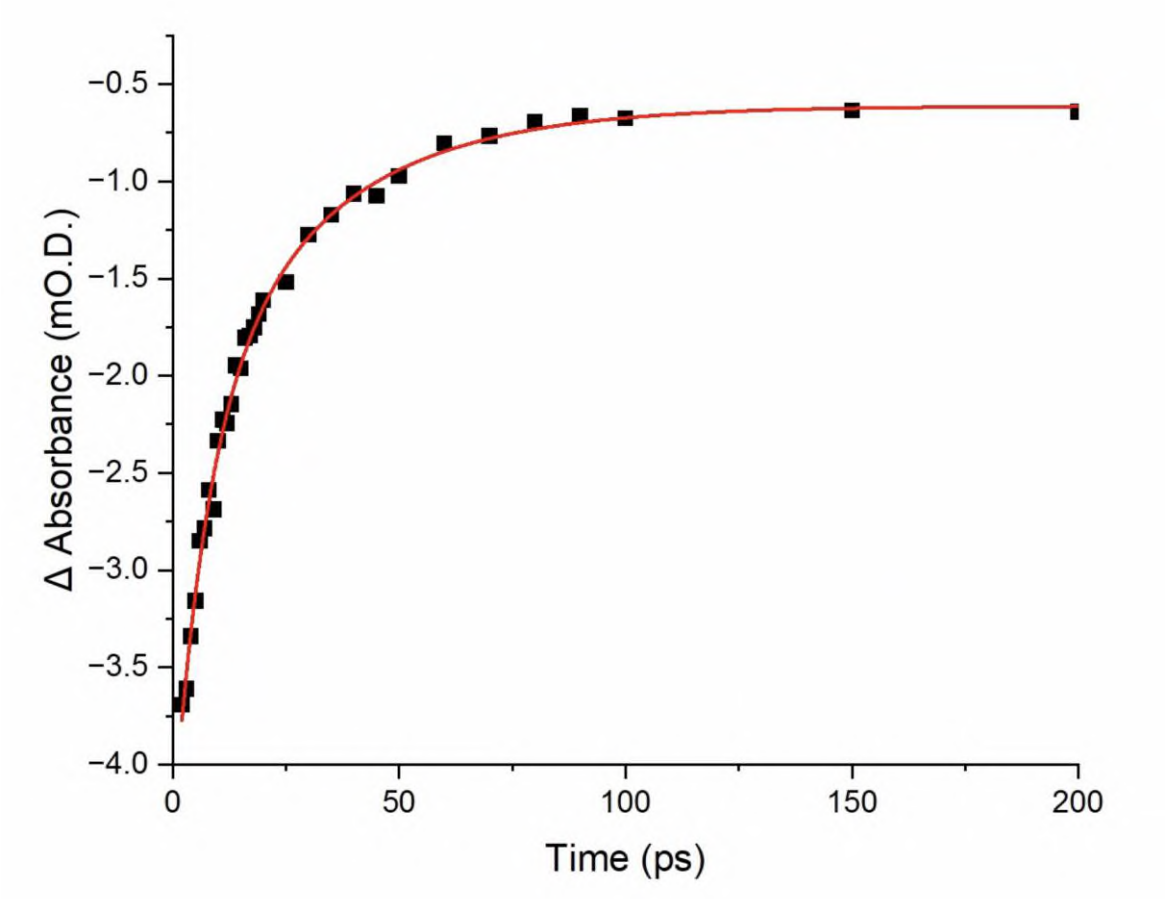

Figure 18. The change in absorbance of the bleach recovery at 2062 cm^{-1} from 2 to 200 ps. The solid red line represents a bi-exponential fit with lifetimes of 7.6 ± 1.7 ps and 29.8 ± 6.7 ps.

2.3.4 Cyclopentyl methyl ether

Cyclopentyl methyl ether was chosen as a solvent system as it has been used in previous research using iron catalysts for HAT, another reason is it is considered a good solvent with a low toxicity and can be derived from sugars. Making it an appropriate solvent system to study the thermal reactions.[46]

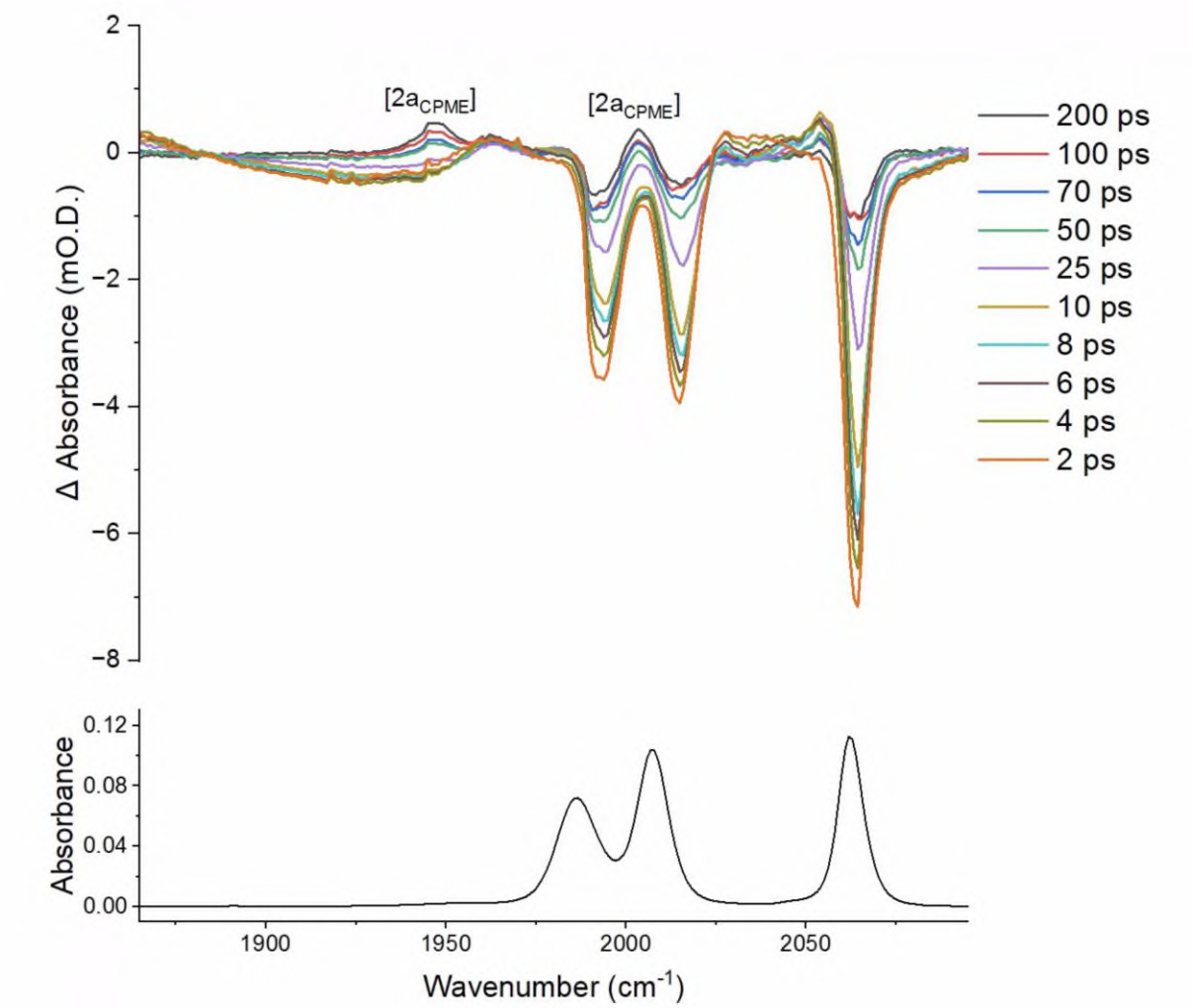

Figure 19. (Top) TRIR spectra of the 330 nm photolysis of the metal carbonyl region of [1a] at selected early pump-probe delays in CPME. The positive bands of [2a$_{CPME}$] represents the solvent coordinated complex. (Bottom) Ground state IR spectrum of [1a] in CPME.

Within a couple of ps, positive bands are observed at 1970 cm^{-1} and another just below 2030 cm^{-1}. From 4 to 50 ps the observed bands are positioned just above 1960 cm^{-1} and 2053 cm^{-1}. From 70 ps the positive band observed at 1960 cm^{-1} shifts to 1945 cm^{-1} and at 200 ps the positive band observed at 2050 cm^{-1} shifts just above 2000 cm^{-1}. The positive bands observed at 1945 cm^{-1} and just above 2000 cm^{-1} are the bands have the largest growth in positive intensity and therefore are assigned as the solvent coordinated complex [2a$_{CPME}$].

Over the course of the first 200 picoseconds of the experiment, the three negative bleach bands for (1993, 2014 and 2064 cm^{-1}) decrease in intensity. This is consistent with the ground state being regenerated on this timescale. As shown in Figure 20, the kinetics of this ground state bleach recovery were modelled using the negative bleach peak at 2064 cm^{-1}. This was effectively fitted to a bi-exponential model with time constants of (11.7 $\pm$ 3.0) ps and (37.5 $\pm$ 11.6) ps (the errors reported are at 95% confidence intervals). The bands also recovers to 14.0% of its original height. This demonstrates that on these time scales the primary fate of the light-activated complex is regeneration of the ground state.

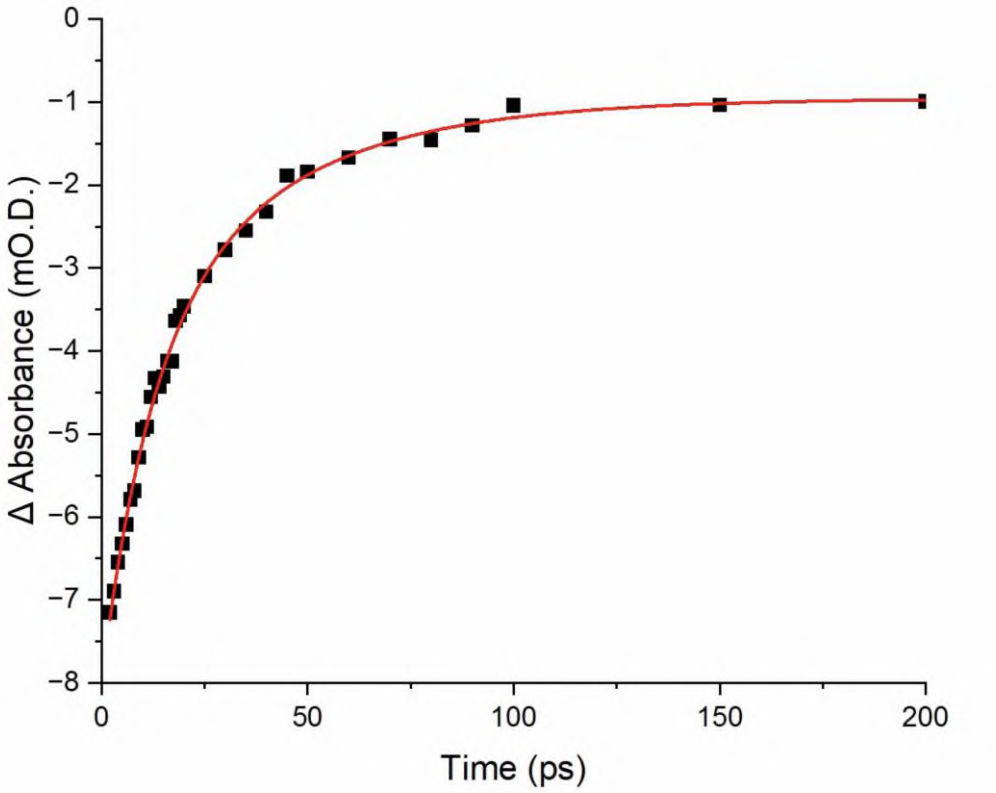

Figure 20. The change in absorbance of the bleach recovery at 2064 cm^{-1} from 2 to 200 ps. The solid red line represents a bi-exponential fit with lifetimes of 11.7 $\pm$ 3.0 ps and 37.5 $\pm$ 11.6 ps.

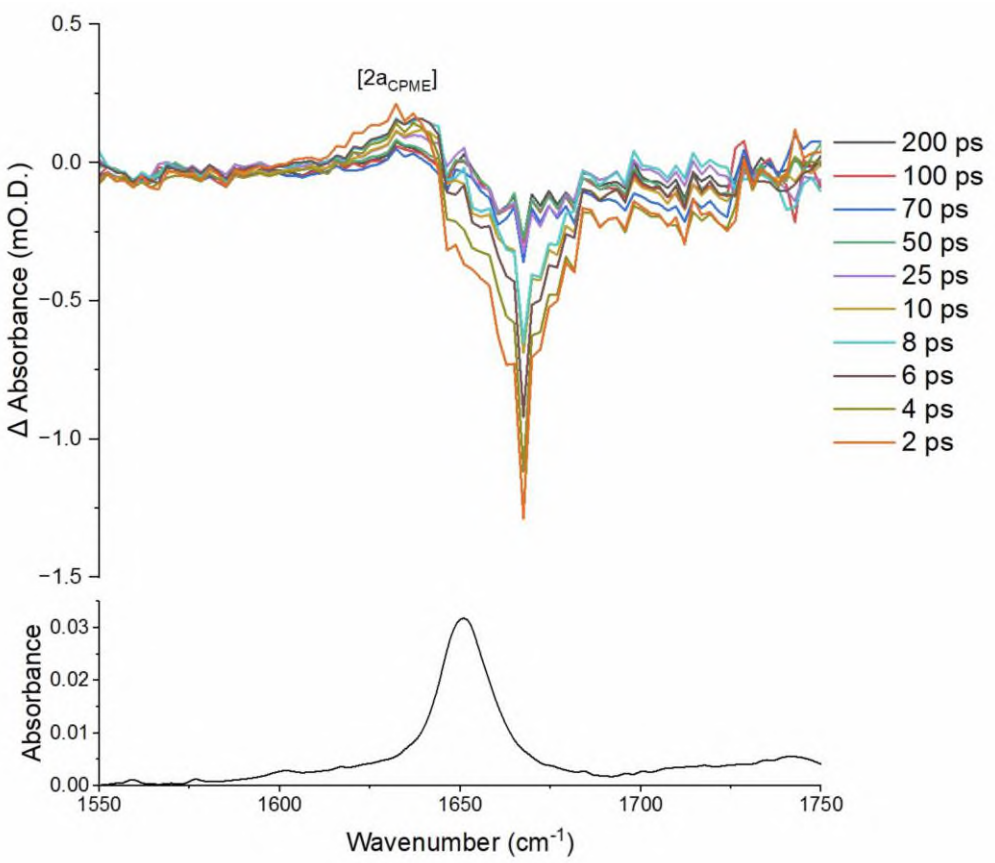

Figure 21. (Top) TRIR spectra of the 330 nm photolysis of the organic carbonyl region of [1a] at selected early pump-probe delays in CPME. The positive band of [2a$_{CPME}$] represents the solvent coordinated complex. (Bottom) Ground state IR spectrum of [1a] in CPME.

Within a couple of ps, a positive band is observed just above 1630 cm^{-1}, over the duration of the early selected pump-probe delays the position of the band shifts only slightly however the intensity decreases at every time interval. This band was assigned to the [2a$_{CPME}$].

2.3.5 Heptane

Heptane was chosen as a solvent system because of its use in the study of $[Mn(ppy)(CO)_4]$ and the interaction of the manganese in heptane, eventually leading to to the aqua complex $[Mn(ppy)(CO)_3(H_2O)]$.[42] In addition, when forming a solvent complex, heptane only shows weak metal-ligand interactions.

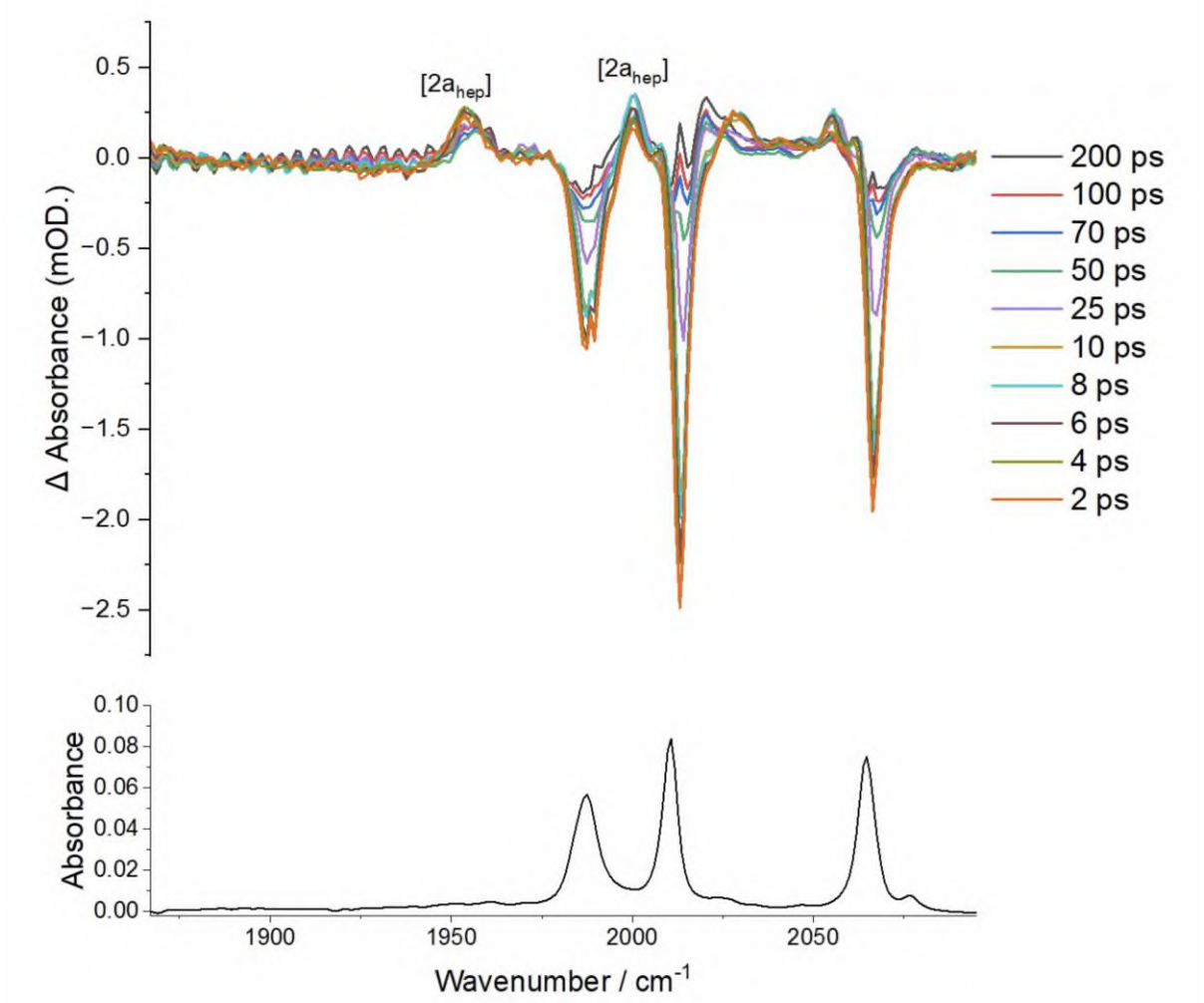

Figure 22. (Top) TRIR spectra of the 330 nm photolysis of metal carbonyl region of [1a] at selected early pump-probe delays in heptane. The positive bands of the [2a$_{hep}$] represents the solvent coordinated complex. (Bottom) Ground state IR spectrum of [1a] in heptane.

In a couple of ps, positive bands are observed at 1955 cm^{-1}, 1978 cm^{-1}, 2000 cm^{-1}, 2028 cm^{-1}, 2041 cm^{-1} and 2053 cm^{-1}. Interestingly these stay within the same position for the rest of the experiment and grow in intensity, the only peak that shifts is the one at 2028 cm^{-1} at 25 ps this peak shifts to 2021 cm^{-1} and stays in the same position until 200 ps this shifts to 2014 cm^{-1} where one of the bleach peaks was originally positioned. Bands at 1955 cm^{-1} and 2000 cm^{-1} are the two bands that maintained a high intensity and these bands were assigned to the solvent coordinated complex [2a$_{hep}$]. One notable feature of this TRIR spectrum is that there are multiple peaks, one possible reason is that there is two ^{3}MLCT states. This has been observed in previous literature using $[Cr(bby)(CO)_4]$ with photolysis using a

wavelength of 400 nm, the recorded ^{3}MLCT bands showed recovery kinetics that are biexponential with lifetimes of (8 ± 3) ps and (76 ± 7) ps.[47]

Over the course of the first 200 picoseconds of the experiment, the three negative bleach bands for (1988, 2014 and 2066 cm^{-1}) decrease in intensity. This is consistent with the ground state being regenerated on this timescale. As shown in Figure 23, the kinetics of this ground state bleach recovery were modelled using the negative bleach peak at 2066 cm^{-1}. This was effectively fitted to a single exponential model with a time constant of (23.3 ± 1.4) ps (the errors reported are at 95% confidence intervals). The bands also recovers to 8.4% of its original height. This demonstrates that on these time scales the primary fate of the light-activated complex is regeneration of the ground state.

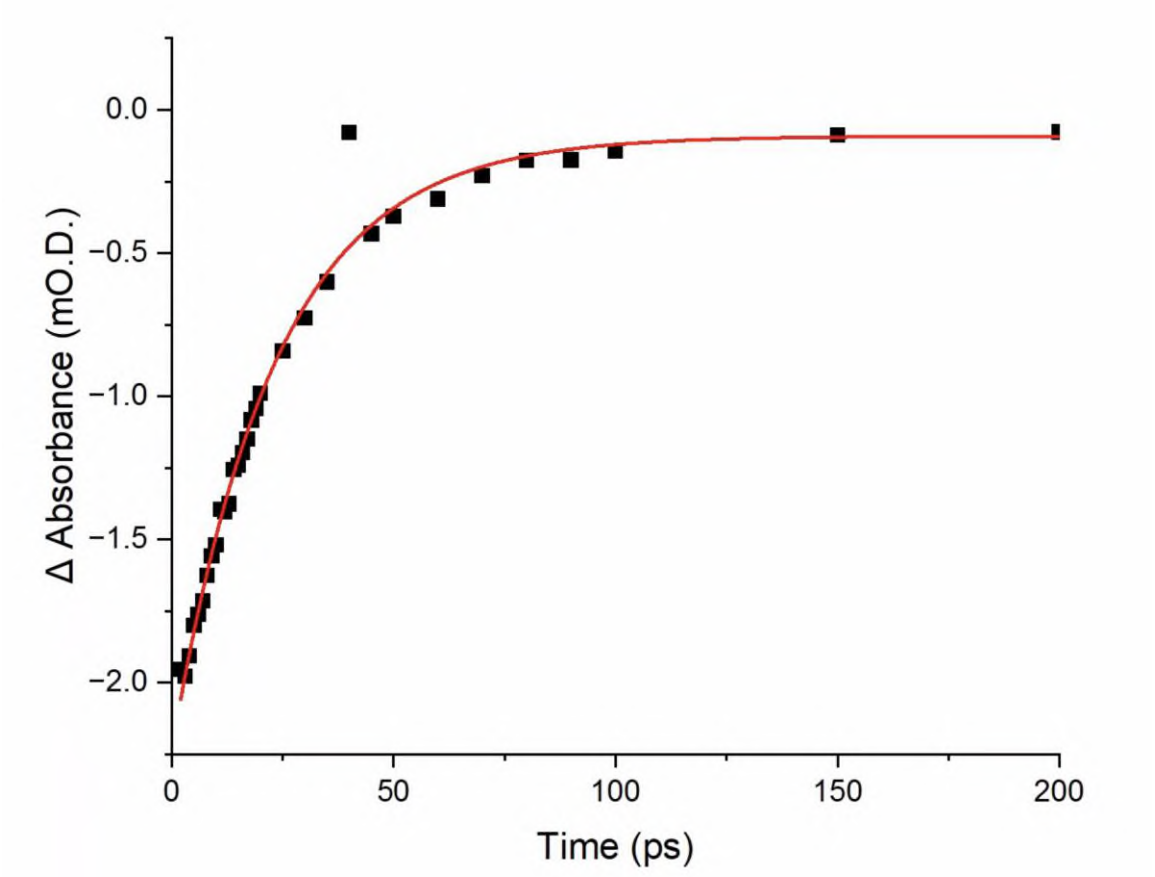

Figure 23. The change in absorbance of the bleach recovery at 2066 cm^{-1} from 2 to 200 ps. The solid red line represents a single exponential fit with a lifetime of 23.3 ± 1.4 ps.

2.3.6 IR$_{PUMP}$-IR$_{PROBE}$ spectroscopic analysis of the metal carbonyl region of [1a] in heptane.

The UV$_{Pump}$-IR$_{Probe}$ data demonstrated that over 75% of the initially formed photoproducts regenerate ground state of the complex over the course of 200 ps.

As mentioned in the case of the IR$_{PUMP}$-IR$_{PROBE}$ analysis [1a] in acetone geminate recombination occurs (section 2.3.2), a similar pattern is observed in THF and in order to observe it geminate recombination does occurs, IR$_{PUMP}$-IR$_{PROBE}$ experiments

were performed using a fs IR pulse to populate vibrational exited states of the sample and the nature is interrogated by a second IR pulse. The vibrational modes can be observed, and their dynamic can give insight into (IVR and T_1) states.

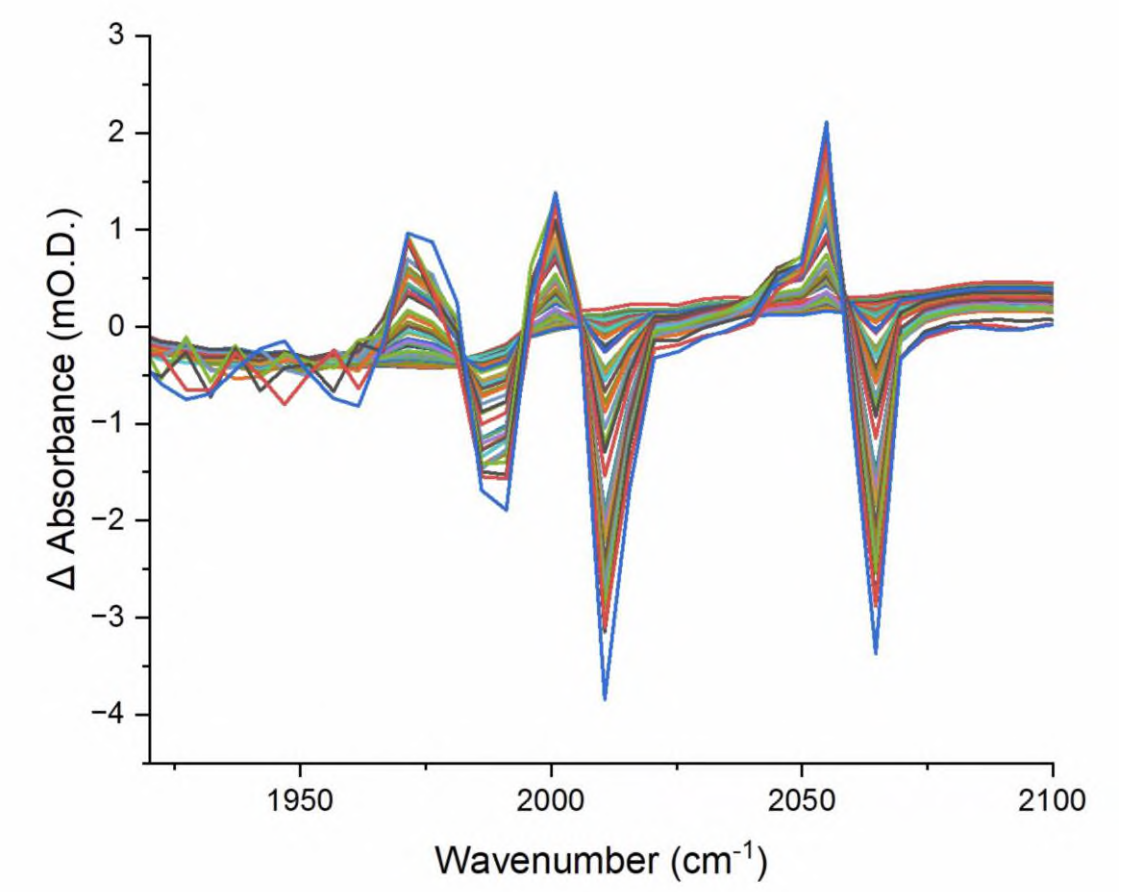

Figure 24. The IR_{PUMP}-IR_{PROBE} spectrum of the metal carbonyl region of [1a] in heptane.

In the IR spectrum three positive bands (1971 cm^{-1}, 2001 cm^{-1} and 2055 cm^{-1}) and four negative bands (1986 cm^{-1}, 1991 cm^{-1}, 2011 cm^{-1} and 2065 cm^{-1}). The experiment was measured using a timescale from 1 to 800 ps. The anharmonicity constants from 1986 cm^{-1} to 1971 cm^{-1} is 15 cm^{-1}, from 2001 $cm^{-1\,t}$ to 1991 cm^{-1} is 10 cm^{-1} and from 2065 cm^{-1} to 2055 cm^{-1} is 10 cm^{-1}.

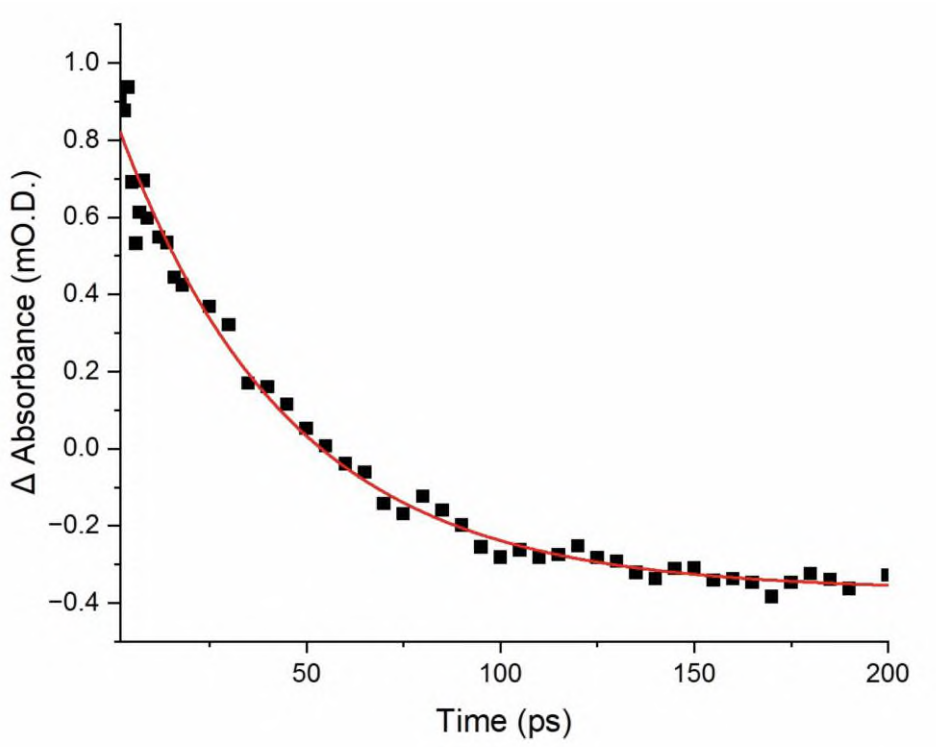

Figure 25. Change in absorbance of the vibrationally excited state at 1971 cm^{-1} from 2 to 200 ps. The solid red line represents a single exponential fit with a lifetime of 44.2 ± 2.5 ps.

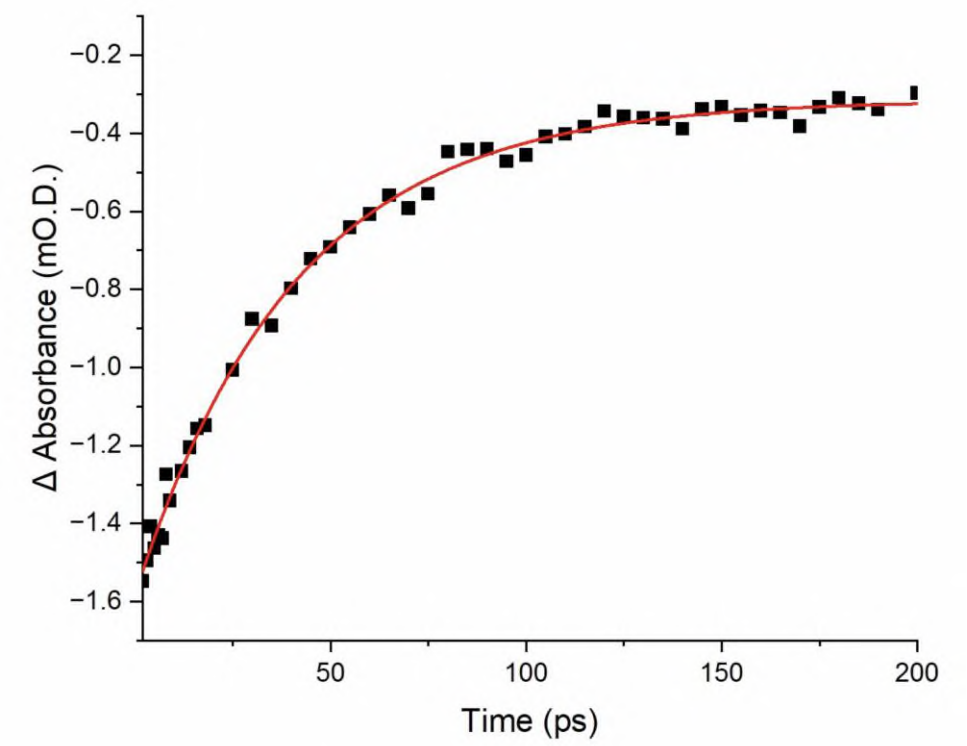

Figure 26. The change in absorbance of the bleach recovery at 1986 cm^{-1} from 2 to 200 ps. The solid red line represents a single exponential fit with a lifetime of 40.9 ± 1.3 ps.

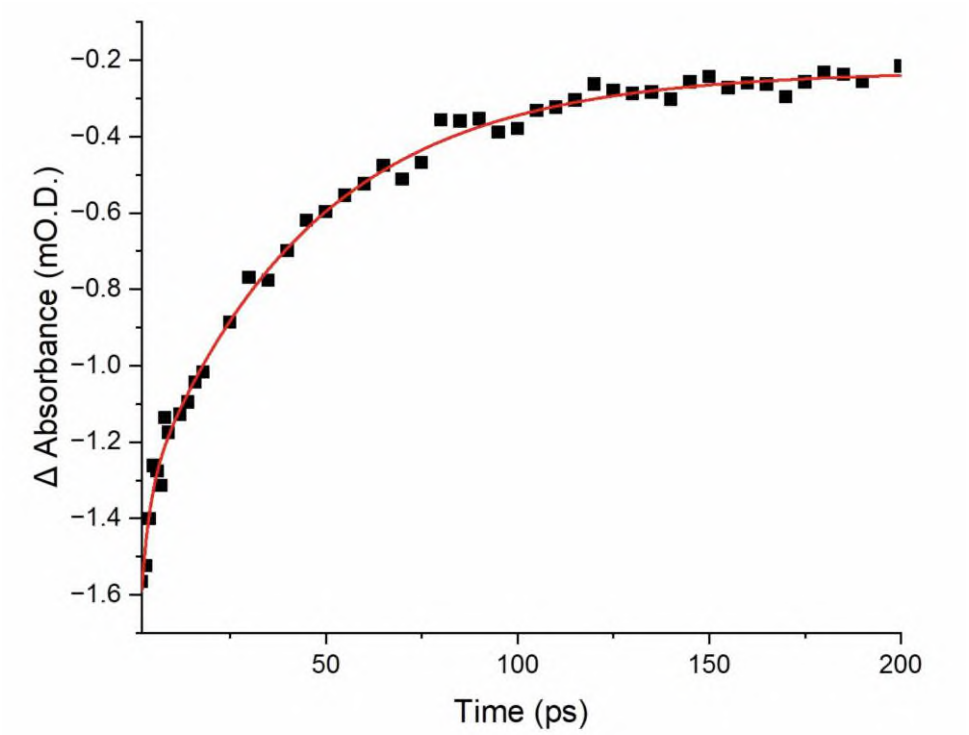

Figure 27. The change in absorbance of the bleach recovery at 1991 cm^{-1} from 2 to 200 ps. The solid red line represents a bi-exponential fit with lifetimes of 2.1 ± 0.7 ps and 43.4 ± 2.1 ps.

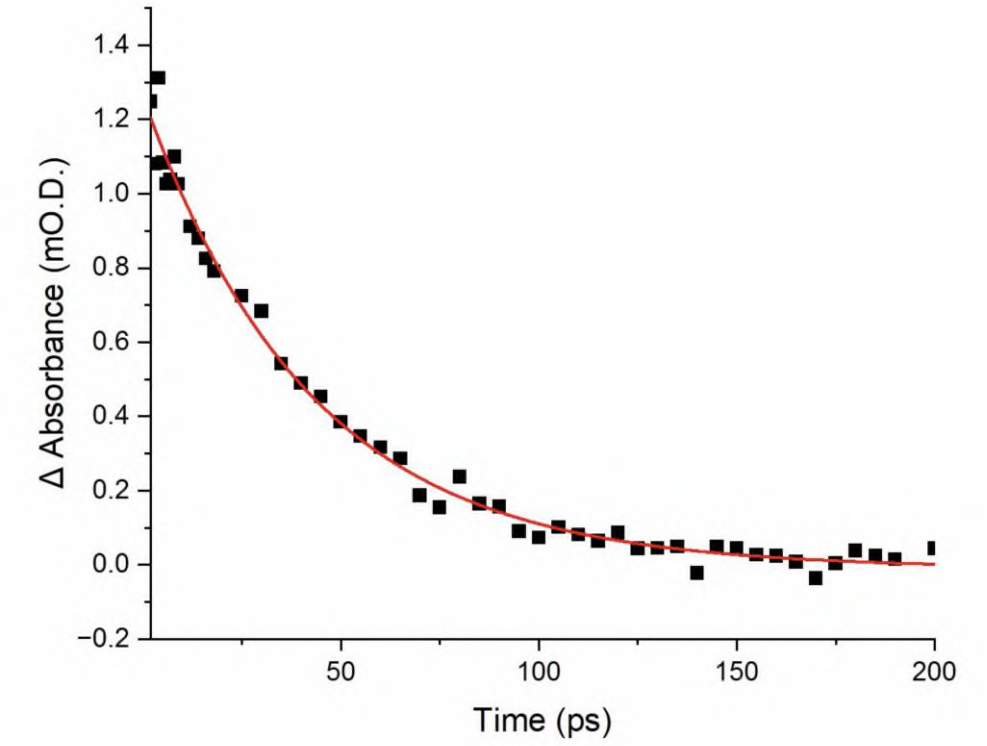

Figure 28. Change in absorbance of the vibrationally excited state at 2001 cm^{-1} from 2 to 200 ps. The solid red line represents a single exponential fit with a lifetime of 42.4 ± 2.0 ps.

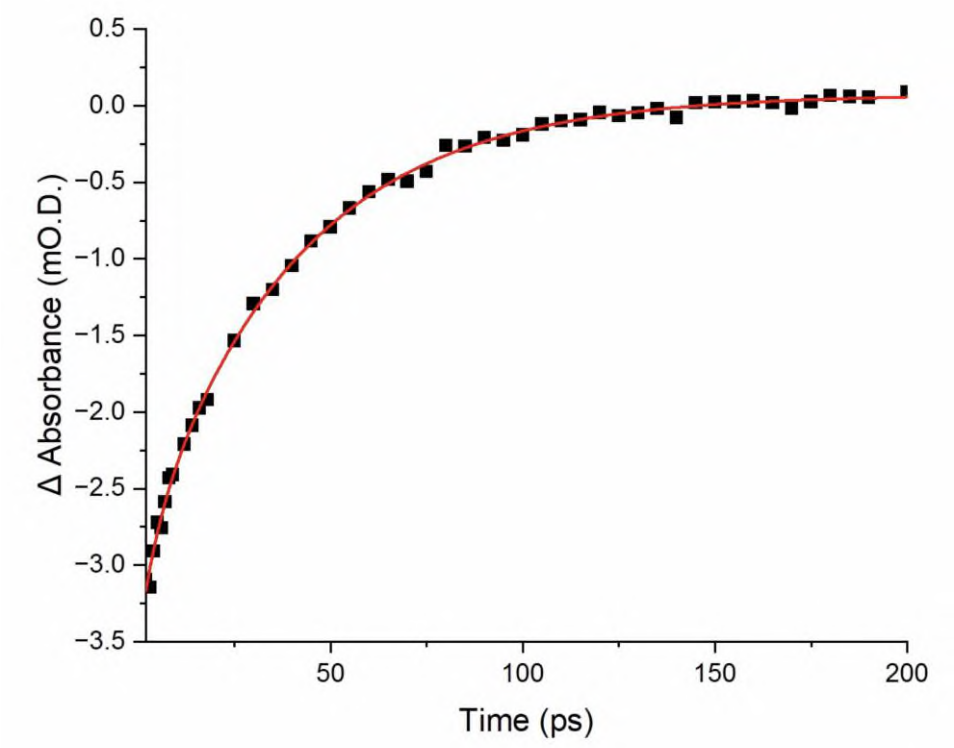

Figure 29. The change in absorbance of the bleach recovery at 2011 cm^{-1} from 2 to 200 ps. The solid red line represents a bi-exponential fit with lifetimes of 4.6 ± 1.6 ps and 39.4 ± 1.3 ps.

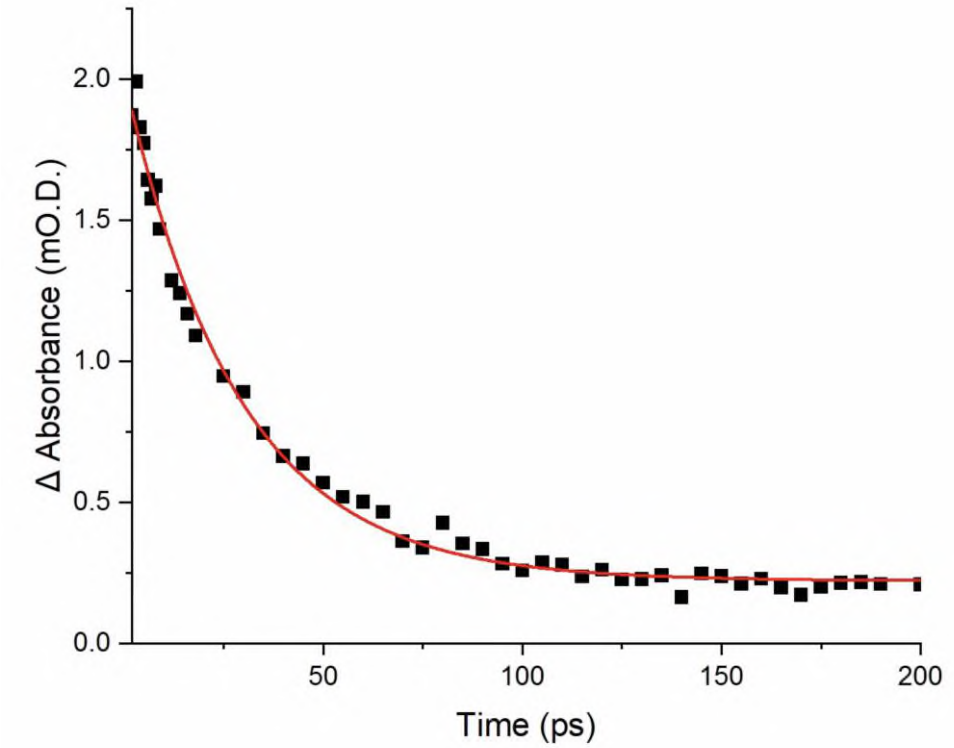

Figure 30. Change in absorbance of the vibrationally excited state at 2055 cm^{-1} from 2 to 200 ps. The solid red line represents a single exponential fit with a lifetime of 28.5 ± 1.1 ps.

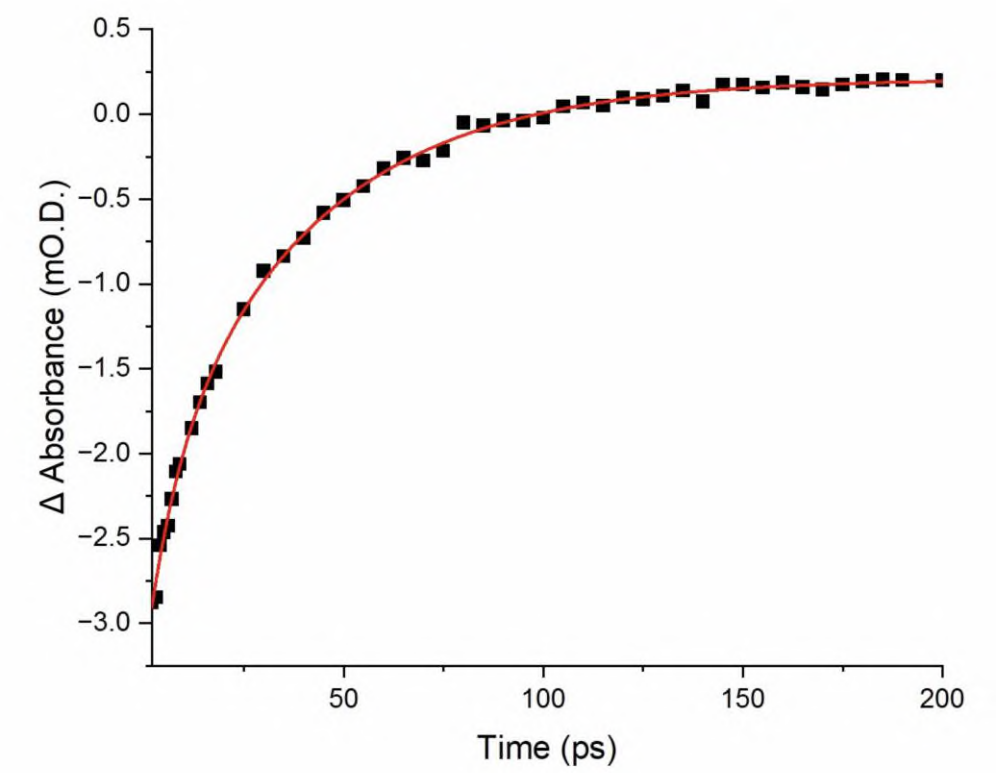

Figure 31. The change in absorbance of the bleach recovery at 2065 cm^{-1} from 2 to 200 ps. The solid red line represents a bi-exponential fit with lifetimes of 7.6 ± 1.4 ps and 39.8 ± 2.1 ps.

At early times (2-20 ps), the TRIR data of [1a] in heptane, there are positive bands positioned between (1950-2055 cm^{-1}). For the IR_{PUMP}-IR_{PROBE} there are three positive bands (1971, 2000 and 2055 cm^{-1}). What is observed, is that the positive bands from the TRIR and the positive bands from the IR_{PUMP}-IR_{PROBE} data occur at the same band position. As previously mentioned in (section 2.3.2) geminate recombination occurs during these reactions, this explains the rapid times.

	Vibrational lifetime (T_1) (ps)							IVR (ps)		
Solvent	1971 cm^{-1}	1986 cm^{-1}	1991 cm^{-1}	2001 cm^{-1}	2011 cm^{-1}	2055 cm^{-1}	2065 cm^{-1}	1991 cm^{-1}	2011 cm^{-1}	2065 cm^{-1}
Heptane	44.2 ± 2.5	40.9 ± 1.3	43.4 ± 2.1	42.4 ± 2.0	39.4 ± 1.3	28.5 ± 1.1	39.8 ± 2.1	2.1 ± 0.7	4.6 ± 1.6	7.6 ± 1.4

Table 4. Vibrational dynamics of the metal carbonyl region of [1a] in heptane obtained from fitting IR_{PUMP}-IR_{PROBE} data to exponential functions.

2.3.7 Isopropyl alcohol

Isopropyl alcohol was chosen as a solvent system because various alcohols have been used within HAT reactions.

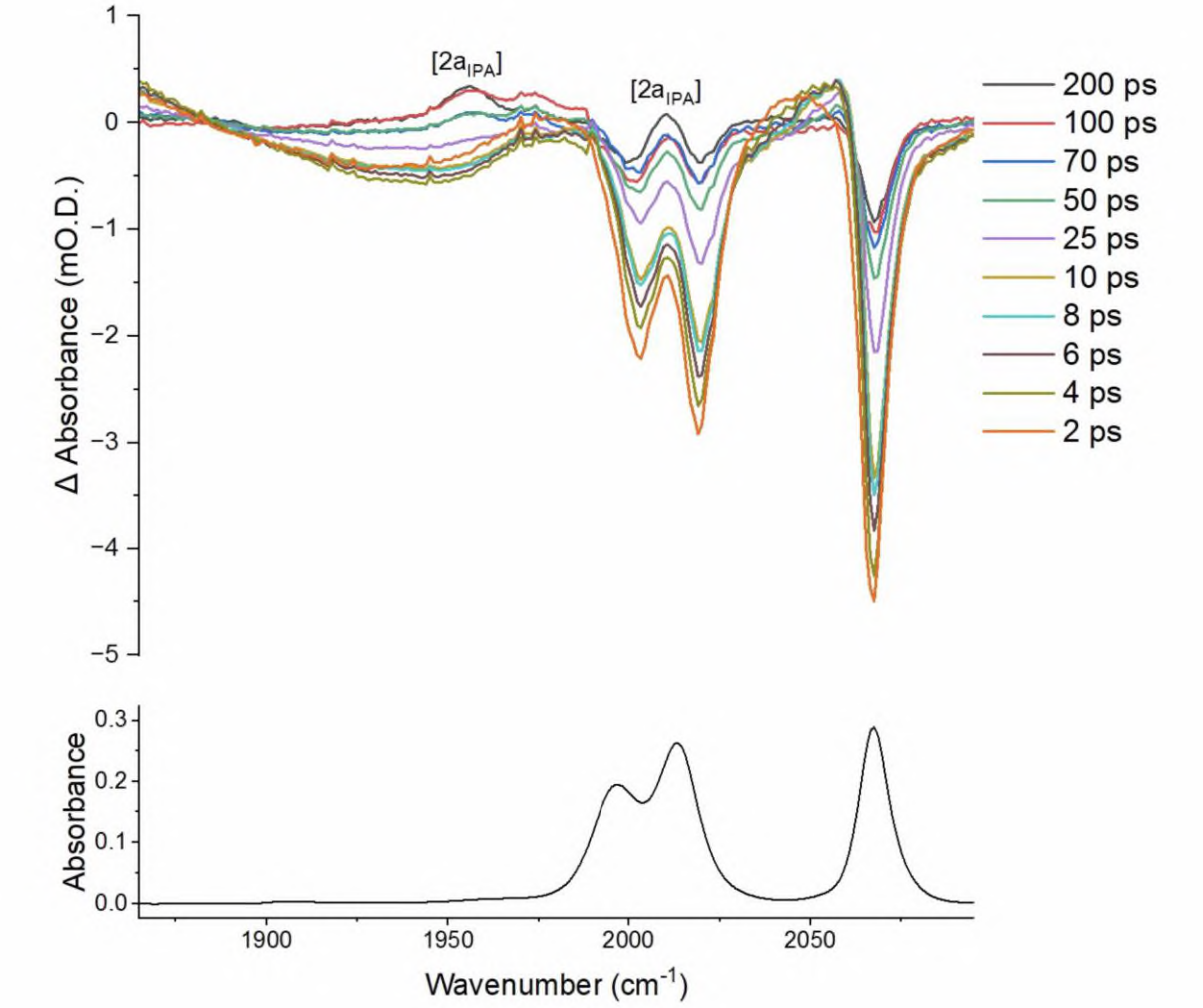

Figure 32. (Top) TRIR spectra of the 330 nm photolysis of the metal carbonyl region of [1a] at selected early pump-probe delays in IPA. The positive bands of [2a$_{IPA}$] represents the solvent coordinated complex. (Bottom) Ground state IR spectrum of [1a] in IPA.

Within a couple of ps, positive bands at 1974 cm^{-1} and 2046 cm^{-1} are observed, at 4 ps these bands shift to 1989 cm^{-1} and 2053 cm^{-1}. From 4 to 100 ps, the positive band observed at 2053 cm^{-1} only shifts within 5 cm^{-1} difference. However, the positive band at 1989 cm^{-1} from 4 to 8 ps shifts between 1970 cm^{-1} and 1989 cm^{-1}, until after 70 ps stays at 1970 cm^{-1} this band at 100 ps shifts to 1957 cm^{-1}. At 200 ps these bands settle at 1956 cm^{-1} and 2010 cm^{-1}, these bands are the bands that grow the largest growth in positive intensity and therefore are assigned to the solvent coordinated complex [2a$_{IPA}$].

Over the course of the first 200 picoseconds of the experiment, the three negative bleach bands for (2003, 2019 and 2068 cm^{-1}) decrease in intensity. This is consistent with the ground state being regenerated on this timescale. As shown in

Figure 33, the kinetics of this ground state bleach recovery were modelled using the negative bleach peak at 2068 cm^{-1}. This was effectively fitted to a bi-exponential model with time constants of (10.6 ± 2.3) ps and (42.3 ± 15.8) ps (the errors reported are at 95% confidence intervals). The bands also recovers to 20.7% of its original height. This demonstrates that on these time scales the primary fate of the light-activated complex is regeneration of the ground state.

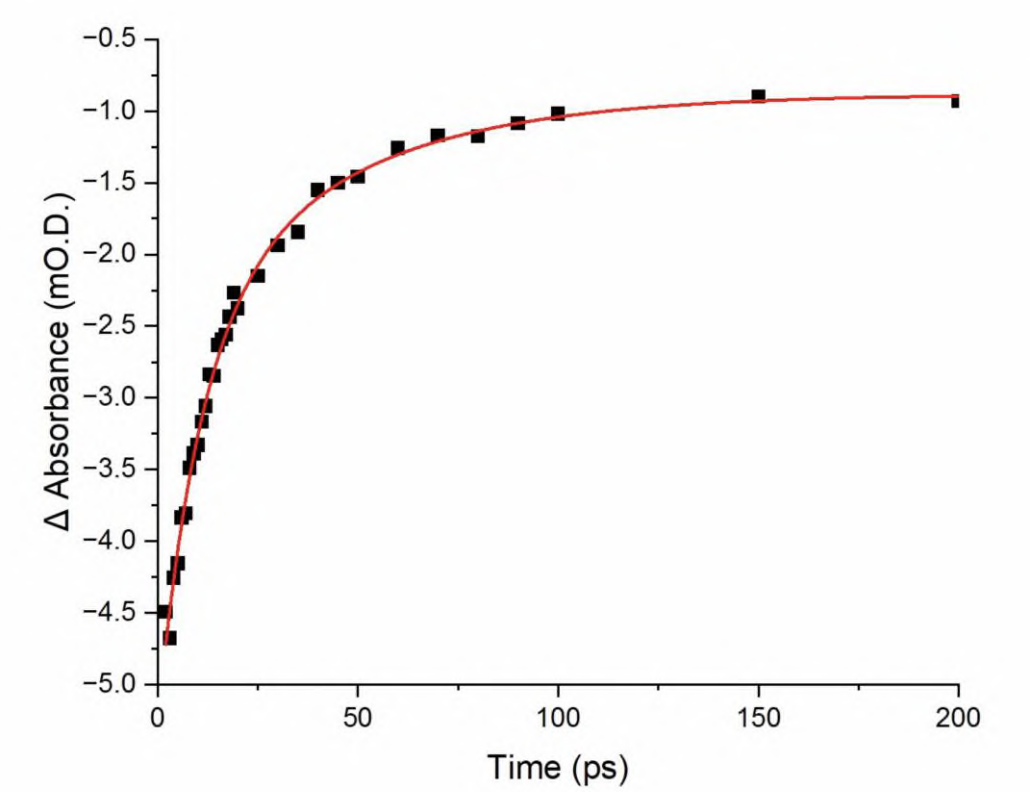

Figure 33. The change in absorbance of the bleach recovery at 2068 cm^{-1} from 2 to 200 ps. The solid red line represents a bi-exponential fit with lifetimes of 10.6 ± 2.3 ps and 42.3 ± 15.8 ps.

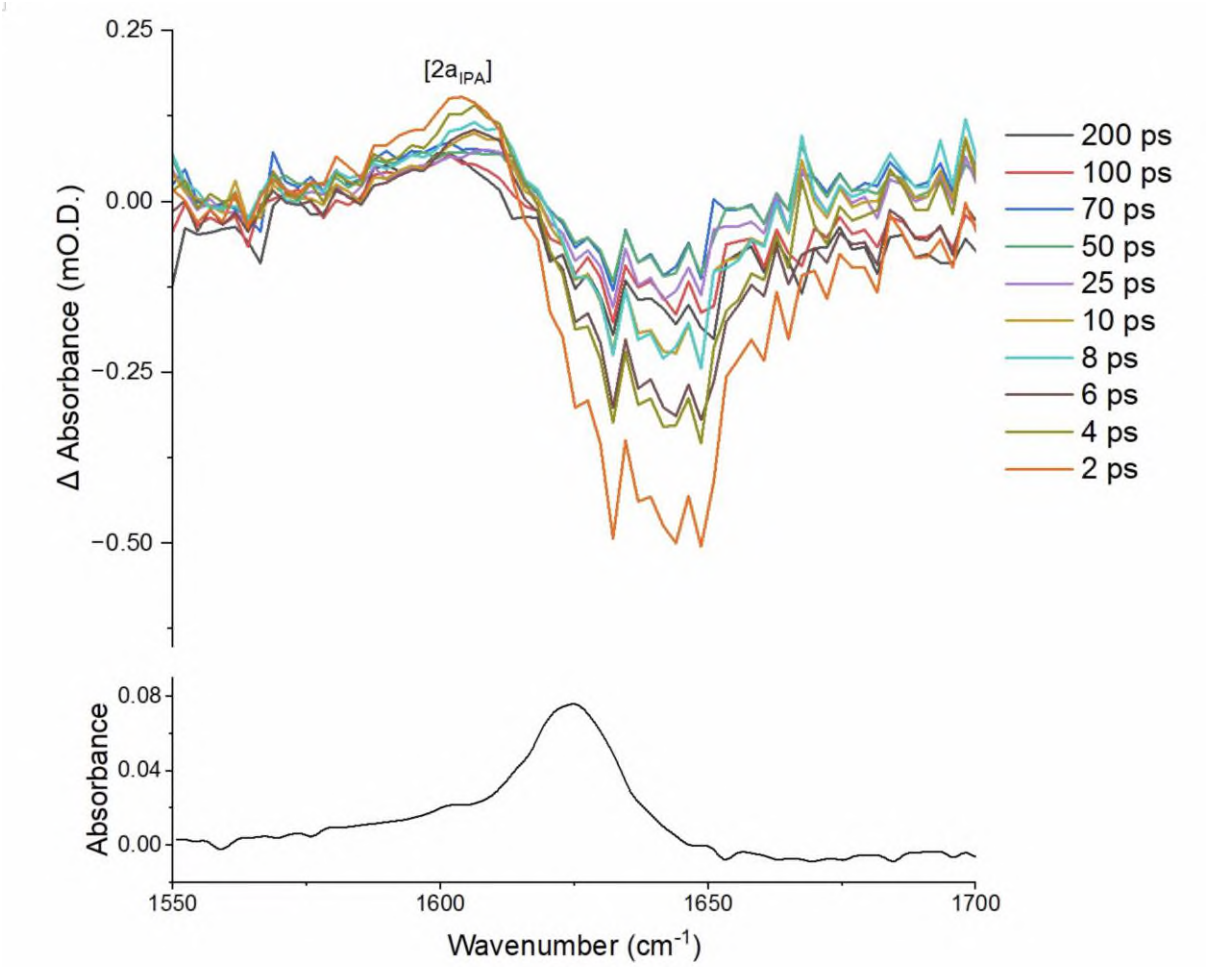

Figure 34. (Top) TRIR spectra of the 330 nm photolysis of the organic carbonyl region of [1a] at selected early pump-probe delays in IPA. The positive band of [2a$_{IPA}$] represents the solvent coordinated complex. (Bottom) Ground state IR spectrum of [1a] in IPA.

Within a couple of ps, a positive band is observed at 1603 cm^{-1}, over the duration of the early pump-probe delays the position of the band shifts only slightly however the intensity decreases at every time interval. This band was assigned to [2a$_{IPA}$].

2.3.8 Tetrahydrofuran

Tetrahydrofuran was chosen as a solvent system because it has been used extensively in the study of manganese catalysed C-H reactions.[42] With this knowledge it was an ideal solvent and an interesting one to examine the interactions between the light activated iron complex with THF.

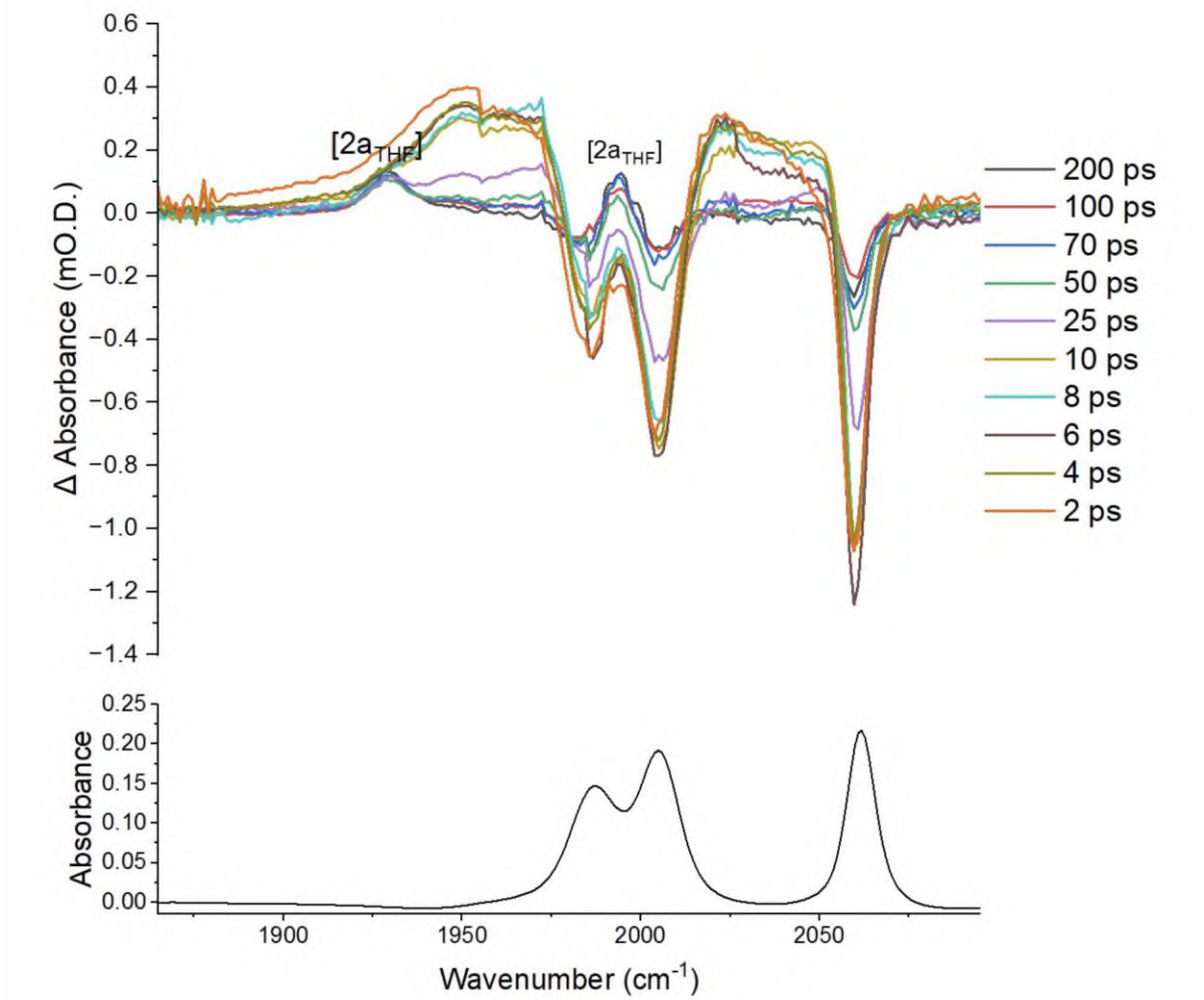

Figure 35. (Top) TRIR spectra of the 330 nm photolysis of the metal carbonyl region of [1a] at selected early pump-probe delays in THF. The positive bands of [2a$_{THF}$] represents the solvent coordinated complex. (Bottom) Ground state IR spectrum of [1a] in THF.

Within a couple of ps two positive bands at 1953 cm^{-1} and 2003 cm^{-1} were observed these bands stay within this position until 50 ps. At 25 ps the band at 1953 cm^{-1} has shifted to 1930 cm^{-1}. At 50 ps the positive bands are observed at 1930 cm^{-1} and 1993 cm^{-1} these bands are observed for the rest of the experiment. These bands were assigned to the solvent coordinated complex [2a$_{THF}$].

Over the course of the first 200 picoseconds of the experiment, the three negative bleach bands for (1985, 2003 and 2059 cm^{-1}) decrease in intensity. This is consistent with the ground state being regenerated on this timescale. As shown in Figure 36, the kinetics of this ground state bleach recovery were modelled using the negative bleach peak at 2059 cm^{-1}. This was effectively fitted to a single exponential

model with a time constant of (24.5 ± 3.6) ps (the errors reported are at 95% confidence intervals). The bands also recovers to 24.8% of its original height. This demonstrates that on these time scales the primary fate of the light-activated complex is regeneration of the ground state.

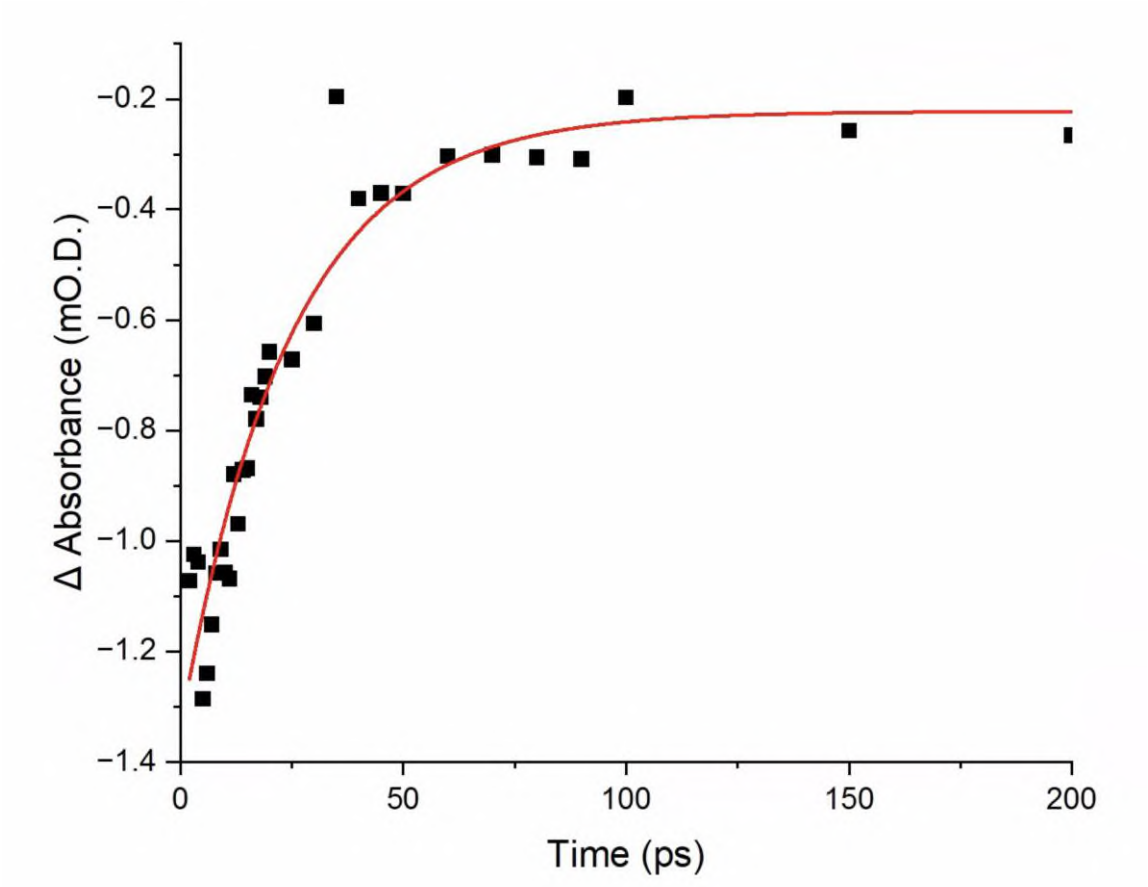

Figure 36. The change in absorbance of the bleach recovery at 2059 cm^{-1} from 2 to 200 ps. The solid red line represents a single exponential fit with a lifetime of 24.5 ± 3.6 ps.

2.3.9 IR_{PUMP}-IR_{PROBE} spectroscopic analysis of the metal carbonyl region of [1a] in THF.

The UV_{Pump}-IR_{Probe} data demonstrated that over 75% of the initially formed photoproducts regenerate ground state of the complex over the course of 200 ps. As mentioned in the case of the IR_{PUMP}-IR_{PROBE} analysis [1a] in acetone and heptane geminate recombination occurs (section 2.3.2 and 2.3.6), a similar pattern is observed in THF and in order to observe it geminate recombination does occurs, IR_{PUMP}-IR_{PROBE} experiments were performed using a fs IR pulse to populate vibrational exited states of the sample and the nature is interrogated by a second IR pulse. The vibrational modes can be observed, and their dynamic can give insight into (IVR and T_1) states.

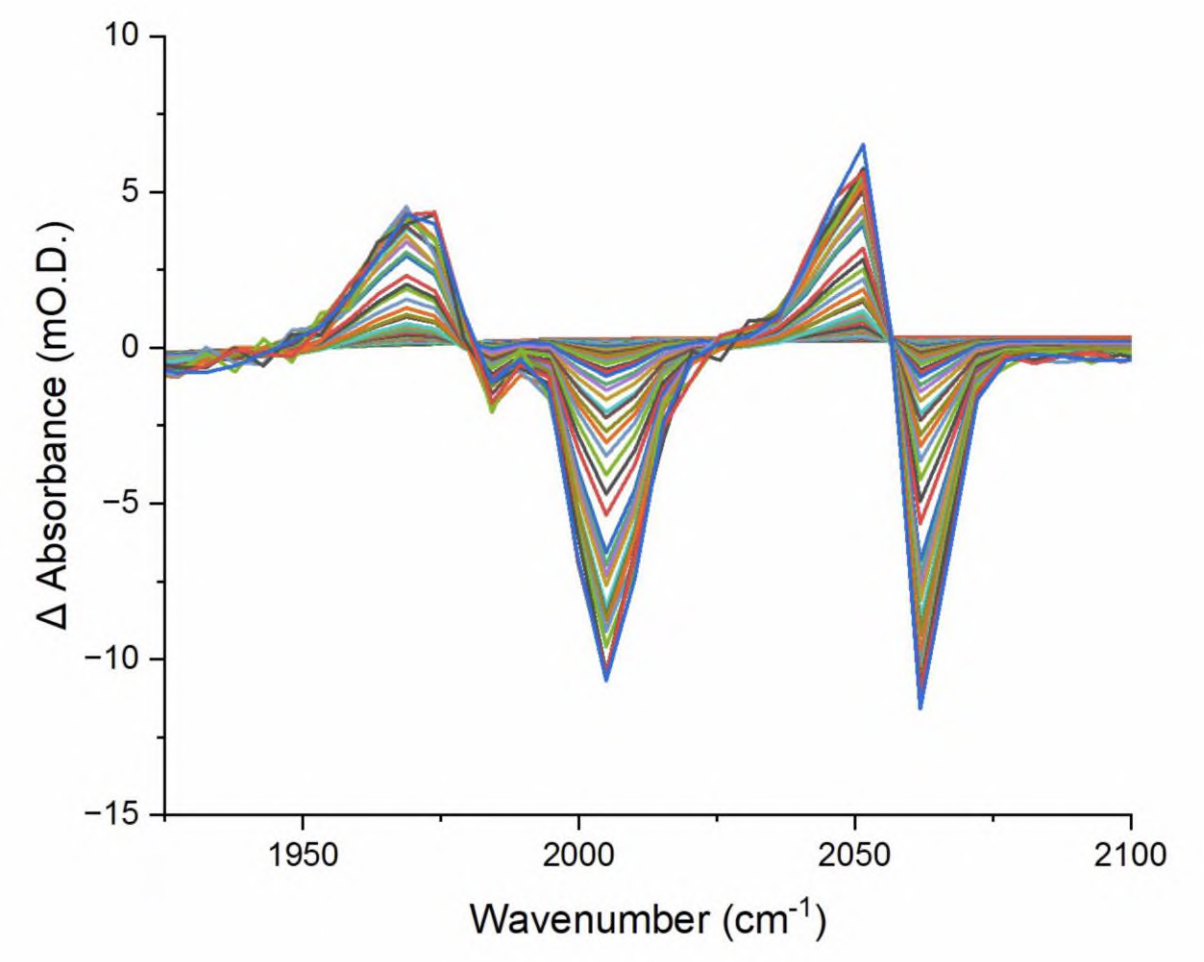

Figure 37. IR_{PUMP}-IR_{PROBE} spectrum of the metal carbonyl region of [1a] in THF.

In the IR spectrum two positive peaks (1969 cm^{-1} and 2051 cm^{-1}) and two negative peaks (2004 cm^{-1} and 2061 cm^{-1}) are observed. The experiment was measured using a timescale of 1 to 800 ps. The anharmonicity constants from 2004 cm^{-1} to 1969 cm^{-1} is 35 cm^{-1}, from 2051 cm^{-1} to 2004 cm^{-1} is 47 cm^{-1} and from 2061 cm^{-1} to 2051 cm^{-1} is 10 cm^{-1}.

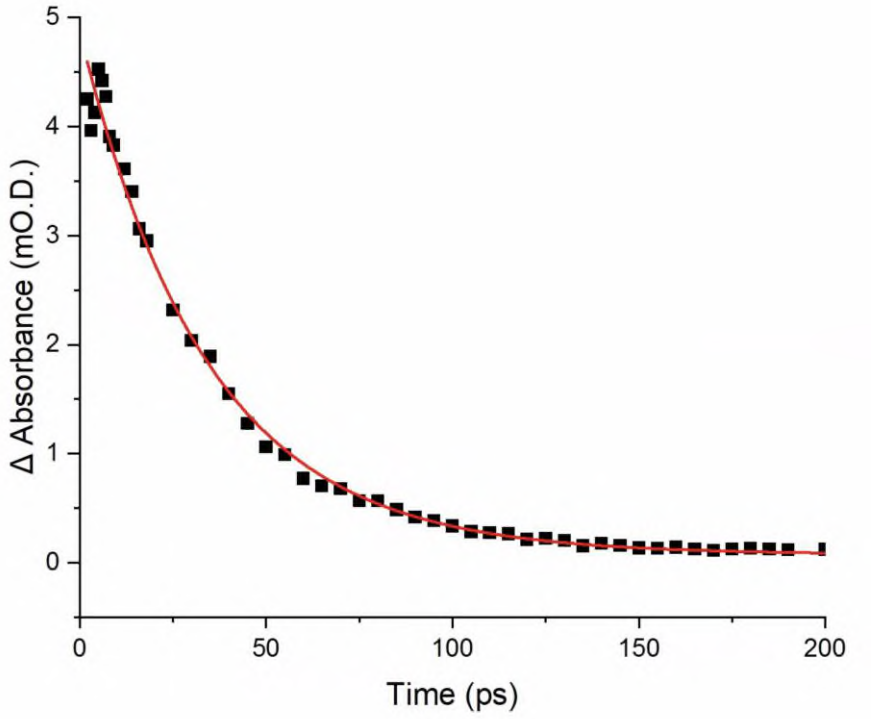

Figure 38. Change in absorbance of the vibrationally excited state at 1969 cm^{-1} from 2 to 200 ps. The solid red line represents a single exponential fit with a lifetime of 34.3 ± 1.3 ps.

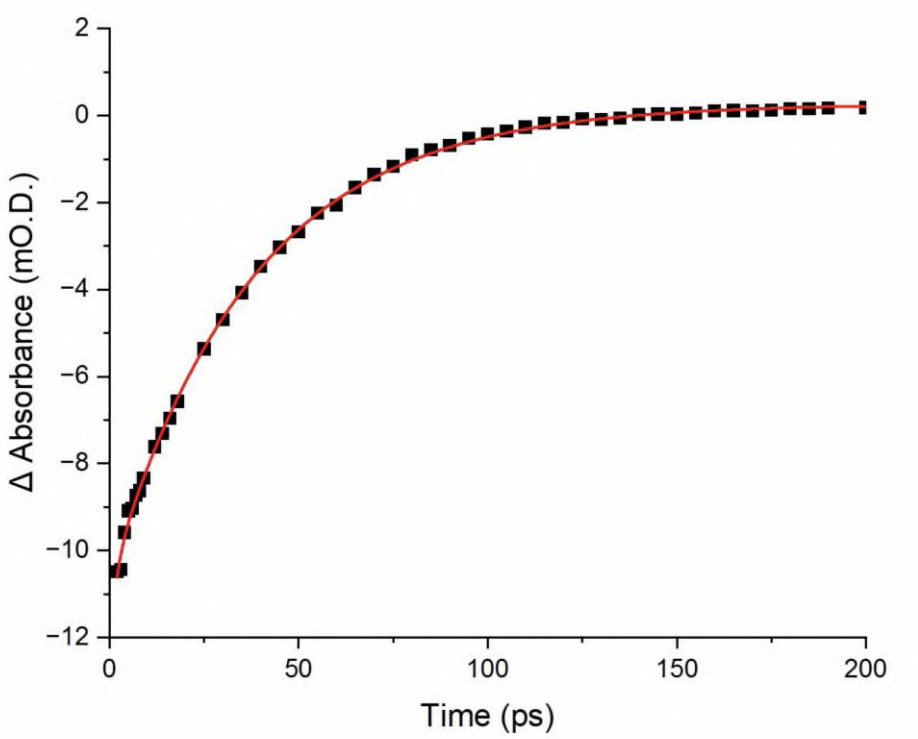

Figure 39. The change in absorbance of the bleach recovery at 2004 cm^{-1} from 2 to 200 ps. The solid red line represents a bi-exponential fit with lifetimes of 1.5 ± 0.7 ps and 37.6 ± 0.5 ps.

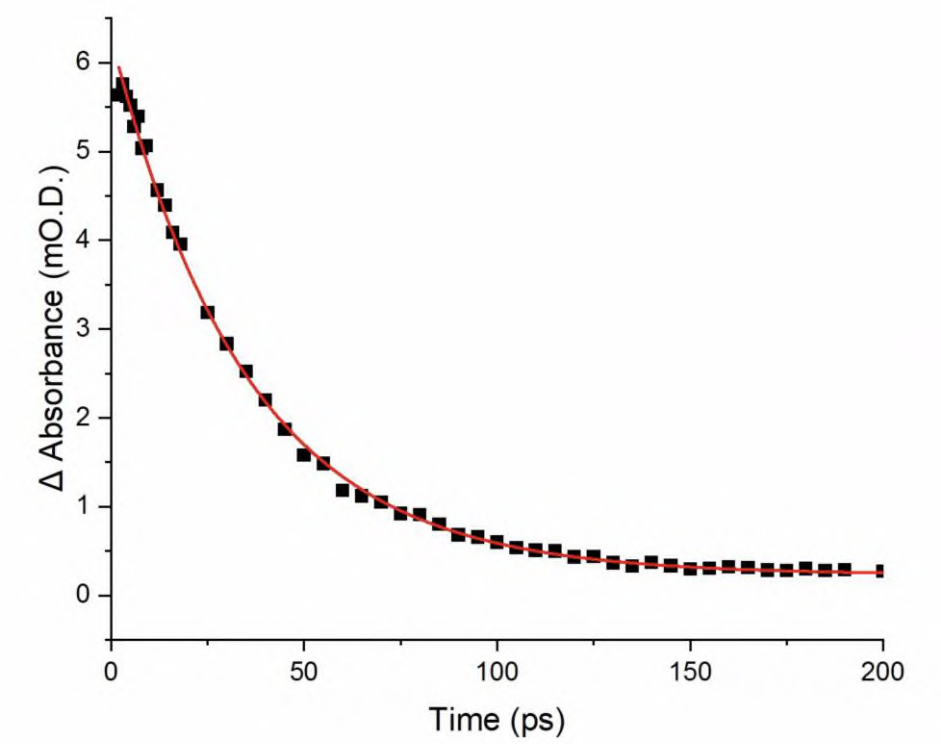

Figure 40. Change in absorbance of the vibrationally excited state at 2051 cm^{-1} from 2 to 200 ps. The solid red line represents a single exponential fit with a lifetime of 35.3 ± 0.6 ps.

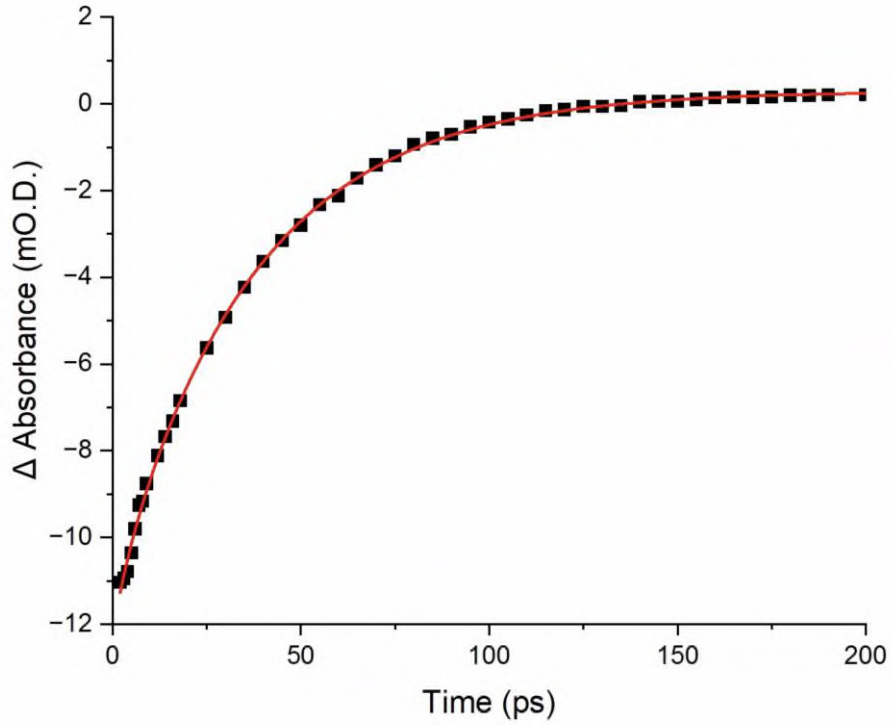

Figure 41. The change in absorbance of the bleach recovery at 2061 cm^{-1} from 2 to 200 ps. The solid red line represents a bi-exponential fit with lifetimes of 4.8 ± 2.4 ps and 37.0 ± 0.8 ps.

IVR (ps)			Vibrational lifetime (T_1) (ps)			
Solvent	2004 cm^{-1}	2061 cm^{-1}	1969 cm^{-1}	2004 cm^{-1}	2051 cm^{-1}	2061 cm^{-1}
THF	1.5 ± 0.7	4.8 ± 2.4	34.3 ± 1.3	37.6 ± 0.5	35.3 ± 0.6	37.8 ± 0.8

Table 5. Vibrational dynamics of the metal carbonyl region of [1a] in THF obtained from fitting IR_{PUMP}-IR_{PROBE} data to exponential functions.

2.4 IR_{PUMP}-IR_{PROBE} spectroscopic analysis of the organic carbonyl region of [1a] in THF.

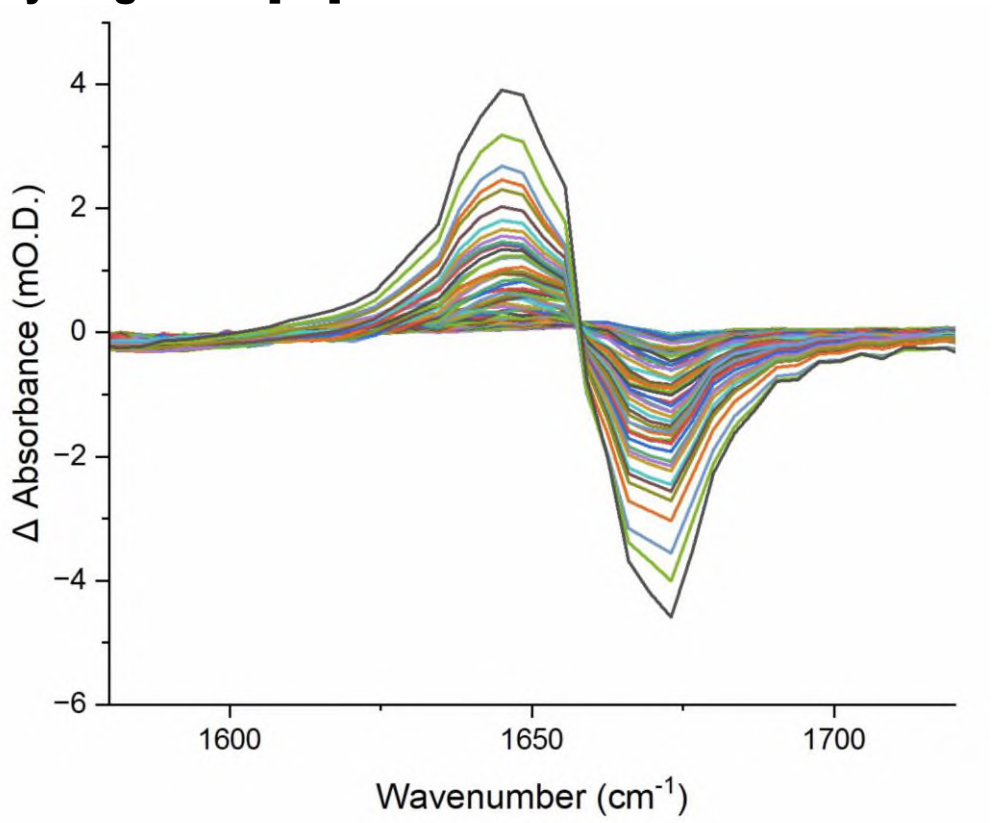

Figure 42. IR_{PUMP}-IR_{PROBE} spectrum of the organic carbonyl region of [1a] in THF.

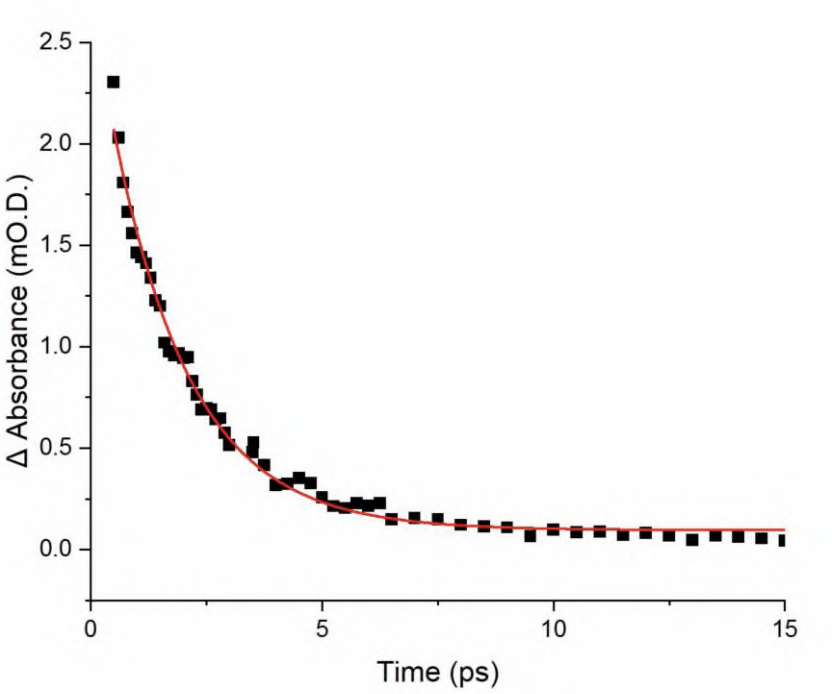

Figure 43. Change in absorbance of the vibrationally excited state at 1645 cm^{-1} from 0.5 to 15 ps. The solid red line represents a single exponential fit with a lifetime of 1.7 ± 0.05 ps.

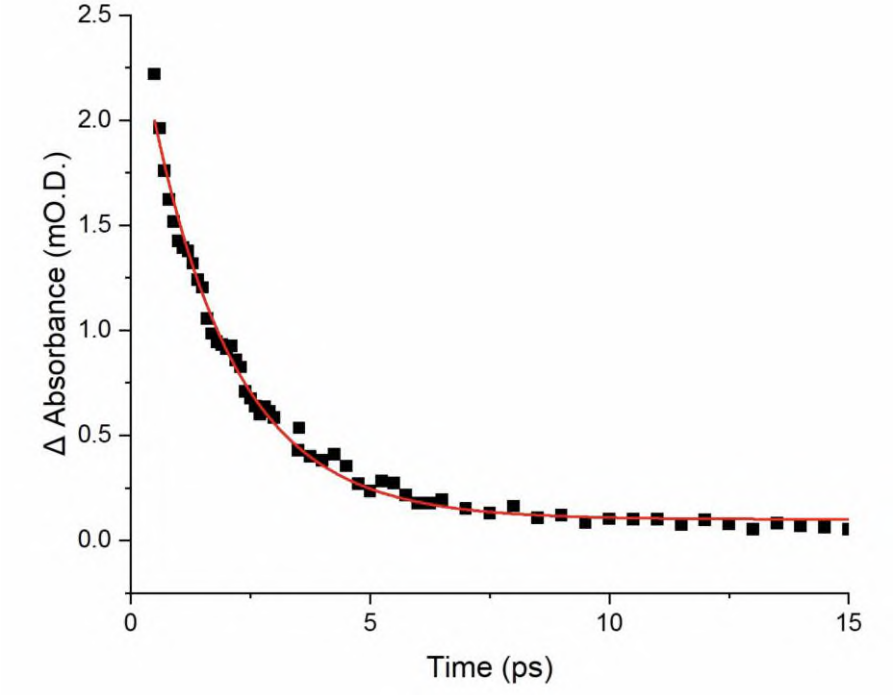

Figure 44. The change in absorbance at 1649 cm^{-1} from 0.5 to 15 ps. The solid red line represents a single exponential fit with a lifetime of 1.8 ± 0.05 ps.

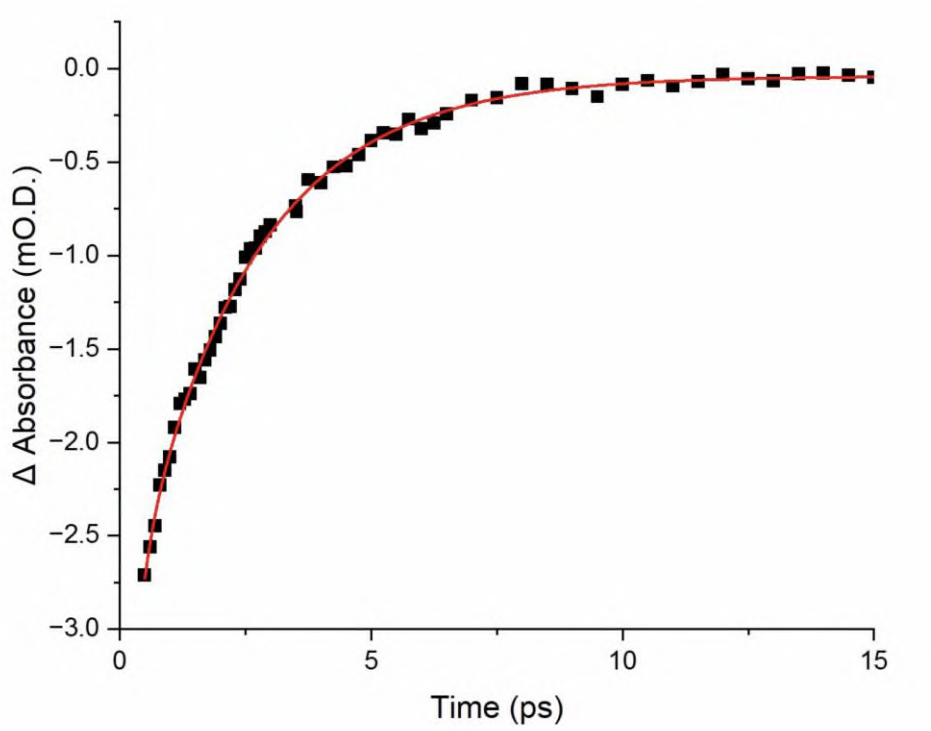

Figure 45. Change in absorbance at 1673 cm^{-1} from 0.5 to 15 ps. The solid red line represents a bi-exponential fit with lifetimes of 0.2 ± 0.1 ps and 2.3 ± 0.07 ps.

IVR (ps)		Vibrational lifetime (T_1) (ps)		
Solvent	1673 cm^{-1}	1645 cm^{-1}	1649 cm^{-1}	1673 cm^{-1}
THF	0.2 ± 0.1	1.7 ± 0.05	1.8 ± 0.05	2.3 ± 0.07

Table 6. Vibrational dynamics of the organic carbonyl region of [1a] in THF obtained from fitting IR_{PUMP}-IR_{PROBE} data to exponential functions.

The positive peaks, excited states were assigned as follows: T_1 (1.7 and 1.8) ps and for the negative peak, excited state was assigned as follows: IVR (0.2) ps and T_1 (2.3) ps. The positive peaks exhibit a $v_1 \rightarrow v_2$ transition and negative peaks exhibit a $v_0 \rightarrow v_1$ transition.

2.4.1 Toluene

Toluene was chosen as a solvent system because it has been used in the study of [Mn(ppy)(CO)$_4$] solvent interactions.[42]

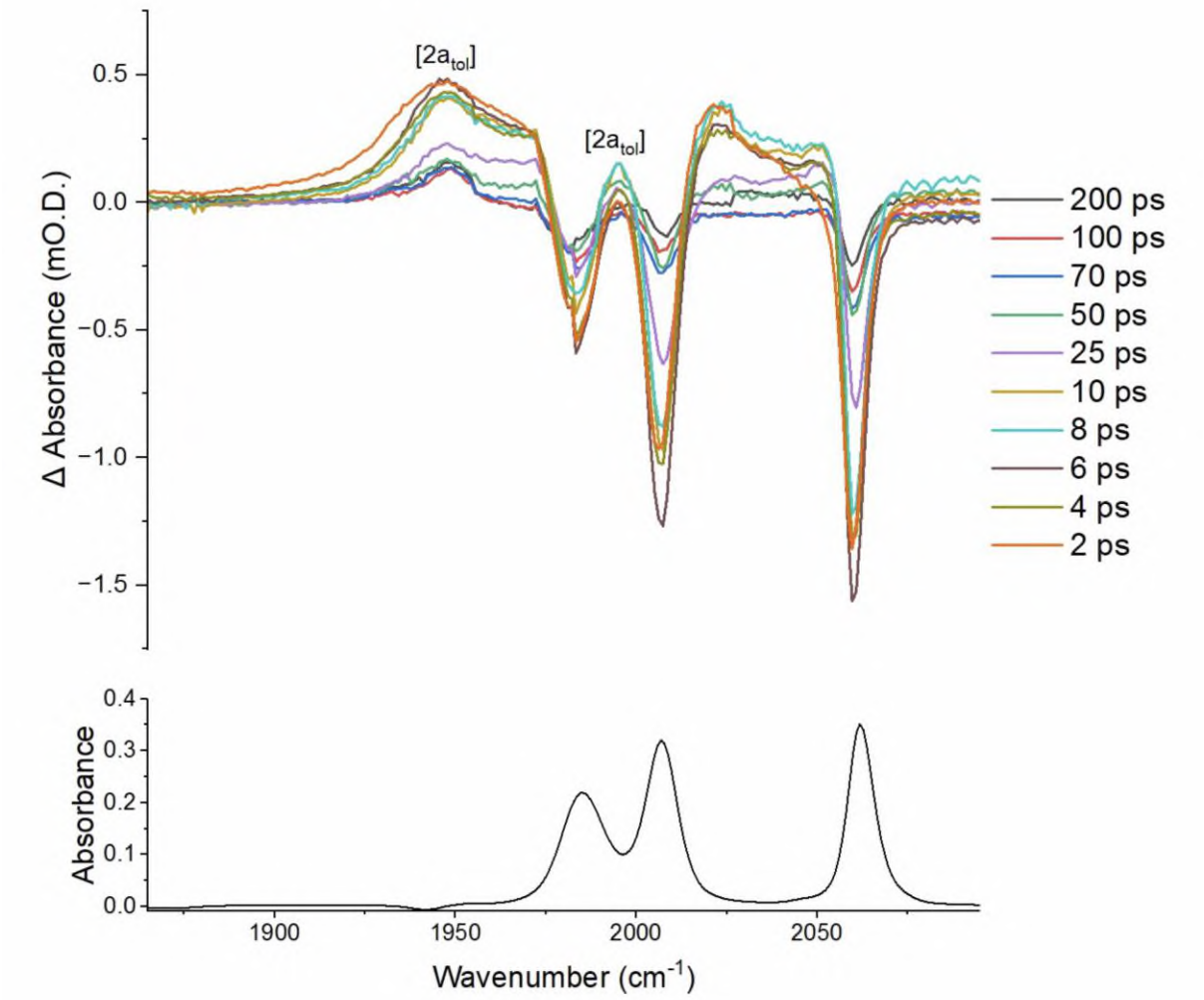

Figure 46. (Top) TRIR spectra of the 330 nm photolysis of the metal carbonyl region of [1a] at selected early pump-probe delays in toluene. The positive bands of [2a$_{tol}$] represents the solvent coordinated complex. (Bottom) Ground state IR spectrum of [1a] in toluene.

Within a couple ps two positive bands at 1947 cm^{-1} and 1994 cm^{-1}, these bands are observed for the rest of the experiment and the only real shift is at 200 ps the band at 1994 cm^{-1} shifts to 2000 cm^{-1} however the band still overlaps with the other bands observed at the various pump-probe delays. These bands were assigned to the solvent coordinated complex [2a$_{tol}$].

Over the course of the first 200 picoseconds of the experiment, the three negative bleach bands for (1983, 2007 and 2059 cm^{-1}) decrease in intensity. This is consistent with the ground state being regenerated on this timescale. As shown in Figure 47, the kinetics of this ground state bleach recovery were modelled using the negative bleach peak at 2059 cm^{-1}. This was effectively fitted to a single exponential model with a time constant of (32.8 $\pm$ 9.4) ps (the errors reported are at 95% confidence intervals). The bands also recover to 18.1% of its original height. This

demonstrates that on these time scales the primary fate of the light-activated complex is regeneration of the ground state.

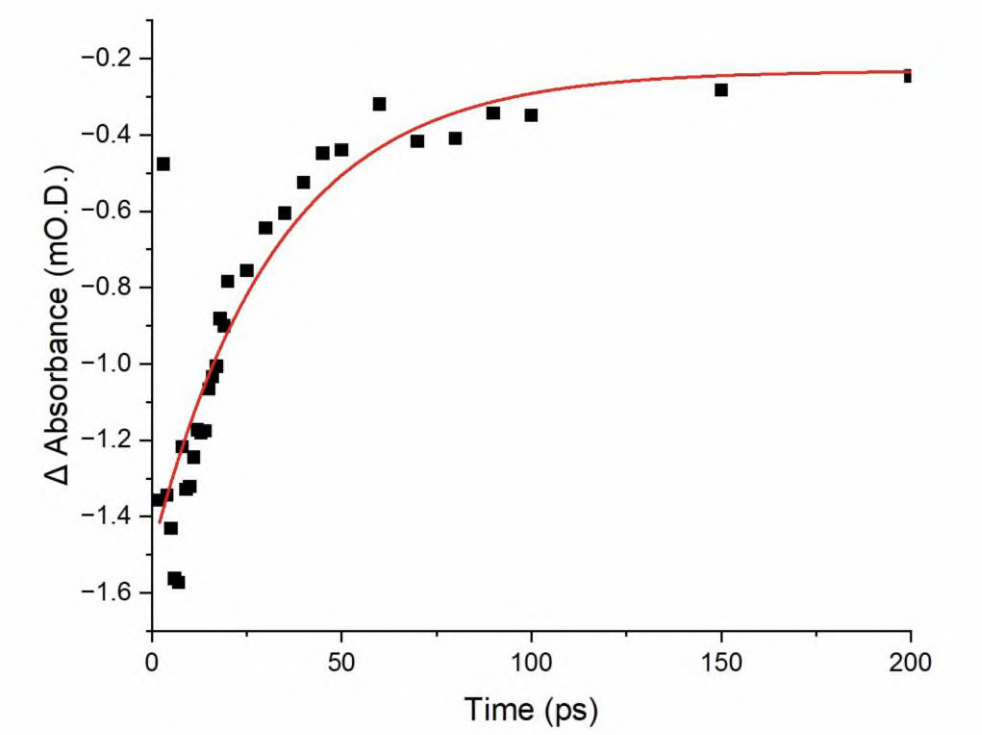

Figure 47. The change in absorbance of the bleach recovery at 2059 cm^{-1} from 2 to 200 ps. The solid red line represents a single exponential fit with a time constant of 32.8 ± 9.4 ps.

2.4.2 Summary of Early pump-probe delays.

Nearly all the TRIR spectrums of the early pump-probe delays, there are intense bleach peaks, that over the period of 2 to 200 ps decrease in negative intensity, this is because of the electronically excited state ^{3}[1a]. The formation of two positive peaks are observed at approximately 50 ps, these peaks grow in intensity and stayed in the same position for the rest of the early pump-probe delays. Heptane behaved differently as there was multiple peaks presumably from two ^{3}MLCT states (section 2.3.5).[48] IR_{PUMP}-IR_{PROBE} was employed, this is a pump-probe method that instead of the sample undergoing a thermal reaction by photolysis. Instead, it was used to study the vibrational dynamics of solvent interactions of the carbonyl ligand stretching modes of [1a] in acetone, heptane and THF.

What is observed similarly to the work on manganese carbonyl complexes is that CO dissociation is rapid (<1 ps) and the formation of the solvent-coordinated species is observed within the ps timescale. Within the ps timescale, TRIR demonstrates that unsaturated iron centres react rapidly with solvent or substrates, this gives evidence to the mechanism where the amine/alcohol substrate will bind to the iron centre to begin the HAT step.

3 Time-resolved Infra-Red Spectra for [1a] from 1 ns to 1 ms.

After analysing the early pump-probe delays, the later pump-probe delays were then analysed. This was done to see if any additional complexes were observed at longer timescales. The later pump-probe delays were measured from 1 ns to 1 ms.

3.1.1 Acetone

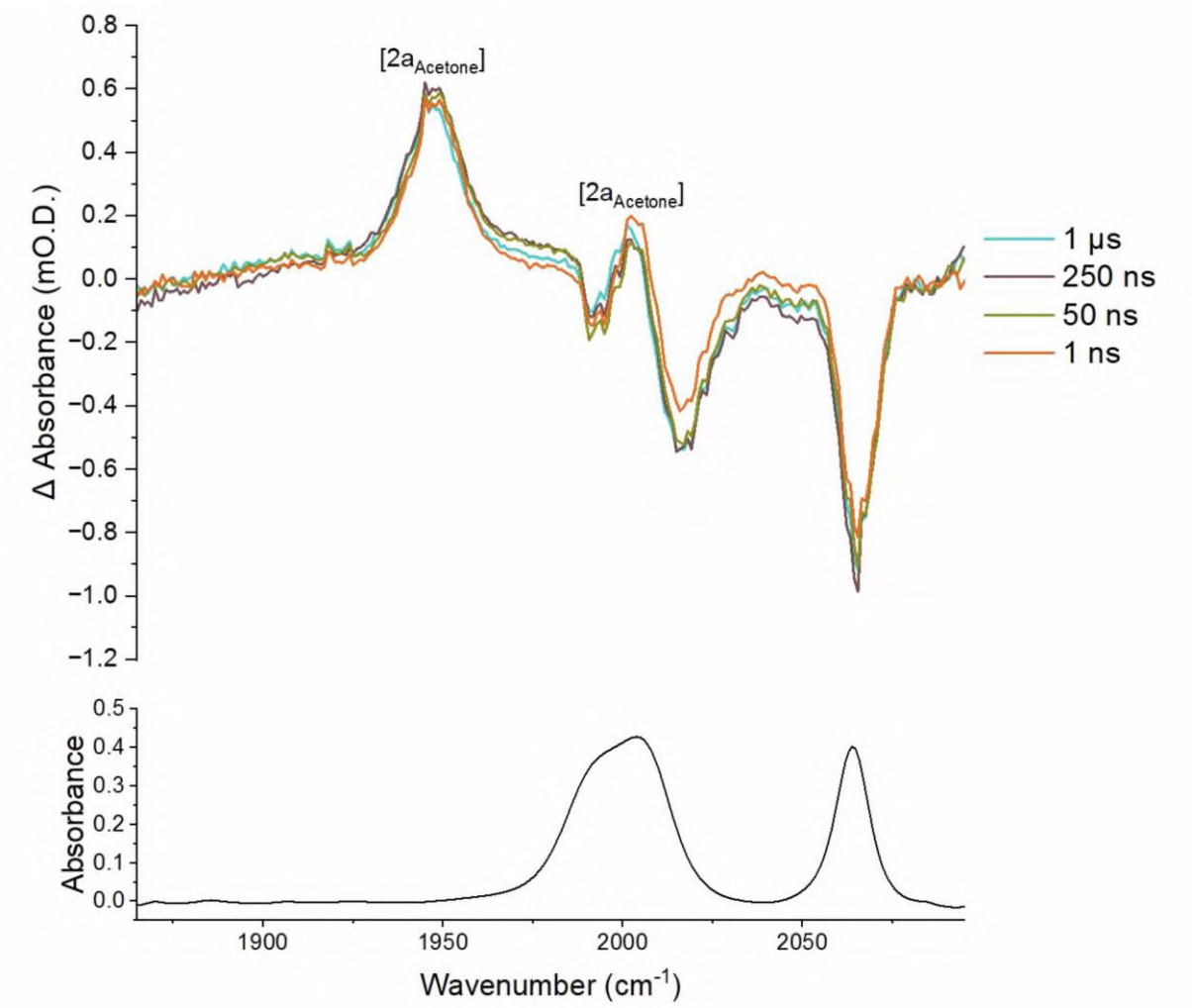

Figure 48. (Top) TRIR spectra of the 330 nm photolysis of the metal carbonyl region of [1a] at selected later pump-probe delays in acetone. The positive bands of [2a$_{acetone}$] represents the solvent coordinated complex. (Bottom) Ground state IR spectrum of [1a] in acetone.

At 1 ns two positive bands are observed at 1945 cm^{-1} and 2002 cm^{-1}, the position of the peaks at 1 ns is the same as what was observed at 200 ps. These peaks are seen throughout the entire experiment only the intensity changes gradually decreasing; however the peak position is the same, meaning that the solvent-coordinated complex is observed even at longer timescales. The reaction scheme proposed in Scheme 37, is what would be expected based on TRIR analysis carried out on the manganese carbonyl complex [Mn(ppy)(CO)$_4$].[42] Within the literature the

timescale in which the solvent-coordinated species *fac*-[Mn(ppy)(S)$(CO)_3$] is observed is within the ps timescale, the solvent-coordinated species [$2a_{acetone}$] is also observed on the ps timescale, this is because geminate recombination occurs on the fs-ps timescale. In terms of reactivity, because the photofragment is trapped within the solvent cage, the complex rapidly coordinates with a solvent molecule (in this case acetone) before it escapes into the bulk solution. The [$2a_{acetone}$] species persisted was the only solvent-coordinated species that lived for the entire experiment and wasn't replaced by the aqua complex. The reason for this is because acetone is a strong ligand when comparing to another ligand such as heptane, the heptane complex only lives on a nanosecond timescale as it is a weak bound ligand and is replaced by the aqua complex.

The assignment of the complex [$2a_{acetone}$] was made because 2 positive bands are observed meaning that a CO ligand has been dissociated and these peaks are in the same position as they were observed at 200 ps. One thing that is observed is that the signals decrease over time one possible reason is that the solvent is flowing out of the cell.

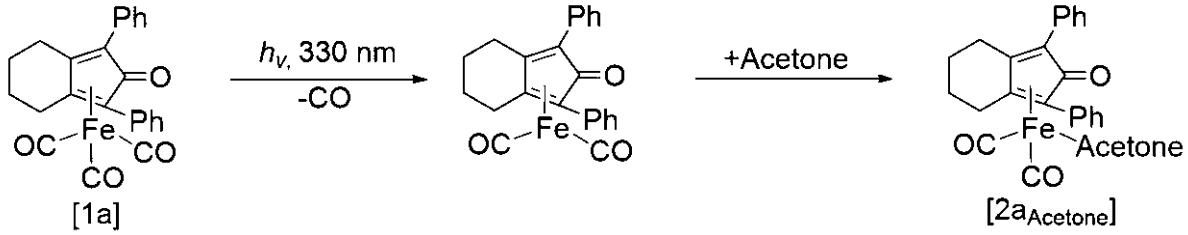

Scheme 37. Proposed mechanism for the photolysis of [1a] in acetone.

3.1.2 Acetonitrile

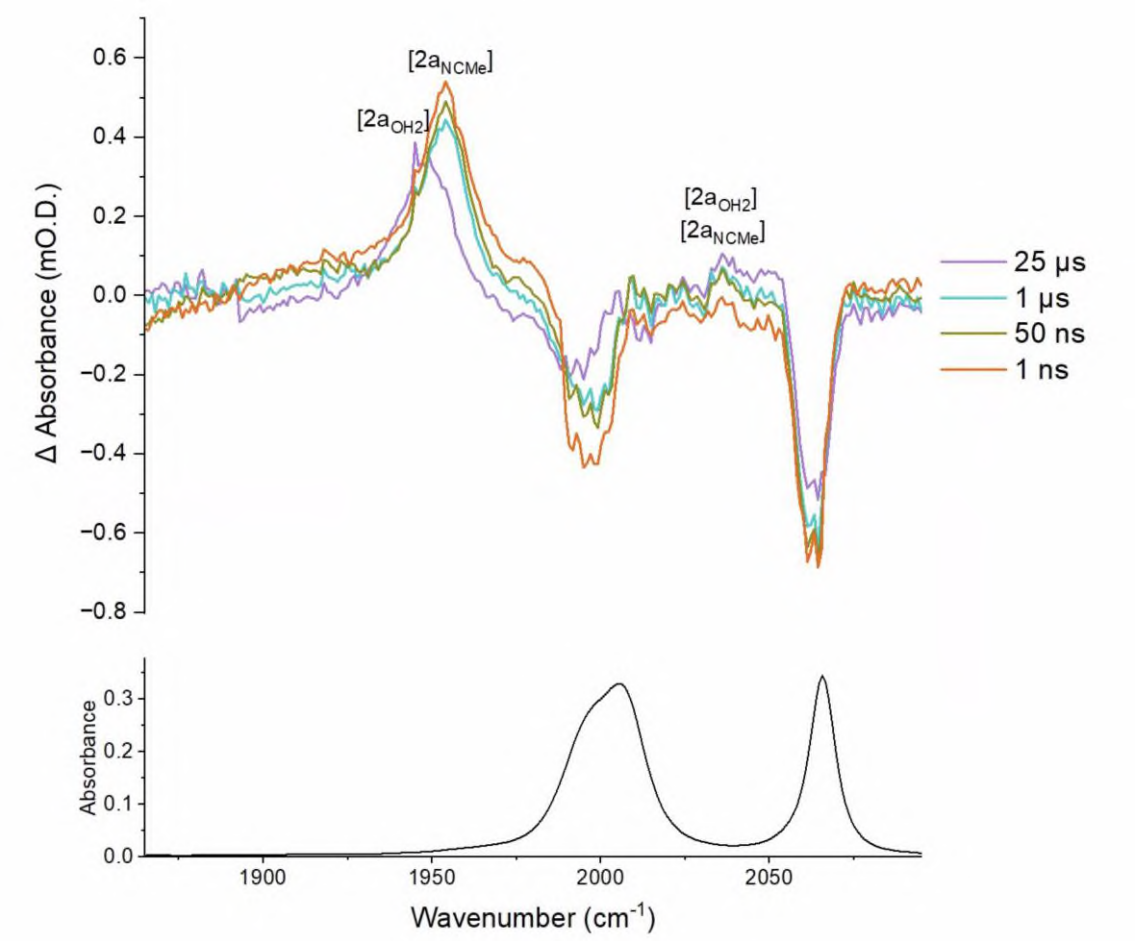

Figure 49. (Top) TRIR spectra of the 330 nm photolysis of the metal carbonyl region of [1a] at selected later pump-probe delays in NCMe. The positive bands of the [2a$_{NCMe}$] represents the solvent coordinated complex. (Bottom) Ground state IR spectrum of [1a] in NCMe.

At 1 ns two positive bands observed at 1954 cm^{-1} and 2035 cm^{-1}, these bands remain in the same position until at 10 µs they begin to decrease in intensity and at 25 µs these bands shift to 1949 cm^{-1} and 2035 cm^{-1}. Because the bands move to a lower wavenumber these were assigned to the aqua complex [2a$_{OH2}$] was assigned, the aqua complex persisted for the rest of the experiment. This was assigned based on heptane based studies using [Mn(C^N)(CO)$_4$] found that the IR bands for the aqua complex shift to a lower wavenumber.[48] An TRIR spectra of the organic carbonyl region of [1a] in NCMe however the signal-to-noise ratio made them inadequate. A proposed mechanism is shown in Scheme 38.

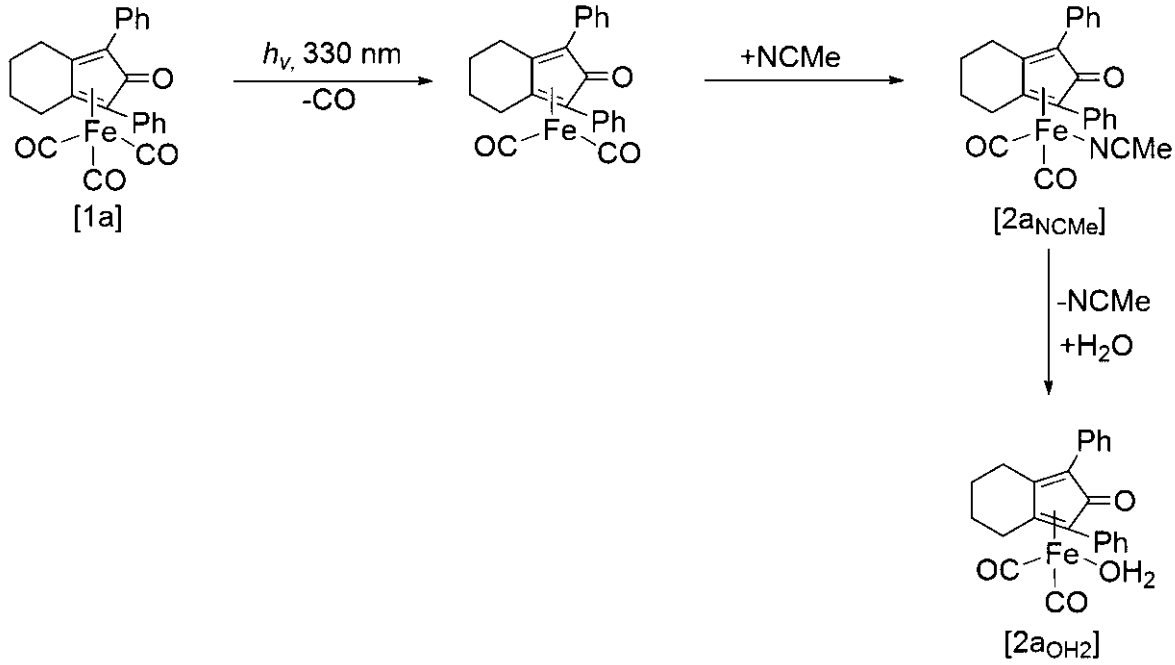

Scheme 38. Proposed mechanism for the photolysis of [1a] in NCMe.

3.1.3 Cyclopentyl methyl ether

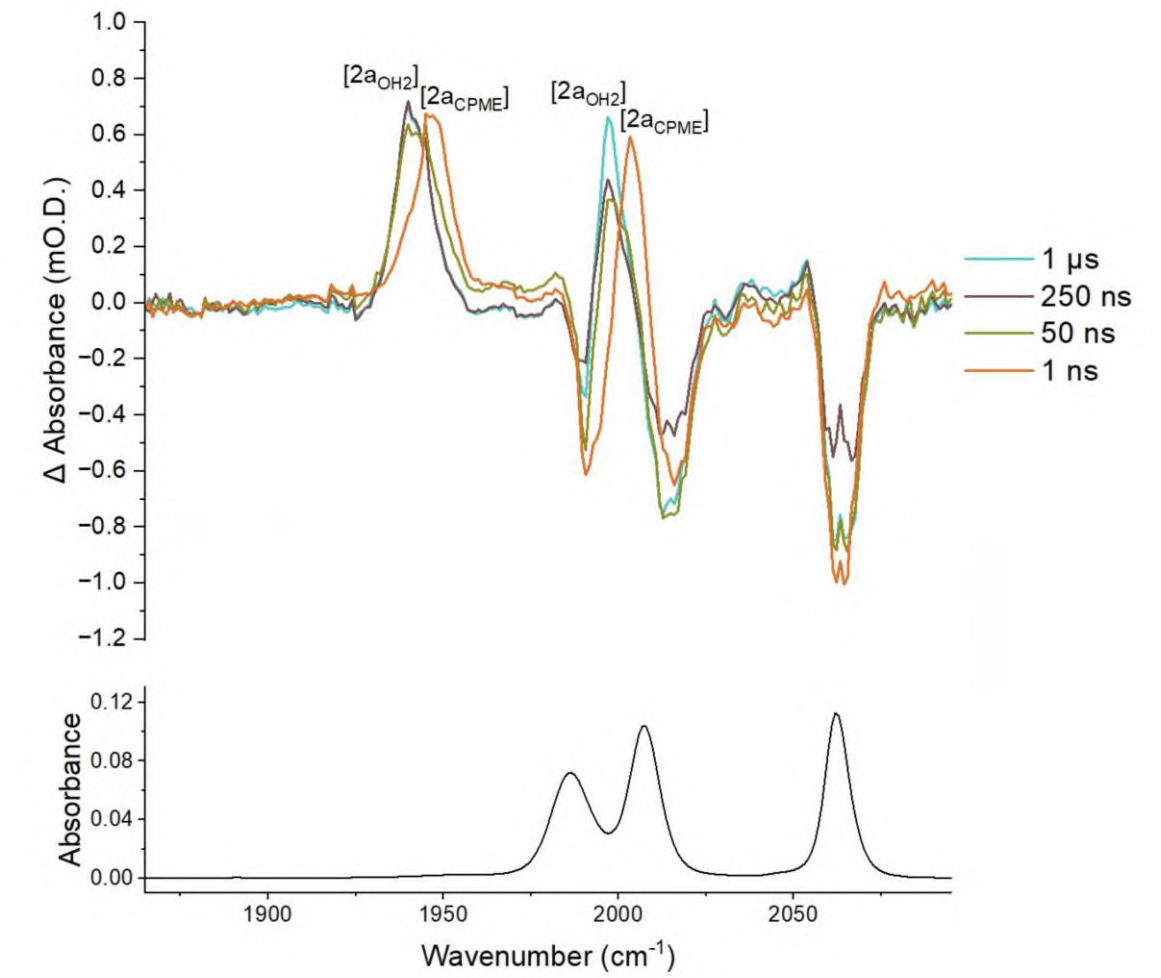

Figure 50. (Top) TRIR spectra of the 330 nm photolysis of the metal carbonyl region of [1a] at selected later pump-probe delays in CPME. The positive bands of [2a$_{CPME}$] represents the solvent coordinated complex. (Bottom) Ground state IR spectrum of [1a] in CPME.

At 1 ns two positive bands are observed at 1945 cm^{-1} and 2003 cm^{-1}, at ~ 50 ns these bands shift to a lower wavenumber, and the bands are now observed at 1940 cm^{-1} and 1996 cm^{-1}. These bands stay in this position for the rest of the experiment. Two complexes are formed at 1 ns the CPME coordinated complex [2a$_{CPME}$] and then at 50 ns bands shift to a lower wavenumber the aqua complex [2a$_{OH2}$] was assigned and persisted for the rest of the experiment.

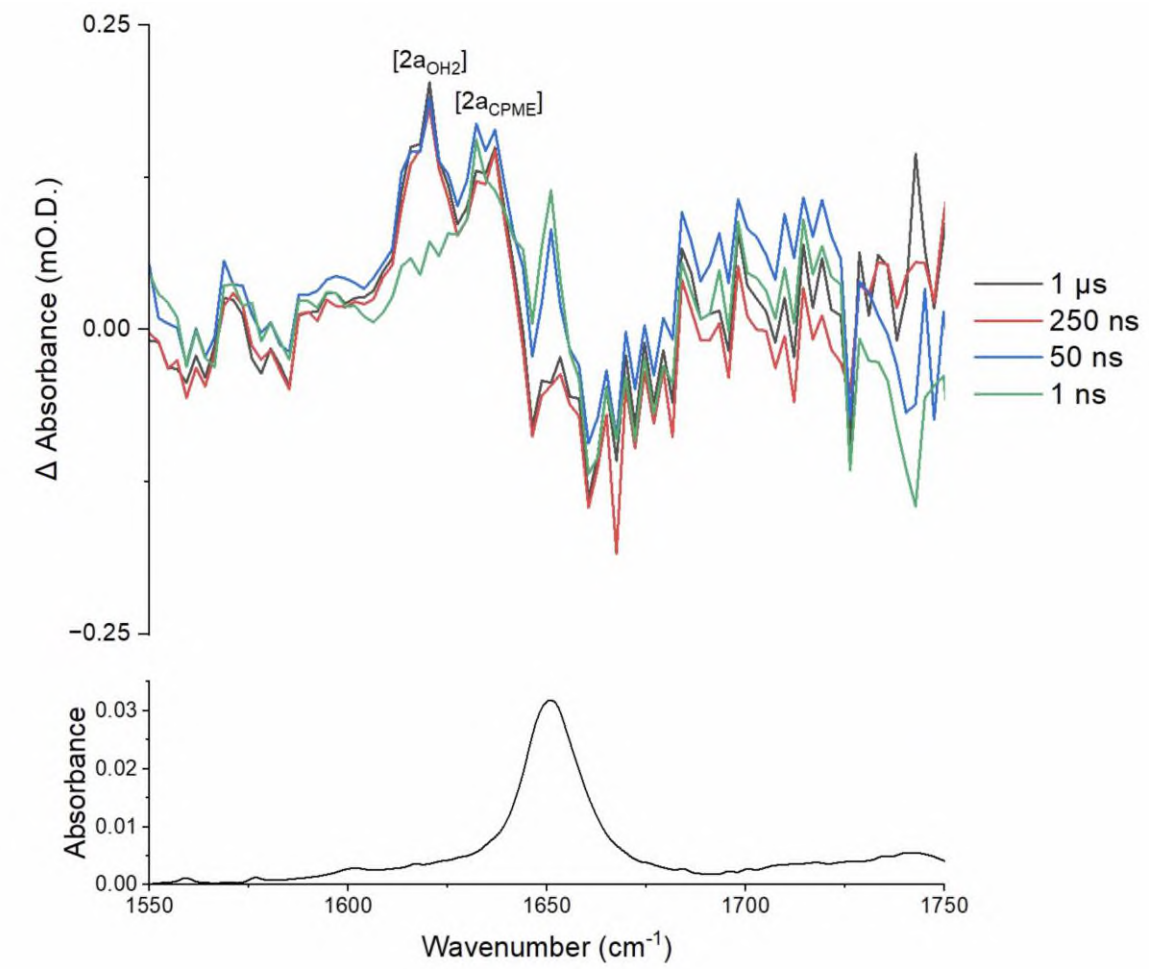

Figure 51. (Top) TRIR spectra of the 330 nm photolysis of the organic carbonyl region of [1a] at selected later pump-probe delays in CPME. The positive band of [2a$_{CPME}$] represents the CPME coordinated complex. (Bottom) Ground state IR spectrum of [1a] in CPME.

At 1 ns a positive band is observed just above 1630 cm^{-1}, at ~50 ns this band shifts to 1620 cm^{-1} and has a slightly higher positive intensity. This band stays in the same position for the rest of the experiment. The band at 1630 cm^{-1} observed at 1 ns is assigned to the CPME coordinated complex [2a$_{CPME}$] and because this band shifts to a lower wavenumber as observed in the metal carbonyl region this band was assigned to the aqua complex [2a$_{OH2}$]. A proposed mechanism is shown in Scheme 39.

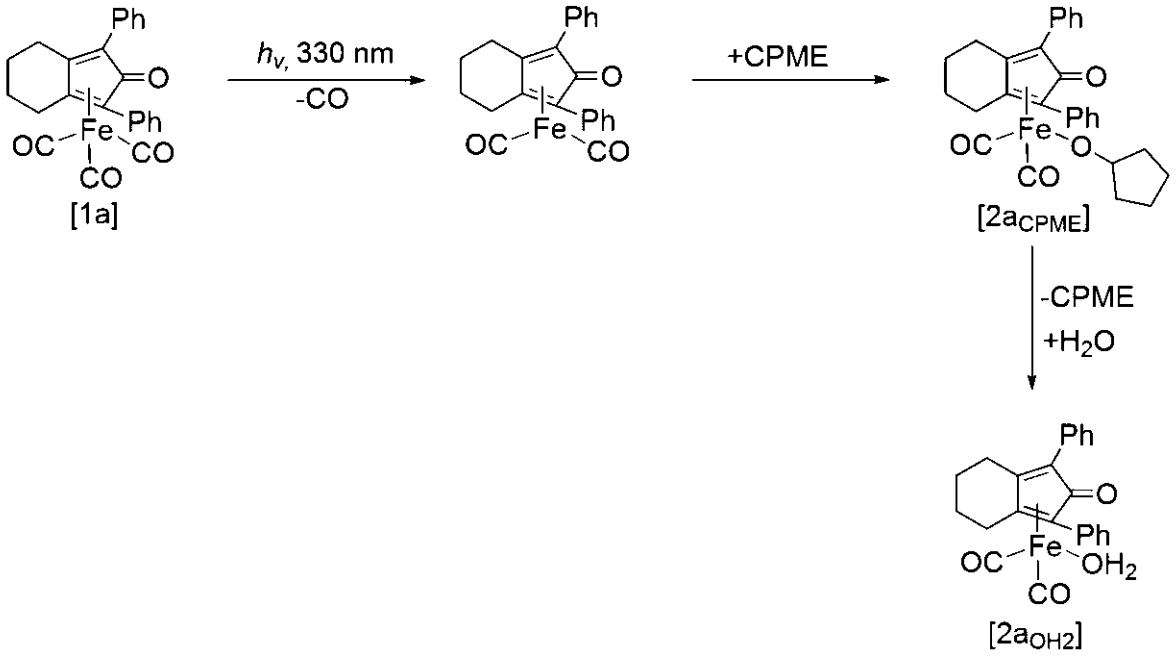

Scheme 39. Proposed mechanism for the photolysis of [1a] in CPME.

3.1.4 Heptane

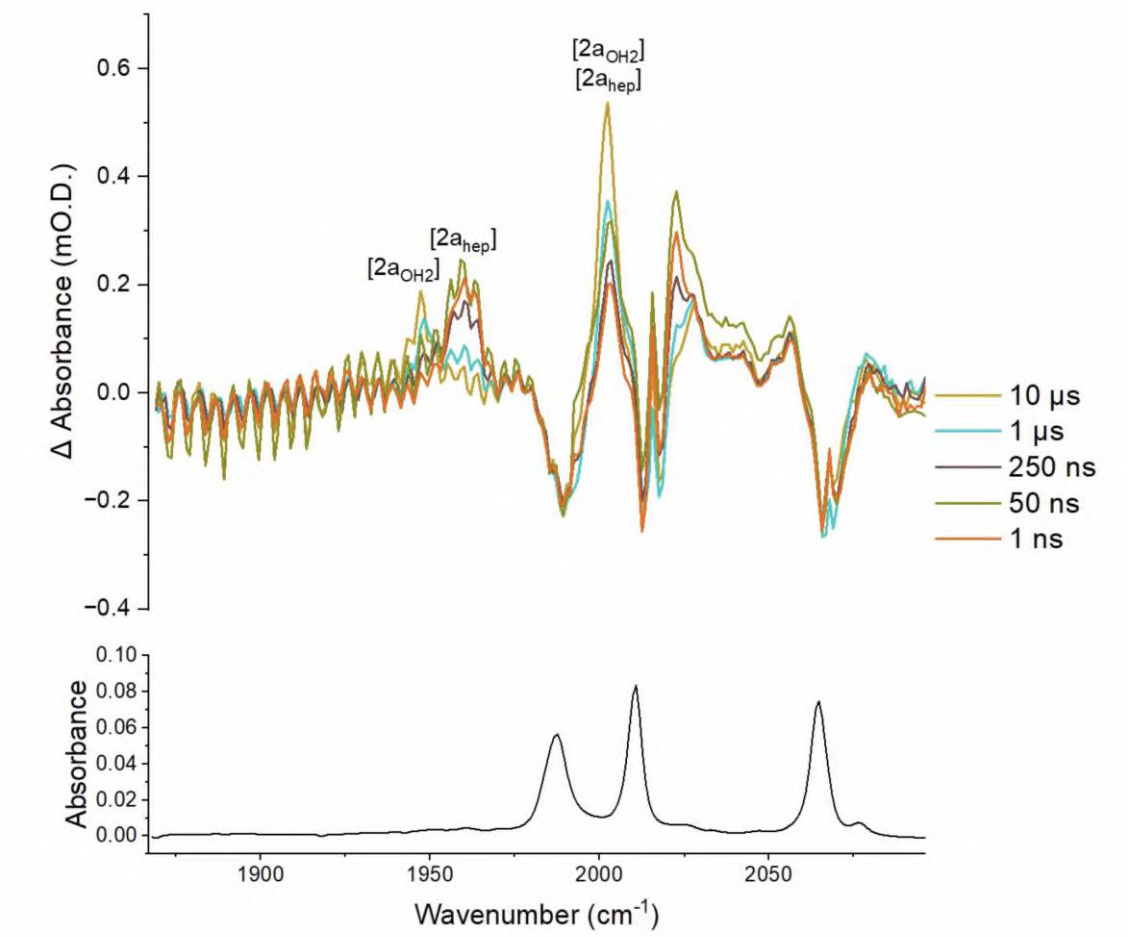

Figure 52. (Top) TRIR spectra of the 330 nm photolysis of the metal carbonyl region of [1a] at selected later pump-probe delays in heptane. The positive bands of [2a$_{hep}$] represents the solvent coordinated complex. (Bottom) Ground state IR spectrum of [1a] in heptane.

At 1 ns, two positive bands at 1958 cm^{-1} and 2001 cm^{-1} are observed. Interestingly these band positions are the same position observed within the early pump-probe delays. These bands remain in the same position until 1 µs the band at 1958 cm^{-1} shifts to 1945 cm^{-1} and remains in that position, the band at 2001 cm^{-1} stays in its position and grows in intensity. Even though there is a shift in band position they overlapped each other and subsequently were assigned to the solvent coordinated complex [2a$_{hep}$]. There is a shift in one of the peaks to a smaller wavenumber this is presumed to be caused by the aqua complex [2a$_{OH2}$] and persisted for the rest of the experiment. A proposed mechanism is shown in Scheme 40.

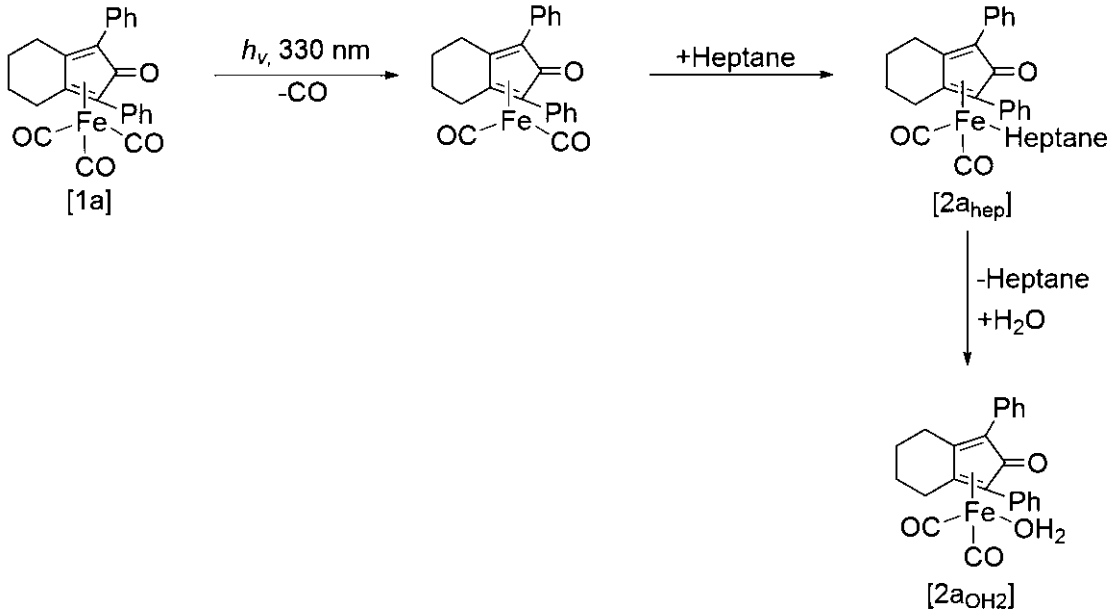

Scheme 40. Proposed mechanism for the photolysis of [1a] in heptane.

3.1.5 Isopropyl alcohol

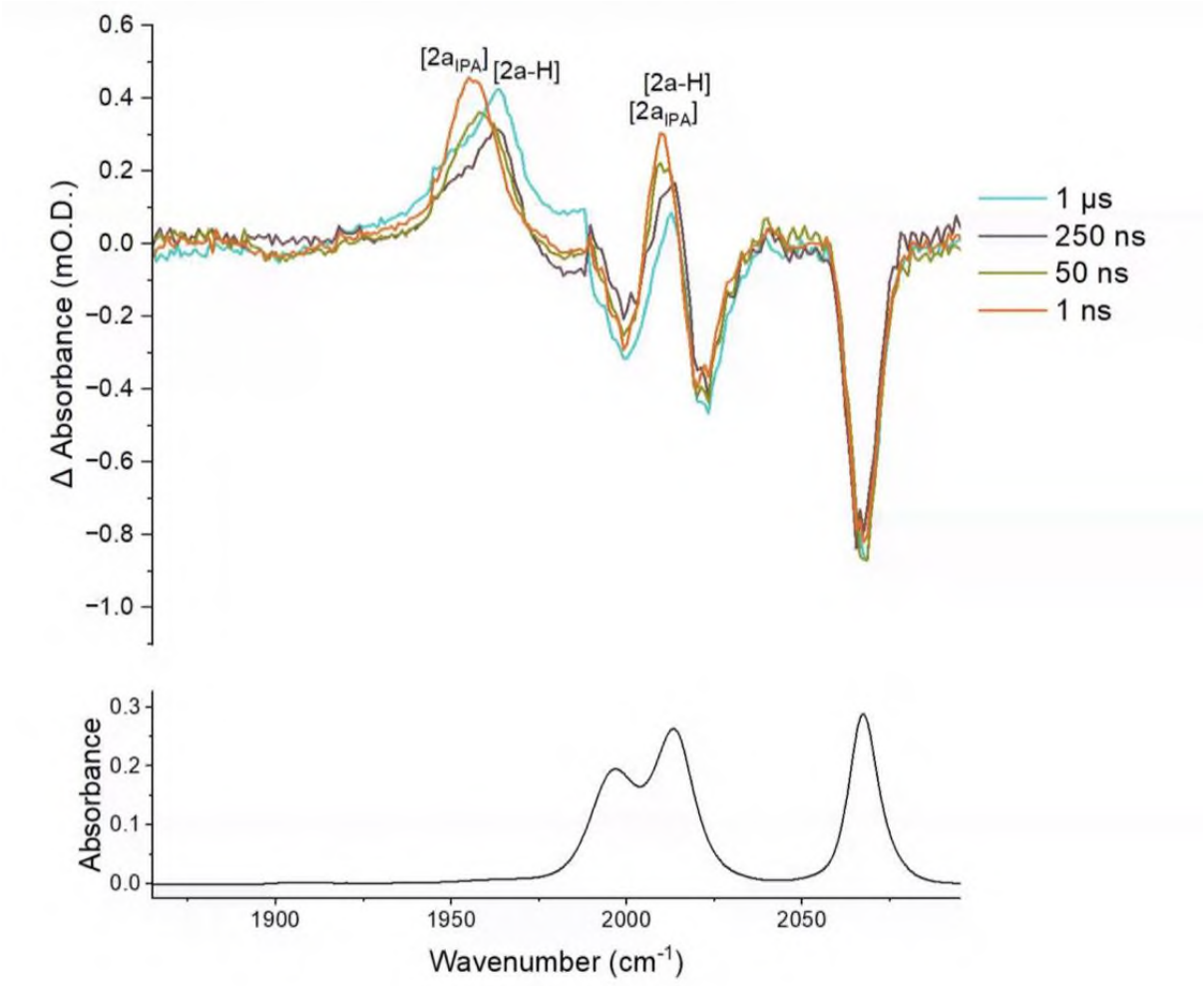

Figure 53. (Top) TRIR spectra of the 330 nm photolysis of the metal carbonyl region of [1a] at selected later pump-probe delays in IPA. The positive bands of [2a$_{IPA}$] represents the solvent coordinated complex. (Bottom) Ground state IR spectrum of [1a] in IPA.

At 1 ns two positive bands are observed at 1955 cm^{-1} and 2009 cm^{-1}, at ~250 ns these bands have shifted to the right and are now observed at 1963 cm^{-1} and 2013 cm^{-1}. These bands stay in the same position for the rest of the experiment. Because these peaks shift to the right, it is caused by the loss of the C=O peak, consistent with transfer dehydrogenation of H_2 from IPA to the metal. As the peak at 1 ns is getting smaller this persisted for the rest of the experiment.

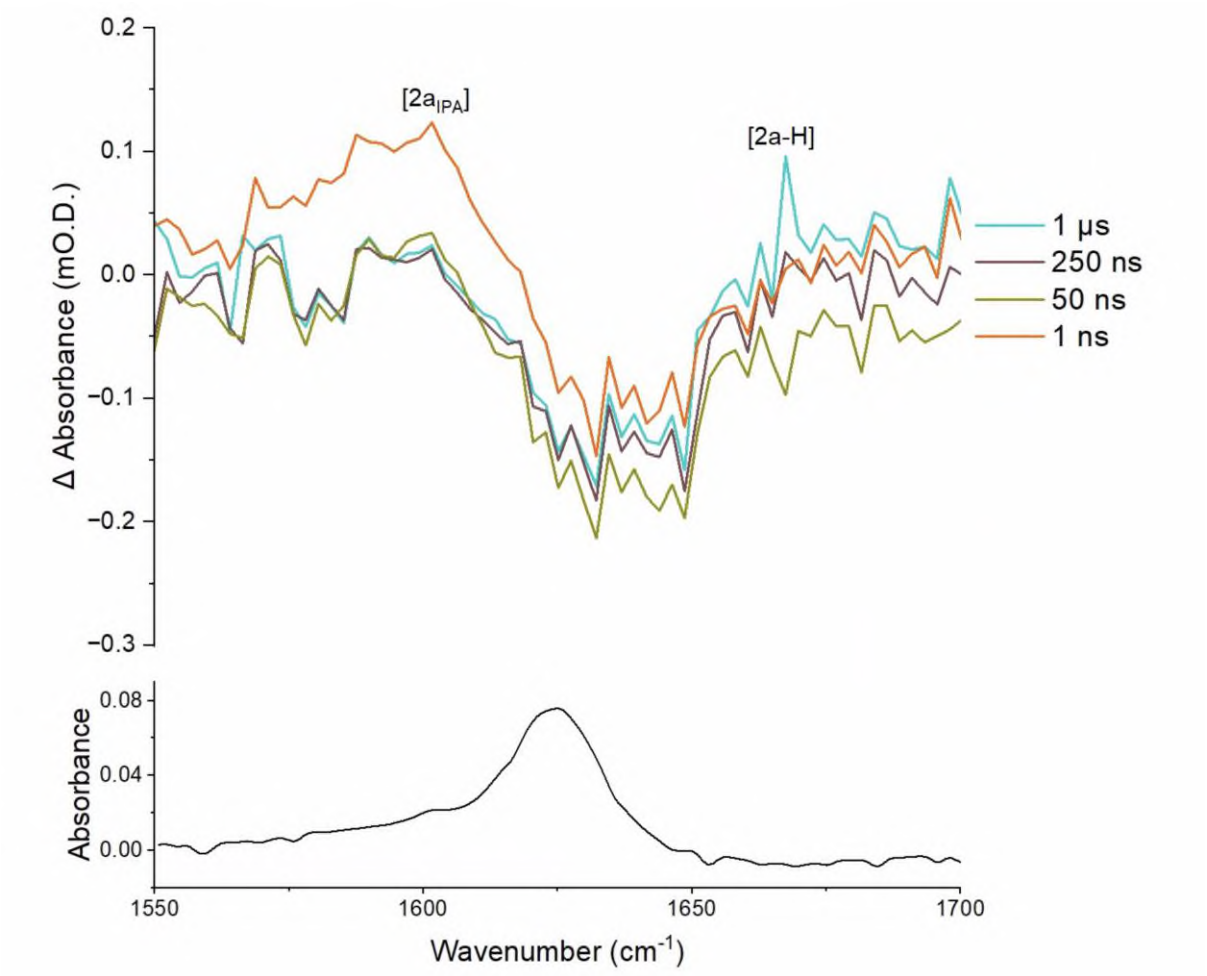

Figure 54. (Top) TRIR spectra of the 330 nm photolysis of the organic carbonyl region of [1a] at selected later pump-probe delays in IPA. The positive band of [2a$_{IPA}$] represents the solvent coordinated complex. (Bottom) Ground state IR spectrum of [1a] in IPA.

At 1 ns a positive band is observed at 1601 cm^{-1}, at 250 ns this band shifts to 1571 cm^{-1}. At 1 µs this band shifts to 1667 cm^{-1} and stays at this position for the rest of the experiment. As the bands after 1 ns decrease it is caused by the loss of the C=O peak consistent with transfer dehydrogenation of H_2 from IPA to the metal, whilst there is a positive peak at 1667 cm^{-1} most likely from poor signal-to-noise ratio in the special region. A proposed mechanism is shown in Scheme 41.

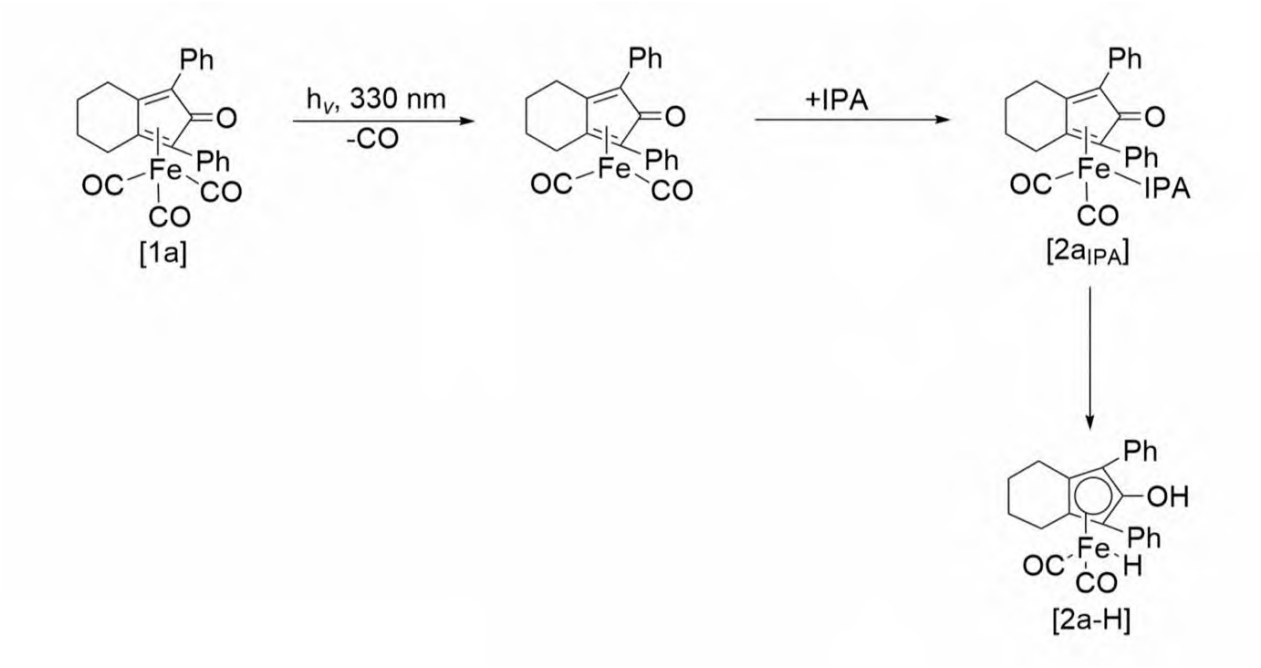

Scheme 41. Proposed mechanisn for the photolysis of [1a] in IPA.

3.1.6 Tetrahydrofuran

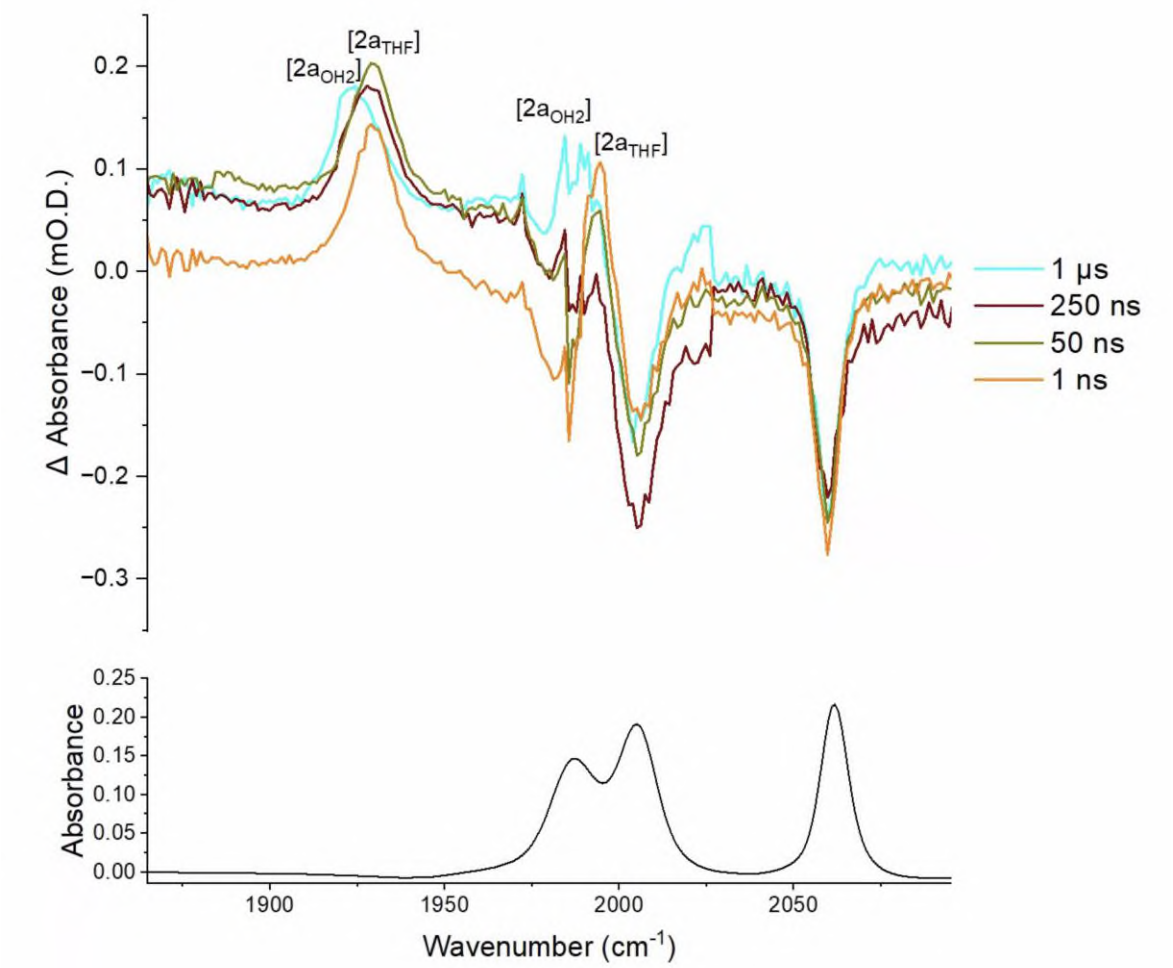

Figure 55. (Top) TRIR spectra of the 330 nm photolysis of the metal carbonyl region of [1a] at selected later pump-probe delays in THF. The positive bands of [2a$_{THF}$] represents the solvent coordinated complex. (Bottom) Ground state IR spectrum of [1a] in THF.

At 1 ns two positive bands are observed at 1928 cm^{-1} and 1994 cm^{-1}. These bands stay within the same band position until 250 ns, the band at 1994 cm^{-1} shifts to 1984 cm^{-1}. At 1 μs the band at 1928 cm^{-1} shifts to 1923 cm^{-1}. These bands are then seen for the rest of the experiment. The bands observed at 1 ns are assigned to the THF coordinated complex [2a$_{THF}$] and at 1 μs shift to a lower wavenumber as seen in CPME and this was assigned to the aqua complex [2a$_{OH2}$] and persisted for the rest of the experiment. A proposed mechanism is shown in Scheme 42.

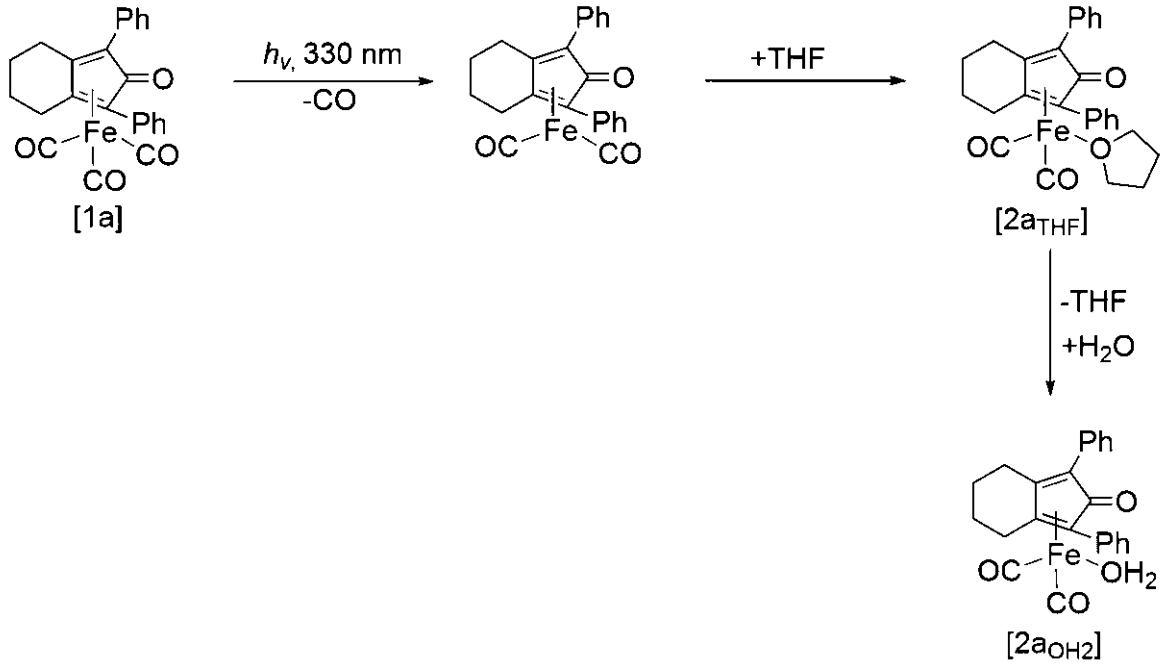

Scheme 42. Proposed mechanism for the photolysis of [1a] in THF.

3.1.7 Toluene

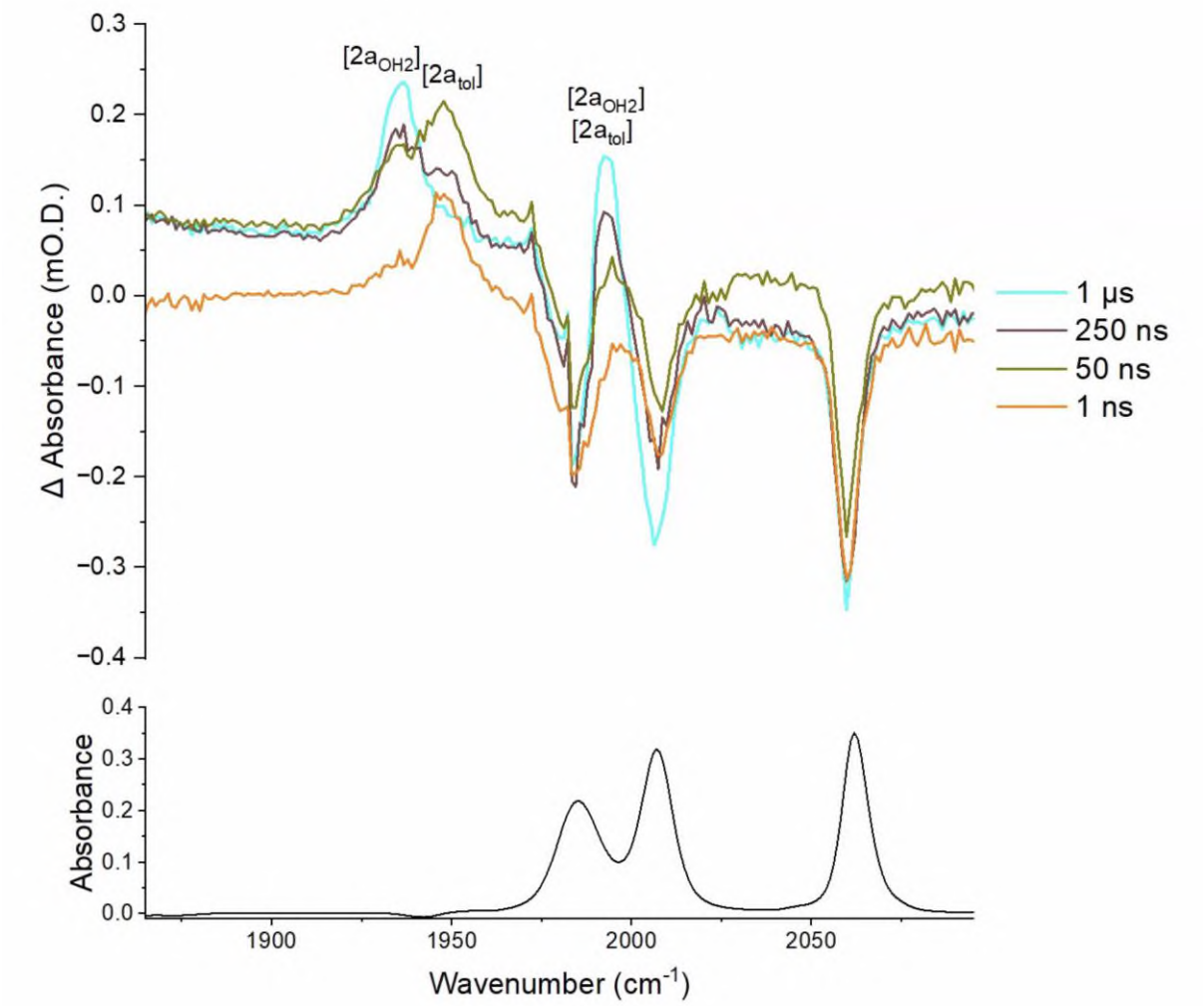

Figure 56. (Top) TRIR spectra of the 330 nm photolysis of the metal carbonyl region of [1a] at selected later pump-probe delays in toluene. The positive bands of [2a$_{tol}$] represents the solvent coordinated complex. (Bottom) Ground state IR spectrum of [1a] in toluene.

At 1 ns two positive bands observed at 1945 cm^{-1} and 1994 cm^{-1}. These bands stay within the same band position until 250 ns, the band at 1945 cm^{-1} shifts to 1936 cm^{-1}. These bands are then for the rest of the experiment. The bands at 1945 cm^{-1} and 1994 cm^{-1} were assigned to the toluene coordinated complex [2a$_{tol}$], however as seen in other solvent systems such as CPME, NCMe and THF, these bands shift to a lower wavenumber this was assigned to the aqua complex [2a$_{OH2}$] and persisted for the rest of the experiment. A proposed mechanism is shown in Scheme 43.

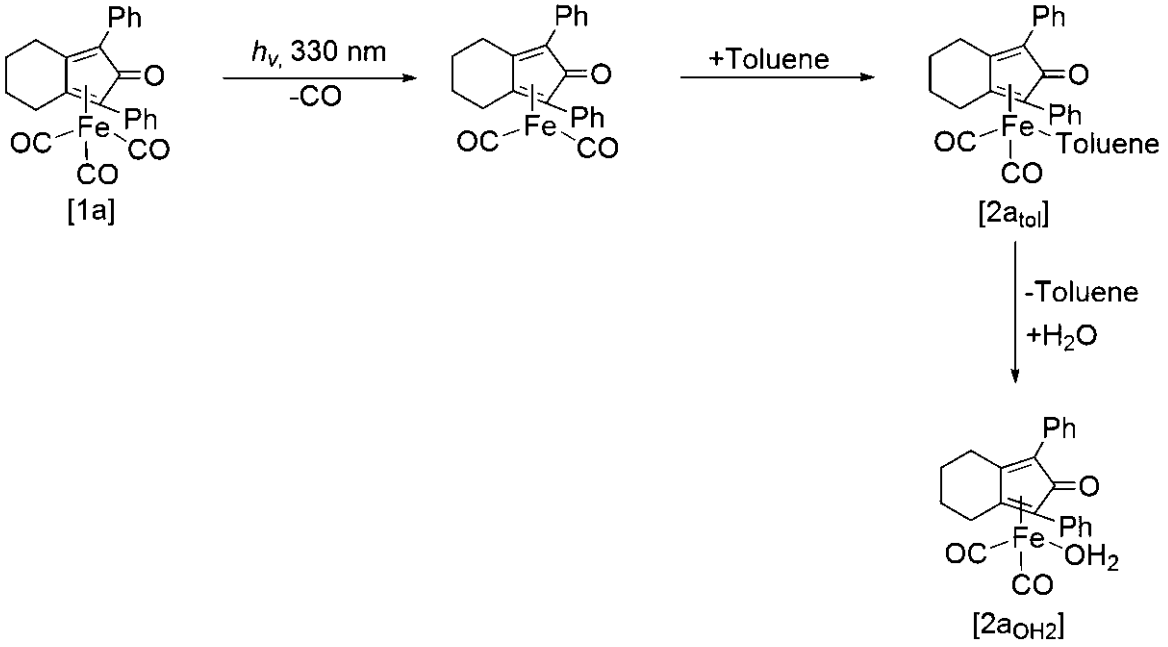

Scheme 43. Proposed mechanism for the photolysis of [1a] in toluene.

3.1.8 Summary of later pump-probe delays

Observing the TRIR data at later pump-probe delays (1 ns–1 ms) showed that at 1 ns the positive peaks are overlapping with the peaks observed at 200 ps shown in chapter 2. Notably the peaks of the TRIR in acetone stayed in the same positions throughout the duration indicating the [2a$_{Acetone}$] is present throughout the entire experiment. In five of the seven solvents, between 50 ns to 25 μs the IR bands shift to a lower wavenumber indicating the formation of the aqua complex [2a$_{OH2}$] and this persisted for the rest of the experiment. In the case of isopropyl alcohol the bands shifted to a higher wavenumber indicating a loss of the C=O peak, this is consistent with transfer dehydrogenation of H_2 from IPA to the metal. To conclude, geminate recombination happens within the ps timescale and in most cases the formation of the aqua complex occurs except with acetone and IPA.

[3a] was also studied using TRIR in acetone, acetonitrile, CPME, IPA, THF and toluene (heptane was unsuccessful as the sample didn't fully dissolve). The behaviour of [3a] in these solvent systems had the same behaviour as [1a] however, the rate of conversion was slower with [1a], this is observable in NCMe. When looking at [1a] in NCMe at 25 μs the peak shifts to a lower wavenumber indicating the formation of the aqua complex, however when studying [3a] there is a shift to a lower wavenumber at 10 μs indicating the formation of the aqua complex.

Two tables with the observed bands in the seven solvents and the bleach recovery percentages of both iron complexes is shown below. All the TRIR spectra for the early and longer pump-probe delays of [3a] are shown in the appendix.

Solvent	Complex	Observed bands (cm^{-1})	Bleach recovery (%)	Complex	Observed bands (cm^{-1})	Bleach recovery (%)
Acetone	[$2a_{acetone}$]	1949 & 2004	19.0	[$4a_{Acetone}$]	1945 & 2003	18.3
Acetonitrile	[$2a_{NCMe}$]	1954 & 2010	17.4	[$4a_{NMCe}$]	1613, 1965 & 2009	19.7
CPME	[$2a_{CPME}$]	1632, 1947 & 2003	14.0	[$4a_{CPME}$]	1632, 1947 & 2003	13.6
Heptane	[$2a_{hept}$]	1955 & 2001	8.4	N/A		
IPA	[$2a_{IPA}$]	1601, 1956 & 2010	20.7	[$4a_{IPA}$]	1601, 1955 & 2010	19.2
THF	[$2a_{THF}$]	1936 & 1994	24.8	[$4a_{THF}$]	1627, 1945 & 1999	17.0
Toluene	[$2a_{tol}$]	1948 & 2000	18.1	[$4a_{tol}$]	1594, 1962 & 2007	12.9

Table 7. Observed TRIR bands for the metal and organic carbonyl vibrations at the end of the early pump-probe delays, along with the bleach recovery percentages of both iron complexes.

Solvent	Complex	Observed bands (cm^{-1})	Complex	Observed bands (cm^{-1})
Acetone	[$2a_{acetone}$]	1945 & 2001	[$4a_{Acetone}$]	1945 & 2001
Acetonitrile	[$2a_{NCMe}$]	1940 & 2035	[$4a_{NMCe}$]	1667, 1960, and 2043
CPME	[$2a_{CPME}$]	1620, 1940, and 1996	[$4a_{CPME}$]	1620, 1940, and 1996
Heptane	[$2a_{hept}$]	1945 & 2000	N/A	
IPA	[$2a_{IPA}$]	1963 & 2012	[$4a_{IPA}$]	1561, 1963 & 2013
THF	[$2a_{THF}$]	1923 & 1984	[$4a_{THF}$]	1613, 1945 & 1999
Toluene	[$2a_{tol}$]	1936 & 1992	[$4a_{tol}$]	1953 & 2002

Table 8. Observed TRIR bands for the metal and organic carbonyl vibrations at the end of the later pump-probe delays for both iron complexes.

4. Conclusions and Future Work

The research within this thesis has focused on analysing and understanding the mechanistic processes of two iron carbonyl complexes. Nearly all the TRIR experiments of the early pump-probe delays, intense bleach peaks over the period of 2 to 200 ps decrease in negative intensity this was due to electronically excited state ^{3}[1a], this was followed by the dissociation of a CO ligand as observed in section 1.6, discussing that light induced reactions of metals carbonyls either have photo dissociation or release of the CO and they are rapid and occur on the picosecond timescale of absorption by light, this is evident that at 50 ps in the TRIR data as there is two positive peaks showing two CO ligands and remain in this position for the rest of the early time delays and because these peaks didn't shift geminate recombination occurred and the solvent attached. When Knölker and co-workers[26] irradiated an iron carbonyl complex with a 150 W medium-pressure mercury lamp to trigger the exchange of a CO ligand to the acetonitrile coordinated to the site previously occupied by the CO ligand.

Interestingly, when observing the TRIR data at later pump-probe delays acetone has the same position as the early pump-probe delays and stayed in this position for the rest of the experiment. In the case of (CPME, IPA, NCMe, THF and toluene) at 50 to 250 ns the peaks would shift approximately 5 to 10 cm^{-1} in wavenumber. Because CPME, heptane, NCMe, THF and toluene all shifted to a lower wavenumber these were assigned to the aqua complex [$2a_{OH2}$]. The case of CPME and THF were surprising, while heptane and toluene as expected: previous research done in the group found [$2a_{OH2}$] is more thermodynamically favourable than [$2a_{hep}$] and [$2a_{tol}$] however is less stable than [$2a_{NCMe}$] and [$2a_{THF}$].[41] One possible explanation is that even though dry solvents were used for every TRIR experiments there is still trace amounts of water present. In the case of IPA transfer dehydrogenation of H_2 from IPA to the metal occurs, a similar situation occurs in section 1.3, figure 3 in the study done by Casey *et* al.[17]

IR_{PUMP}-IR_{PROBE} was employed because it is a pump-probe method that instead of the sample undergoing a thermal reaction by photolysis. Instead, it was used to study the vibrational dynamics solvent interactions of the carbonyl ligand stretching vibrational modes of [1a] in (acetone, heptane and THF). This study was used to investigate the vibrational modes of [$Mn(CO)_{10}$].[45]

These vibrational modes are close within the lifetimes obtained from the excited state of the TRIR samples. The negative peaks go from v = 0 → 1 and the positive bands are between v = 1 → 2 bands. This provided evidence that the bands observed at the end of the early pump-probe delays is the solvent coordinated complex as the positive bands in IR_{PUMP}-IR_{PROBE} spectrum showed the "hot bands" have different peak positions.

Comparing the IVR vibrational modes of [$Mn_2(CO)_{10}$] in heptane was 0.50 ± 0.02 comparing that to 2.1 ± 0.7, 4.6 ± 1.6 and 7.6 ± 1.4 vibrational modes of [1a], means that [$Mn_2(CO)_{10}$] is faster than the IVR of [1a]. For the T_1 of [$Mn_2(CO)_{10}$] the vibrational modes were 165 ± 2 and 200 ± 4 comparing that to 44.5 ± 2.5, 40.9 ± 1.3, 43.4 ± 2.1, 42.4 ± 2.0, 39.4 ± 1.3, 28.5 ± 1.1 and 39.8 ± 2.1. The T_1 vibrational modes of the [$Mn_2(CO)_{10}$] is slower when comparing the T_1 of [1a]. For the IVR of [$Mn_2(CO)_{10}$] in THF was 0.67 ± 0.03 comparing that to 1.5 ± 0.7 and 4.8 ± 2.4 of [1a],

means that $[Mn_2(CO)_{10}]$ is faster than the IVR of [1a]. For the T_1 of $[Mn_2(CO)_{10}]$ the two vibrational modes were 113 $\pm$ 2 and 123 $\pm$ 8 comparing that to 34.3 $\pm$ 1.3, 37.6 $\pm$ 0.5, 35.3 $\pm$ 0.6 and 37.0 $\pm$ 0.8. The T_1 of the $[Mn_2(CO)_{10}]$ is slower when comparing the T_1 of [1a]. Acetone was not a solvent chosen in literature studies however based on the IR_{PUMP}-IR_{PROBE} data the values of IVR and T_1 are similar to [1a] in THF and the T_1 values for [1a] in heptane are slower. In a previous literature, a scenario was discussed, detailing that the vibrational modes could potentially relax through an intramolecular route. Notably, having a large organic carbonyl ligand possess a substantial amount of low-frequency modes which could contribute to an increased amount of channels for vibrational relaxation. This is potential reason the incredibly rapid relaxation times and the intensity of the relaxation time scale to the nature of the solvent system, obtaining values within a range of 28-44.5 ps measured across the three solvents studied.

Solvent coordination to metal carbonyl complexes affects their reactivity by occupying coordination sites, stabilising intermediates, altering electron density at the metal centre and influencing the rate of ligand substitution, this is because coordinated solvent molecules act as a liable ligand that can either stabilise or when they are too strong, can deactivate the metal centre.[49,50] One example is the photochemical excitation of $Cr(CO)_6$ creates CO dissociation, this leads to the formation of a transient, unsaturated $Cr(CO)_5$ species which coordinates to the solvent molecule (THF). The solvent coordinated species $Cr(CO)_5$(Solvent), acts as the short-lived intermediate, that coordinates through the oxygen in polar solvents or C-H bonds in alkanes, and is necessary for ligand substitution reactions. One very noticeable similarity is that CO dissociation occurs at a rapid timescale (reference of 100 fs) meaning geminate recombination occurs at a rapid timescale. When using transient UV-absorption spectroscopy, the time constant for the formation of the σ-complex was defined as a mean 8.2 $\pm$ 0.4 ps and a slower time constant of 53 $\pm$ 12 ps. What is observed is that the time constants for [1a] is faster than the bi-exponential fits of $Cr(CO)_6$.[44] These insights can help us to design better catalysts because ultrafast laser spectroscopy analyses how solvent-assisted relaxation affects the excited state lifetimes and nonadiabatic dynamics of the iron complex, this permits for optimisation of photochemical pathways.[51] Another way is to help develop a better understanding of the “on-cycle” of iron hydride against the “off-cycle” solvent addicts permitting for designing iron catalysts for hydrogenation, thus making sure that the active unsaturated species is available.[52]

For future work, as previously mentioned geminate recombination occurs in rapid timescales (femtosecond to picosecond), TRIR could be used to study timescales in the femtosecond region however the vibrational coherence is longer than the femtosecond timescale meaning there is nothing observable. One method that could be useful to observe geminate recombination is known as Transient absorption spectroscopy (TA), this technique can cover the dynamic range in charge generation, for both geminate and non-geminate reactions that occur at sub-100 fs and can go past microseconds.[53,54] In a research paper published in 2018[55] discussed a specific setup that was used in their experiments to analysis a wide temporal (fs to μs) along with a spectral range of (350 nm to 1600 nm) along with the use of methods such as multivariate curve resolution that is used to analyse spectra composed of various components and obtains the component-associated spectra and the dynamics.[56] By using this technique on the iron carbonyl complexes will help

gain a better understanding of these reactions within a femtosecond timescale and aid in making more accurate predictions.

5. Experimental Section

5.1 Experimental details

Both iron compounds were by prepared by a previous MSc by Research student. All solvents were purchased from Sigma Aldrich and used as received unless stated otherwise.

5.2 Preparation of the LIFEtime samples

All solvents used were freshly opened and kept under a sure-seal bottle under nitrogen. All samples were prepared in a sealed Duran bottle and degassed with argon for 20 minutes. Solutions were prepared at a concentration of approximately 190 μM for [3a] and 2.34 mM for [1a], unless stated otherwise. During the experiment, the bottle was kept under a positive pressure of argon and light was excluded. The bottle was connected to a Harrick cell fitted with a 250 μm spacer and flowed through the cell using a perstalic pump. During the experiment the cell was rastered in the path of the beam.

5.3 Preparation of the IR_{PUMP}-IR_{PROBE} samples

25 mg of [1a] was dissolved in 1 mL of three solvents (acetone, heptane and THF), this level of concentration was used to ensure that the maximum absorbance of the ν_{CO} bands were over 0.3 depending on the solvent, this concentration was used to get a measurement of both the metal and organic carbonyl region typical concentrations are usually 0.6-0.9 OD, however because of a low quantity of sample available 0.3 OD was agreed.

5.4 IR spectroscopy

Ground states spectra were recorded at room temperature on a Bruker Vertex 70 spectrometer with a spectral resolution of 1 cm^{-1}, solution of approximately 1.91 mM and 2.34 mM were made up and injected into a standard transmission cell (Harrick), with two CaF_2 windows that are separated using a PTFE spacer of 150 μm thickness.

5.5 IR spectroscopy measurements for IR_{PUMP}-IR_{PROBE}

IR_{PUMP}-IR_{PROBE} experiments were performed using a regeneratively amplified Ti:sapphire laser system that produced mid-IR pulses via difference frequency mixing of the signal and idler beams produced by using an optical parametric amplifier (OPA). The central frequency of the mid-IR pulses was selected to be resonant with the vibrational modes of [1a]. The pulse had a bandwidth of 200 cm^{-1}, 100 fs pulse duration, and were generated with a repetition rate of 1 kHz. The output of the OPA was split using a CaF_2 beam splitter to give pump and probe pulses. The two beams were overlapped spatially in the sample, and the pump-probe delay time was controlled through a optical delay line. After the sample, the probe beam was frequency dispersed using a spectrograph and detected using a 64 channel mercury cadmium telluride (MCT, HdCdTe) array detector giving a probe frequency resolution of 4.5-5 cm^{-1}. For data acquisition the pump bream was cut off at 500 Hz to permit the collection of $pump_{on}$-$pump_{off}$ difference spectra. The delay time was scanned from -5 to 800 ps.

5.6 Time-Resolved Infrared Spectroscopy (LIFEtime)

Time-Resolved Infrared (TRIR) Spectroscopic experiments were performed at the Central Laser Facility (Science & Technology Facilities Council (STFC), Rutherford Appleton Laboratories, Oxfordshire, UK) using Time-Resolved Multiple Probe Spectroscopy (TR^MPS) at the ULTRA facility. Experiments were driven by 100 kHz repetition rate Yb:KGW amplifier (Pharos) as pump source, producing 260 fs pulses at 1030 nm. The laser output was used to pump a BBO-based 515 nm pumped Optical Parametric Amplifier (OPA). The pump beam was collimated, travelled along a programmable optical delay line (0-16 ns 1200 mm long double pass), then focused onto the sample. The probe beam sources from a 100 kHz repetition rate Yb:KGW amplifier (Pharos) providing 6 W, 180 fs pulses at 1030 nm, this drove two 3 W BBO/KTA based OPAs. The two Pharos sources shared an 80 MHz oscillator, allowing pump-prove delay steps of 12.5 ns. The probe beam was split to provide probe and reference pulses. The probe beams were collimated, synchronised by a fixed optical delay, and focused by a gold parabolic mirror onto the sample. The three beams were overlapped on the sample using a 50 μm pinhole. The probe beams were measured by two separate 128-element detectors. In order to go beyond 12.5 ns, subsequent seed pulses can be selected from the 80 mHz oscillator. The data were collected using pump-probe delays ranging from 1 ps to 988.5 μs.

5.7 Data Analysis

Data were exported into ULTRA VIEW v2. Appropriate peaks and spectra were identified and the desired single pixel kinetics and and spectra were exported as comma separated variable files. These files were exported into OriginPro. Pixels were converted to wavenumbers by comparing spectra of $Mnppy(CO)_4$ (metal carbonyl region) and polystyrene (organic carbonyl region) taken on the LIFEtime instrument reference spectra. Overlap between the two detectors was removed by inspection. Kinetic plots were fitted using ExpDec ($y = yo + A_1e^{-x/t_1}$) and ExpGro ($y = y_0 + A_1e^{x/t_1}$). For the IR_{PUMP}-IR_{PROBE}: baselines were created for each time-point in each experiment these were then removed from the value of the pump-probe data and averaged over the total number of runs of the experiments. The calibration of the metal carbonyls was done by using the Ground state spectrum done approximately 5-10 minutes before the experiment started and matching them with the negative bleach peaks. For the organic carbonyl region a reference known as TFA had a point of 1673 cm^{-1} and was plotted along with the peak from the organic carbonyl.

6 Appendix

6.1 Acetone

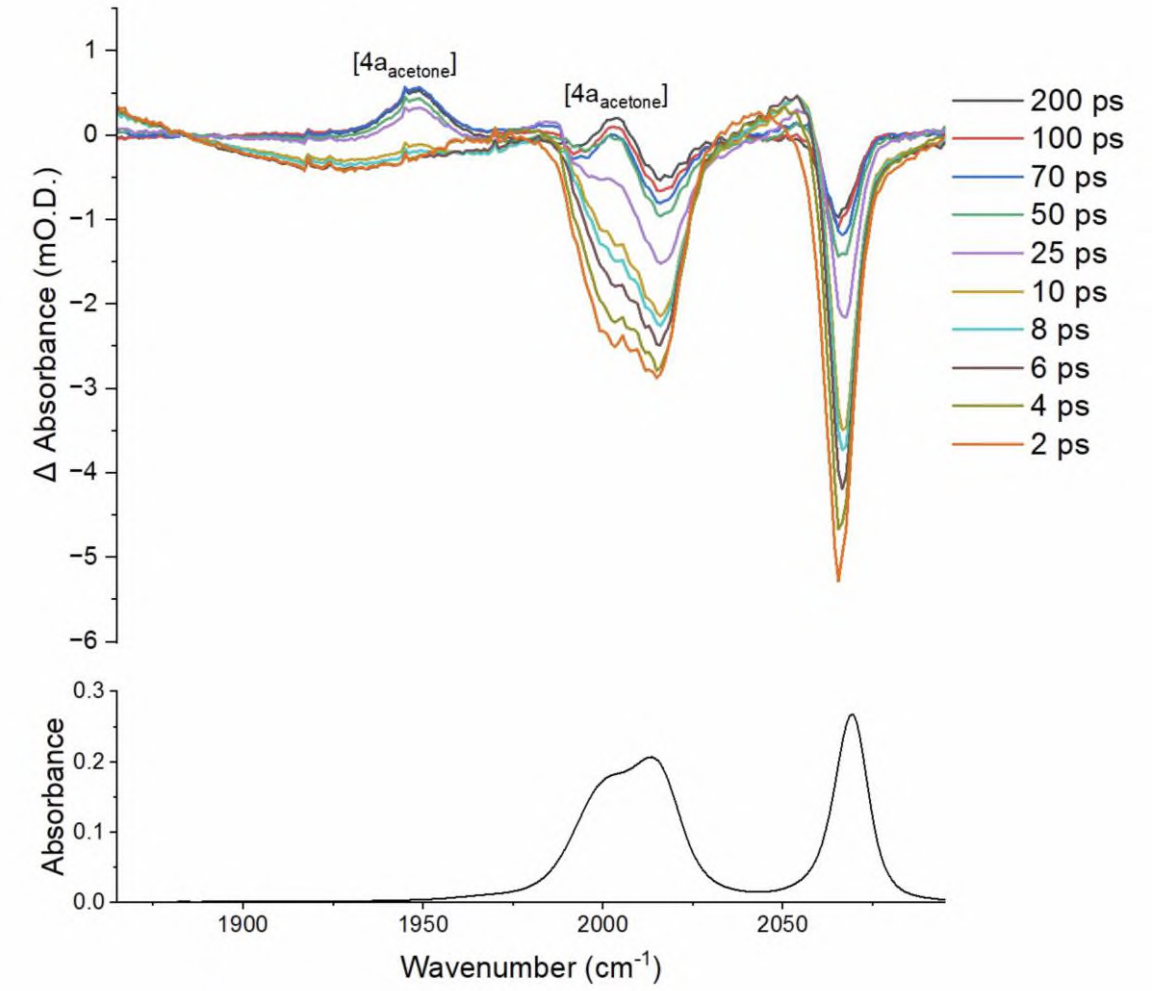

Figure 57. (Top) TIRR spectra of the 330 nm photolysis of the metal carbonyl region of [3a] at selected early pump-probe delays in acetone. The positive bands of [4a$_{acetone}$] represents the solvent coordinated complex. (Bottom) Ground state IR spectrum of [3a] in acetone.

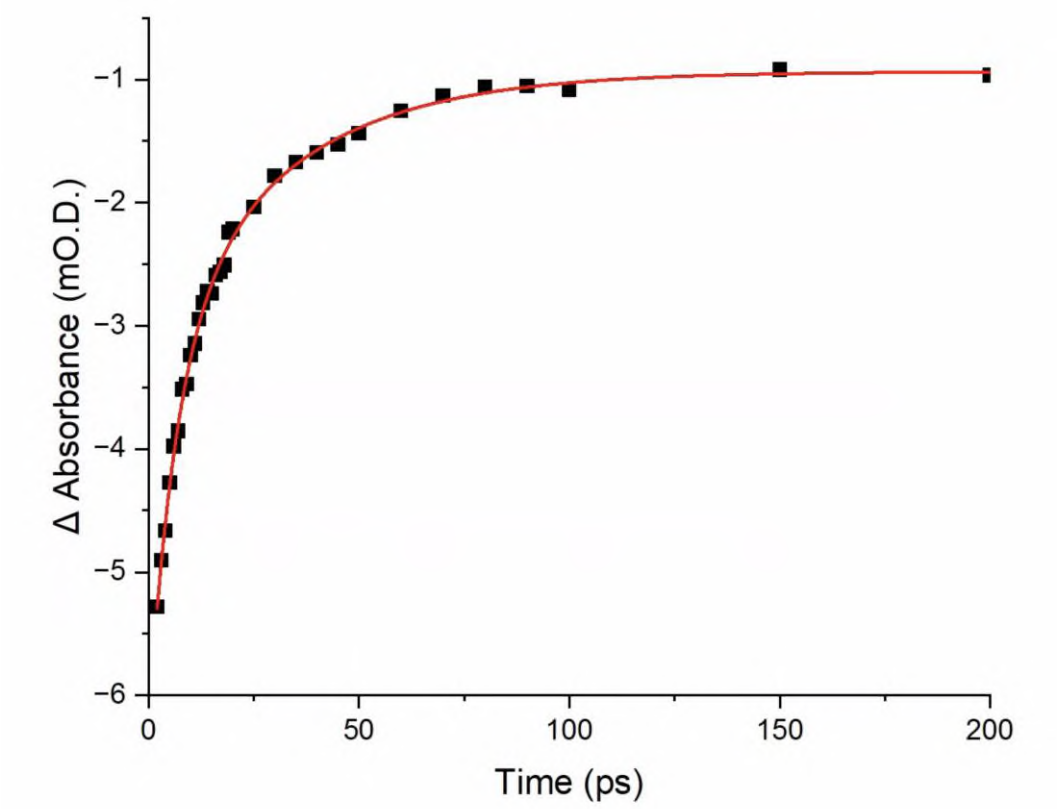

Figure 58. The change in absorbance of the bleach recovery at 2065 cm^{-1} from 2 to 200 ps. The solid red line represents a bi-exponential fit with lifetimes of 6.6 ± 0.8 ps and 31.0 ± 4.0 ps.

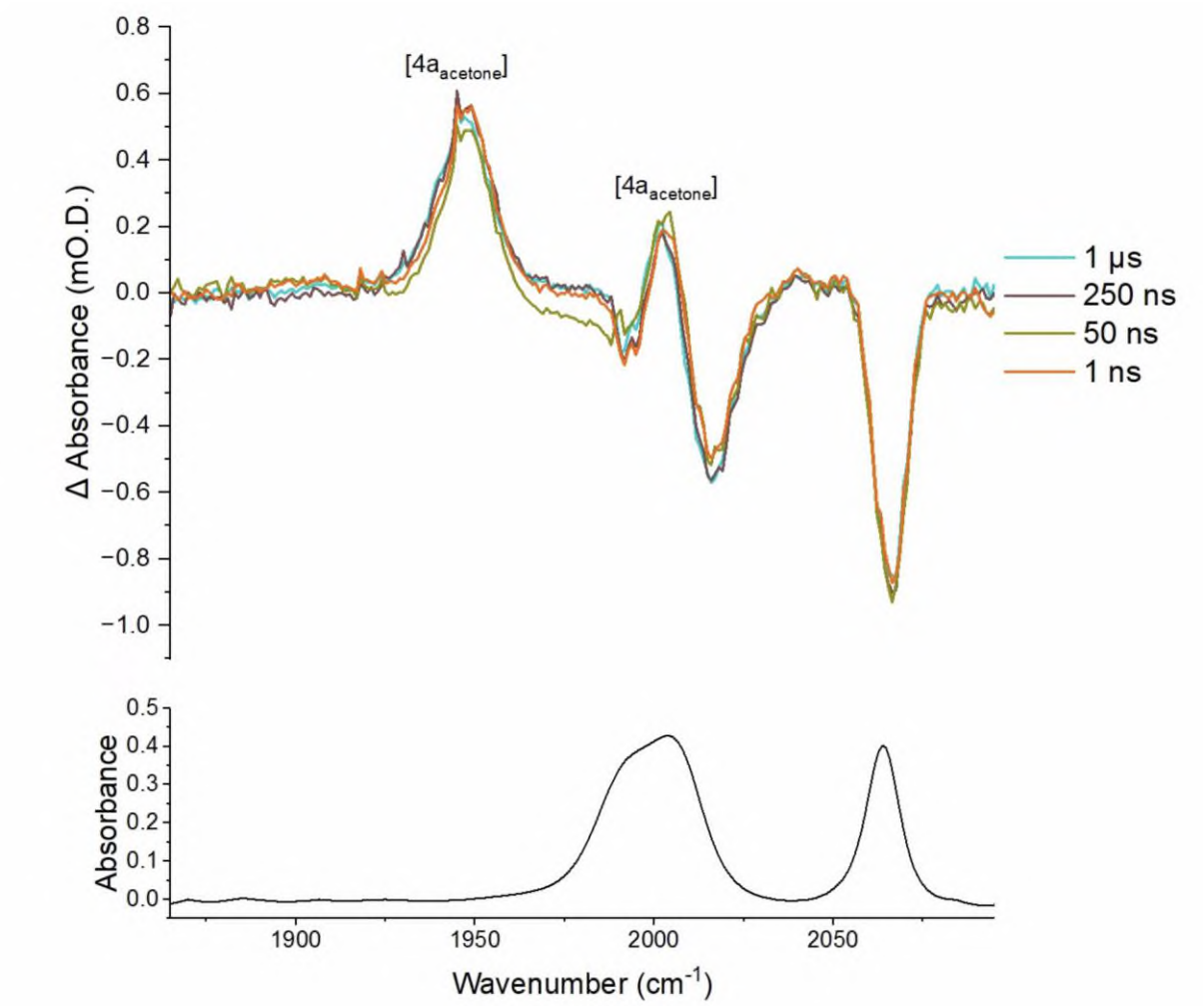

Figure 59. (Top) TRIR spectra of the 330 nm photolysis of the metal carbonyl region of [3a] at selected later pump-probe delays in acetone. The positive bands of [4a$_{acetone}$] represents the solvent coordinated complex. (Bottom) Ground state IR spectrum of [3a] in acetone.

6.2 Acetonitrile

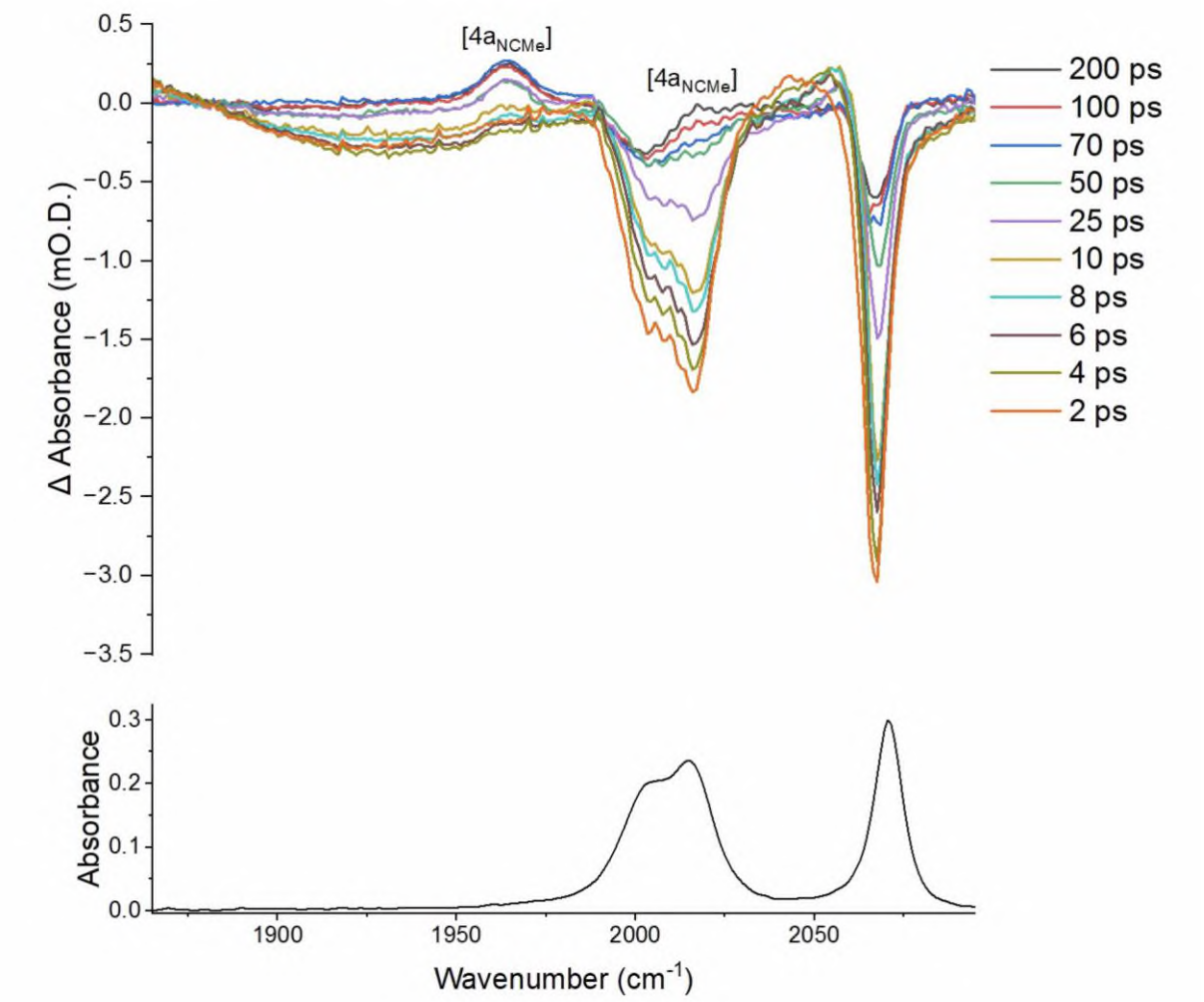

Figure 60. (Top) TRIR spectra of the 330 nm photolysis of the metal carbonyl region of [3a] at selected early pump-probe delays in NCMe. The positive bands of [4a$_{NCMe}$] represents the solvent coordinated complex. (Bottom) Ground state IR spectrum of [3a] in NCMe.

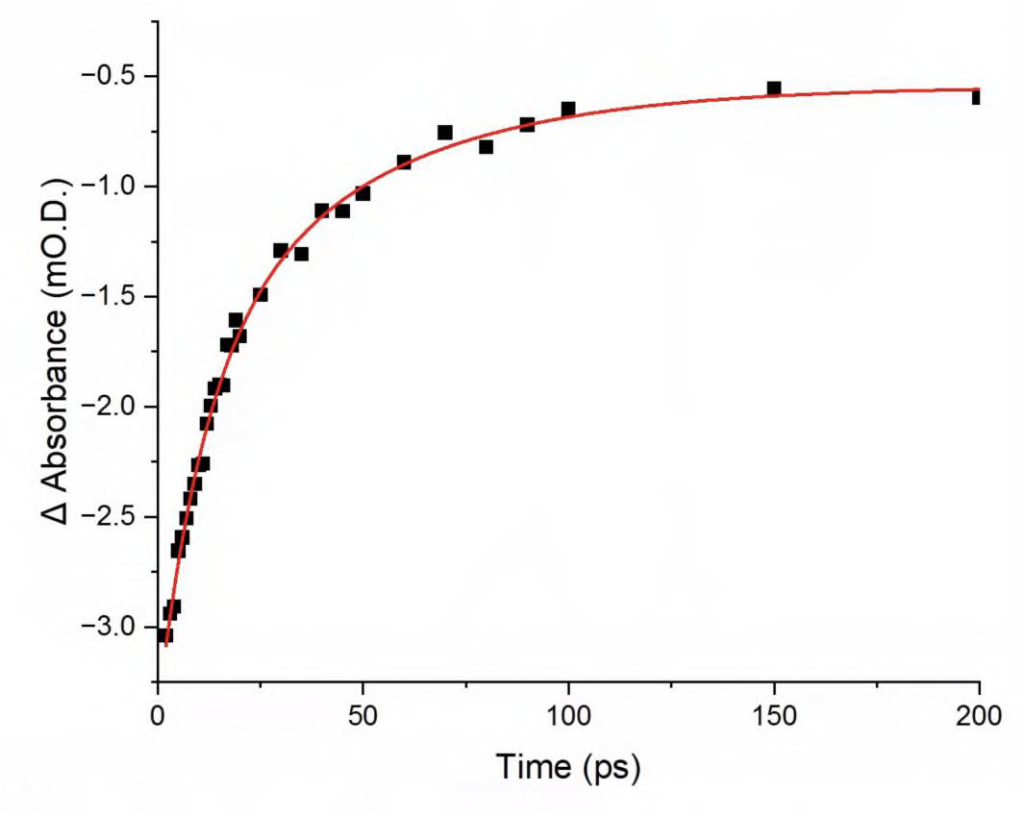

Figure 61. The change in absorbance of the bleach recovery at 2068 cm^{-1} from 2 to 200 ps. The solid red line represents a bi-exponential fit with lifetimes of 11.2 ± 2.7 ps and 43.8 ± 12.9 ps.

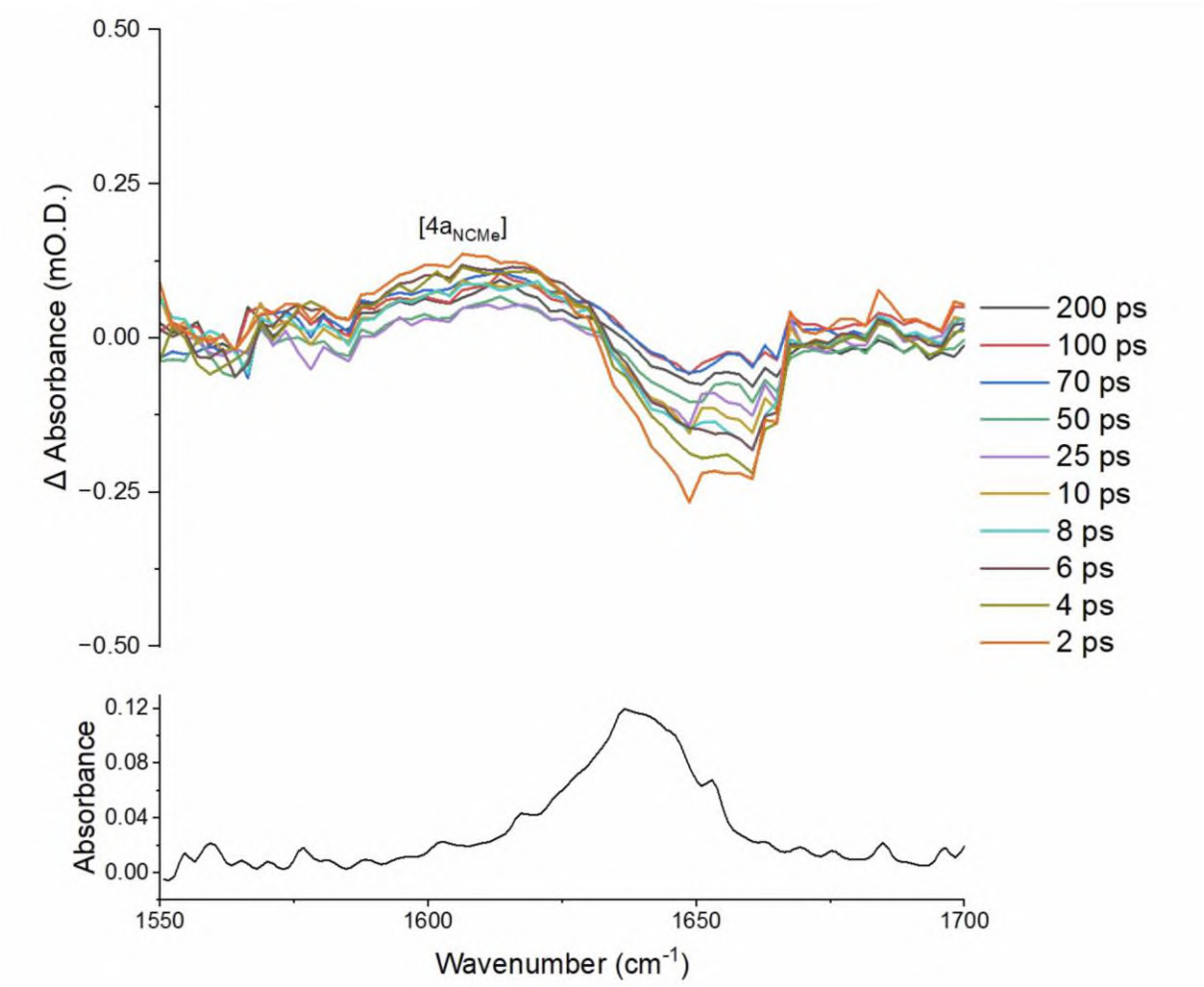

Figure 62. (Top) TRIR spectra of the 330 nm photolysis of the organic carbonyl region of [3a] at selected later pump-probe delays in NCMe. The positive band of [4a$_{NCMe}$] represents the solvent coordinated complex. (Bottom) Ground state IR spectrum of [3a] in NCMe.

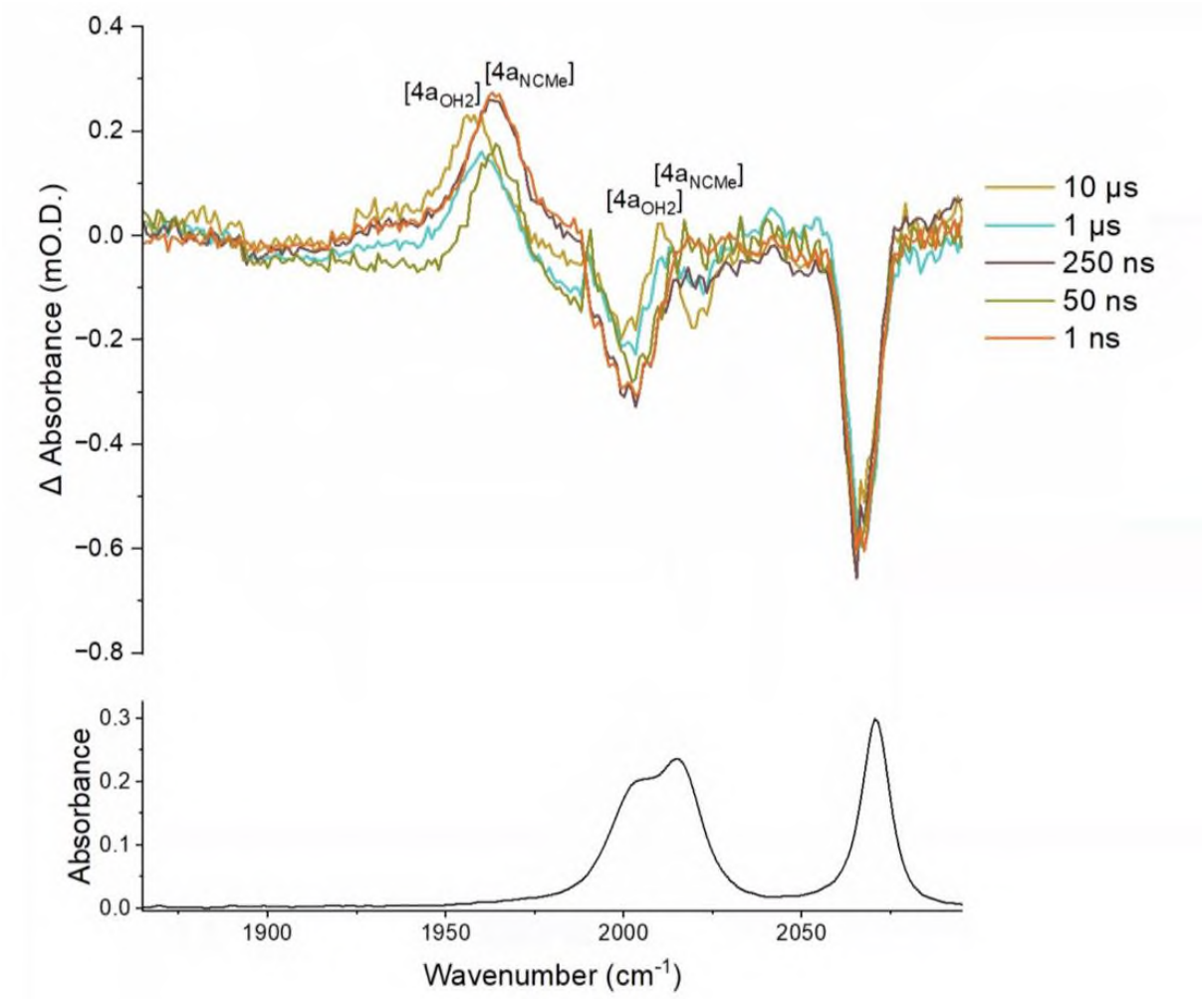

Figure 63. (Top) TRIR spectra of the 330 nm photolysis of the metal carbonyl region of [3a] at selected early pump-probe delays in NCMe. The positive bands of [4a$_{NCMe}$] represents the solvent coordinated complex. (Bottom) Ground state IR spectrum of [3a] in NCMe.

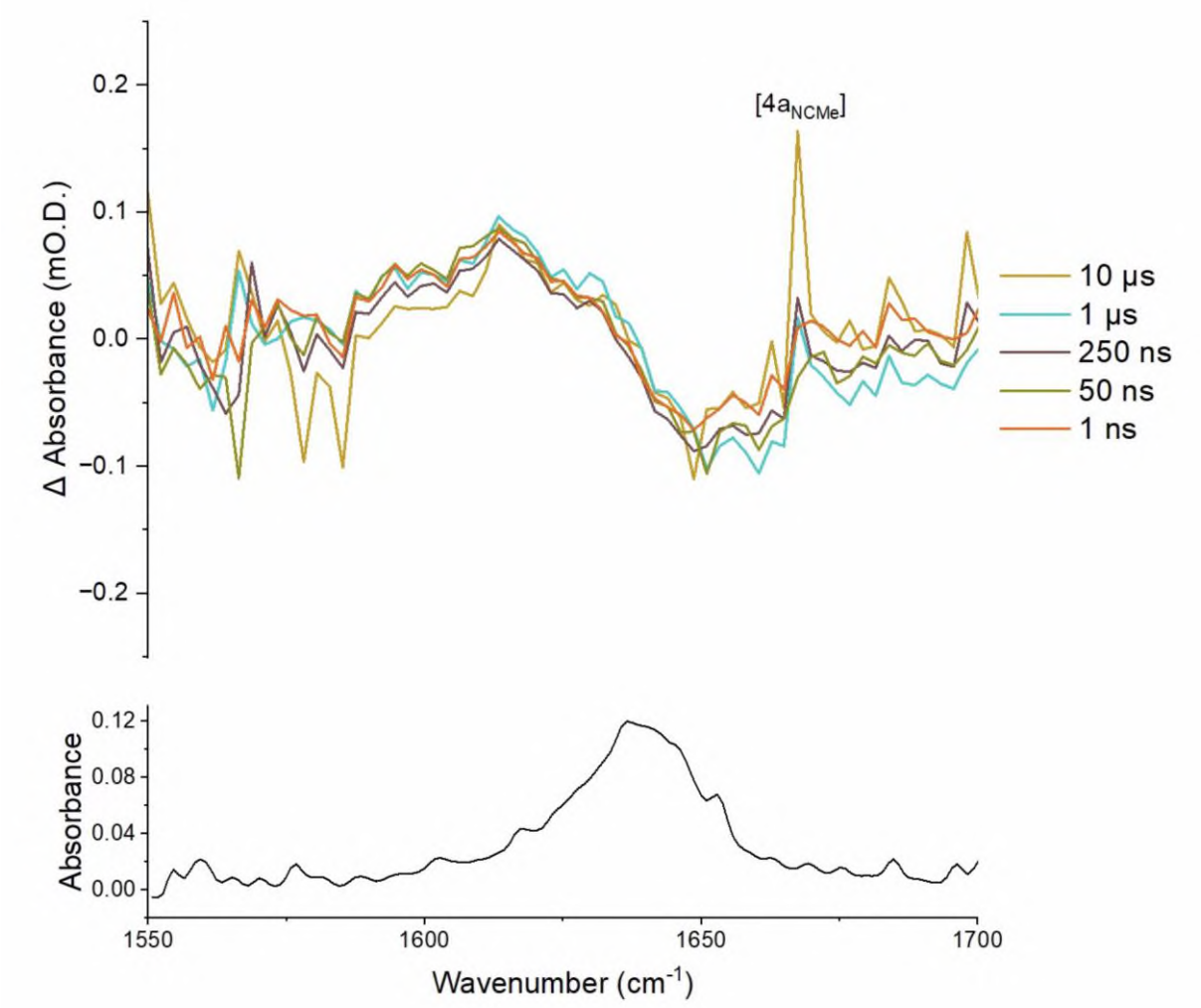

Figure 64. (Top) TRIR spectra of the 330 nm photolysis of the organic carbonyl region of [3a] at later pump-probe delays in NCMe. The positive of band of [4a$_{NCMe}$] represents the solvent coordinated complex. (Bottom) Ground state IR spectrum of [1a] in NCMe.

6.3 Cyclopentyl methyl ether

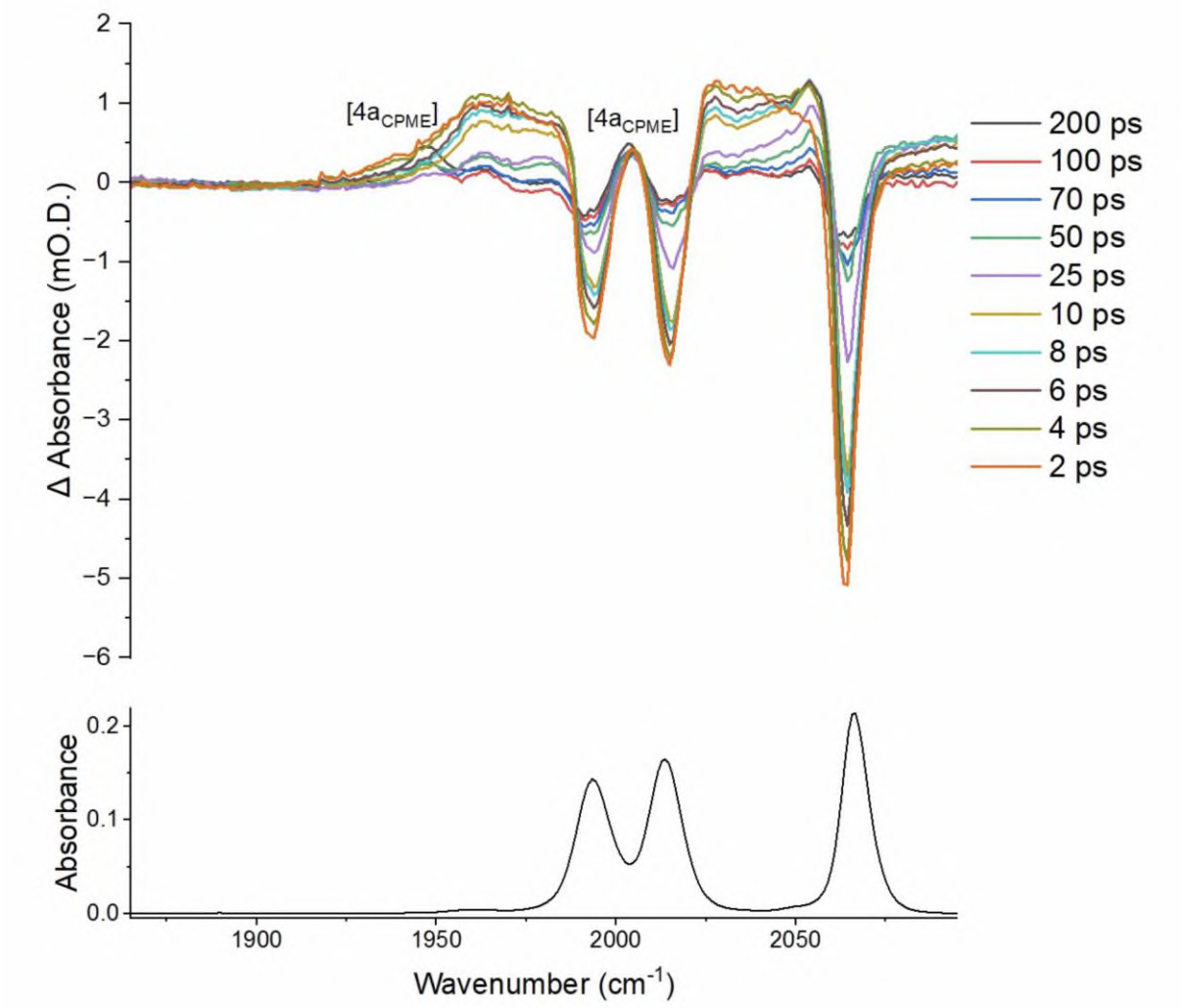

Figure 65. (Top) TRIR spectra of the 330 nm photolysis of the metal carbonyl region of [3a] at selected early pump-probe delays in CPME. The positive bands of [4a$_{CPME}$] represents the solvent coordinated complex. (Bottom) Ground state IR spectrum of [3a] in CPME.

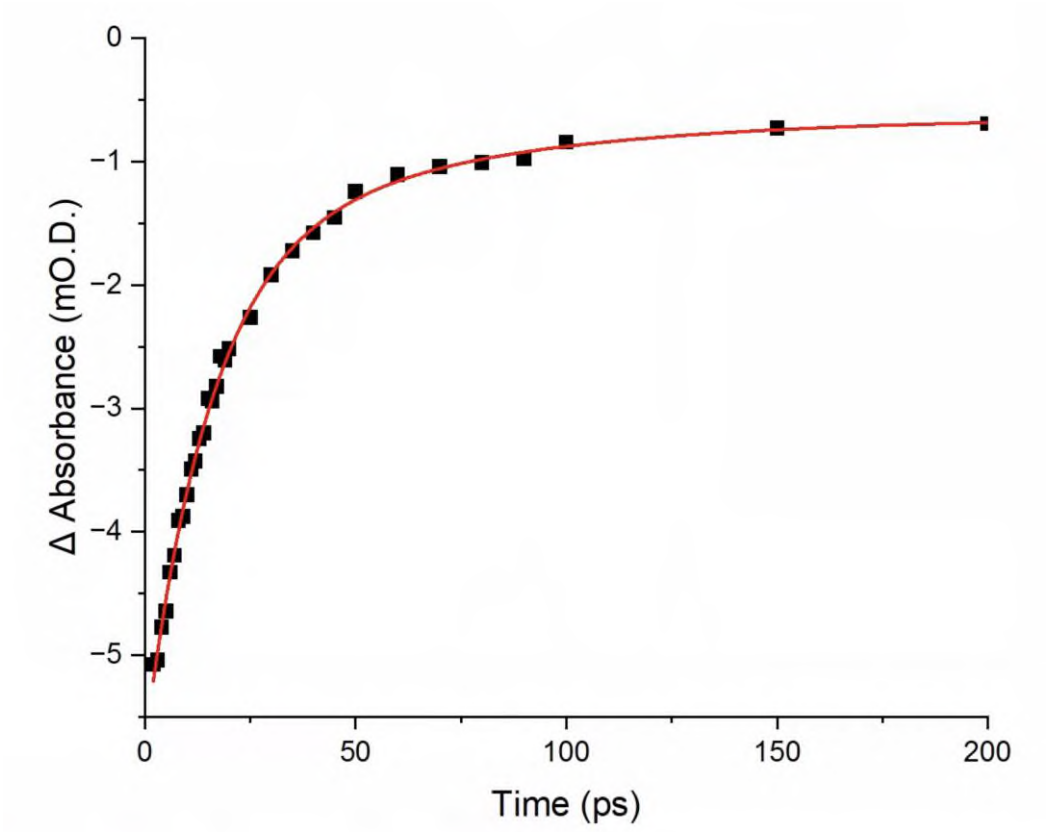

Figure 66. Change in absorbance of the excited state at 2064 cm^{-1} from 2 to 200 ps. The solid red line represents a bi-exponential fit with lifetimes of 15.3 ± 1.8 ps and 62.4 ± 38.0 ps.

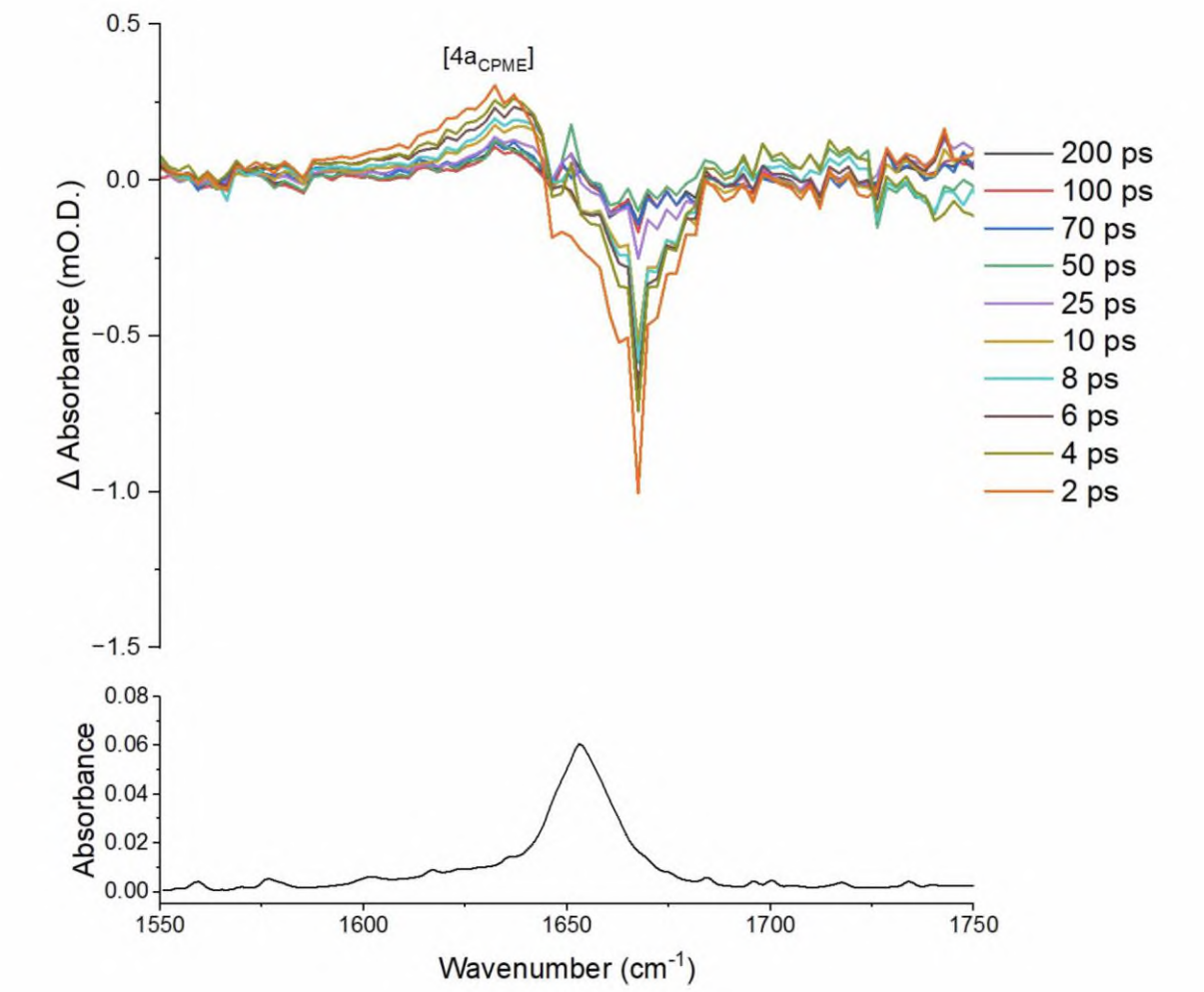

Figure 67. (Top) TRIR spectra of the 330 nm photolysis of the organic carbonyl region of [3a] at selected early pump-probe delays in CPME. The positive band of [4a$_{CPME}$] represents the solvent coordinated complex. (Bottom) Ground state IR spectrum of [3a] in CPME.

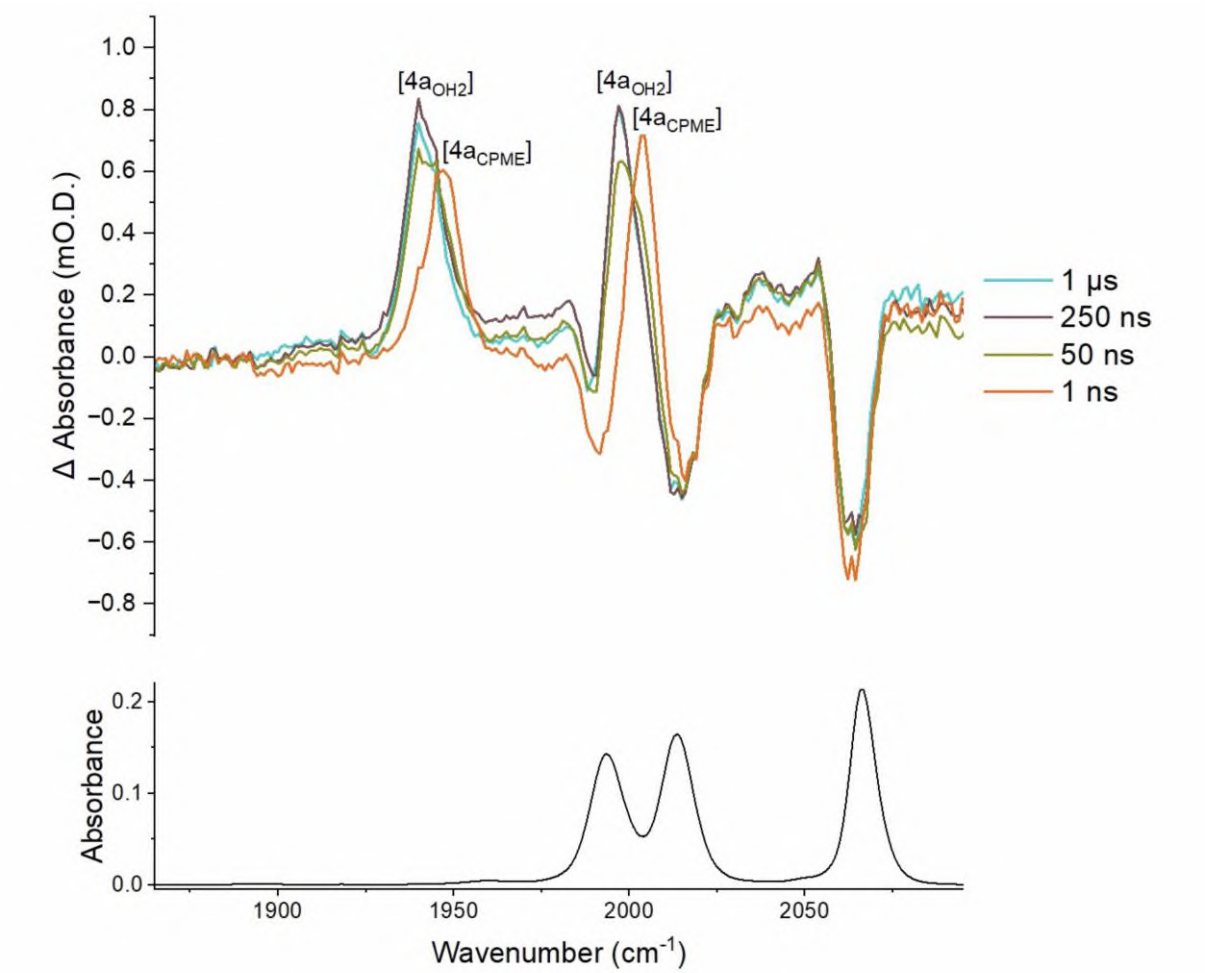

Figure 68. (Top) TRIR spectrum of the 330 nm photolysis of the metal carbonyl region of [3a] at selected later pump-probe delays in CPME. The positive bands of [4a$_{CPME}$] represents the solvent coordinated complex. (Bottom) Ground state IR spectrum of [3a] in CPME.

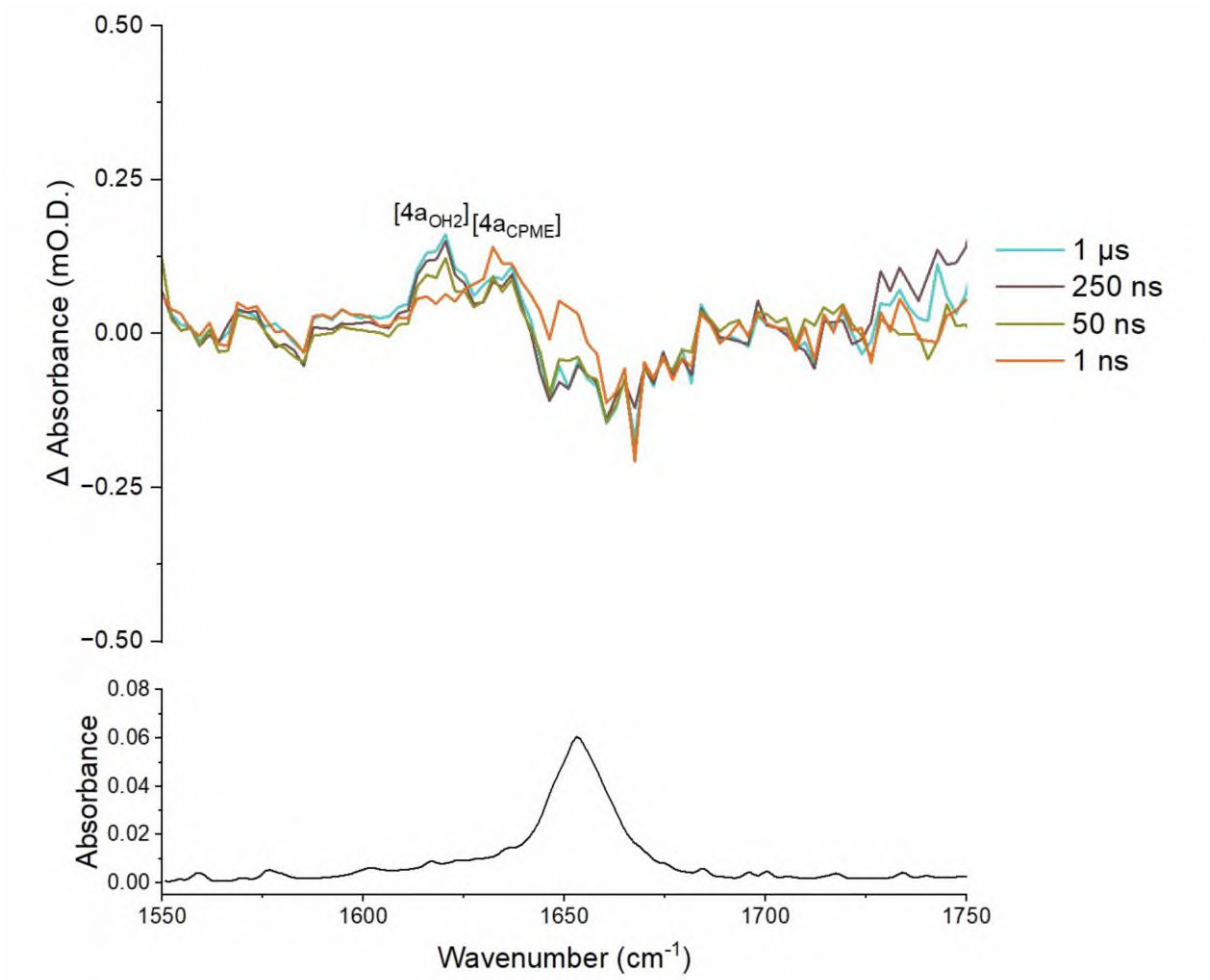

Figure 69. (Top) TRIR spectra of the 330 nm photolysis of the organic carbonyl region of [3a] at selected later pump-probe delays in CPME. The positive band of [4a$_{CPME}$] represents the solvent coordinated complex. (Bottom) Ground state IR spectrum of [3a] in CPME.

6.4 Isopropyl alcohol

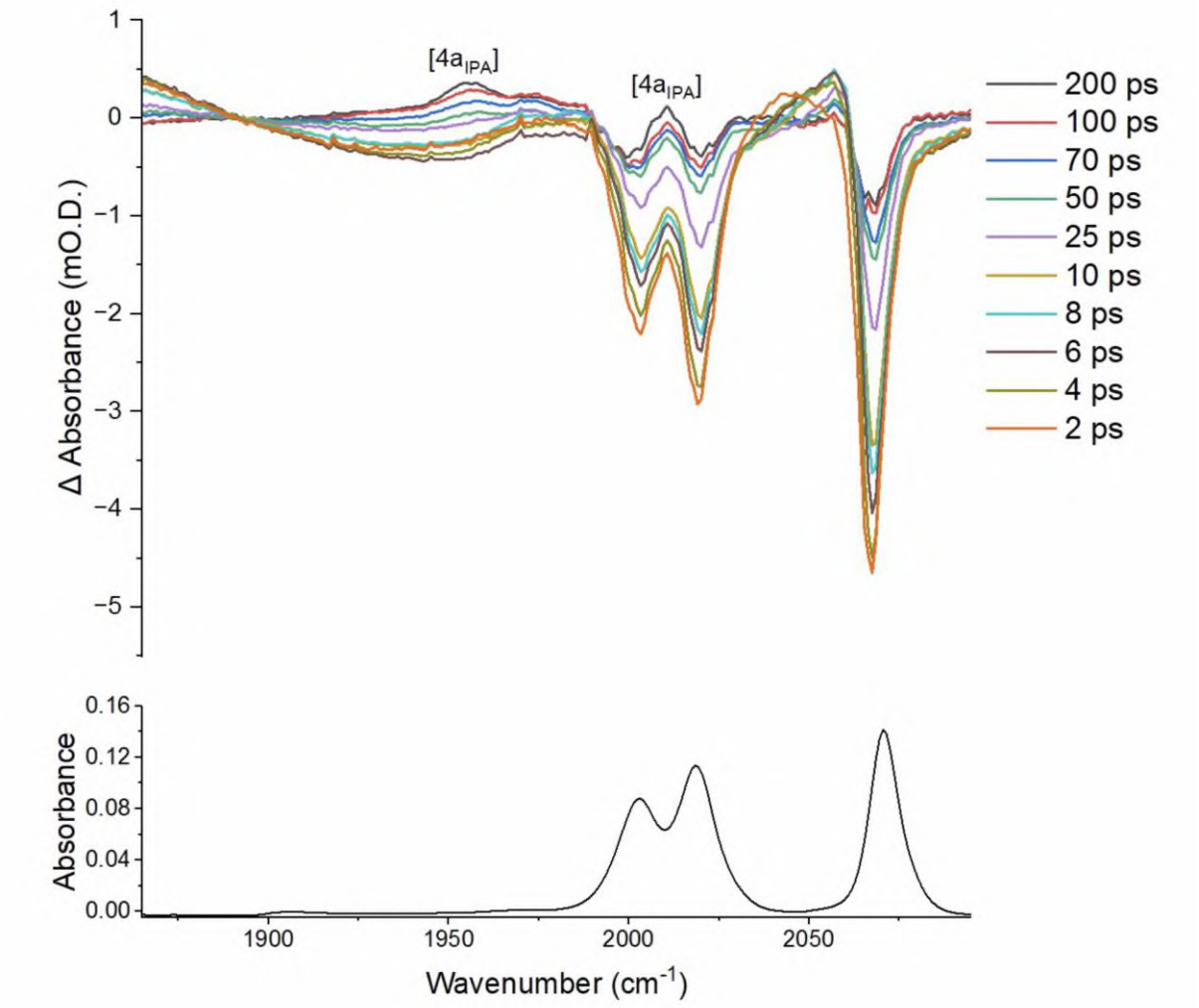

Figure 70. (Top) TRIR spectra of the 330 nm photolysis of the metal carbonyl region of [3a] at selected pump-probe delays in IPA. The positive bands of [4a$_{IPA}$] represents the solvent coordinated complex. (Bottom) Ground state IR spectrum of [3a] in IPA.

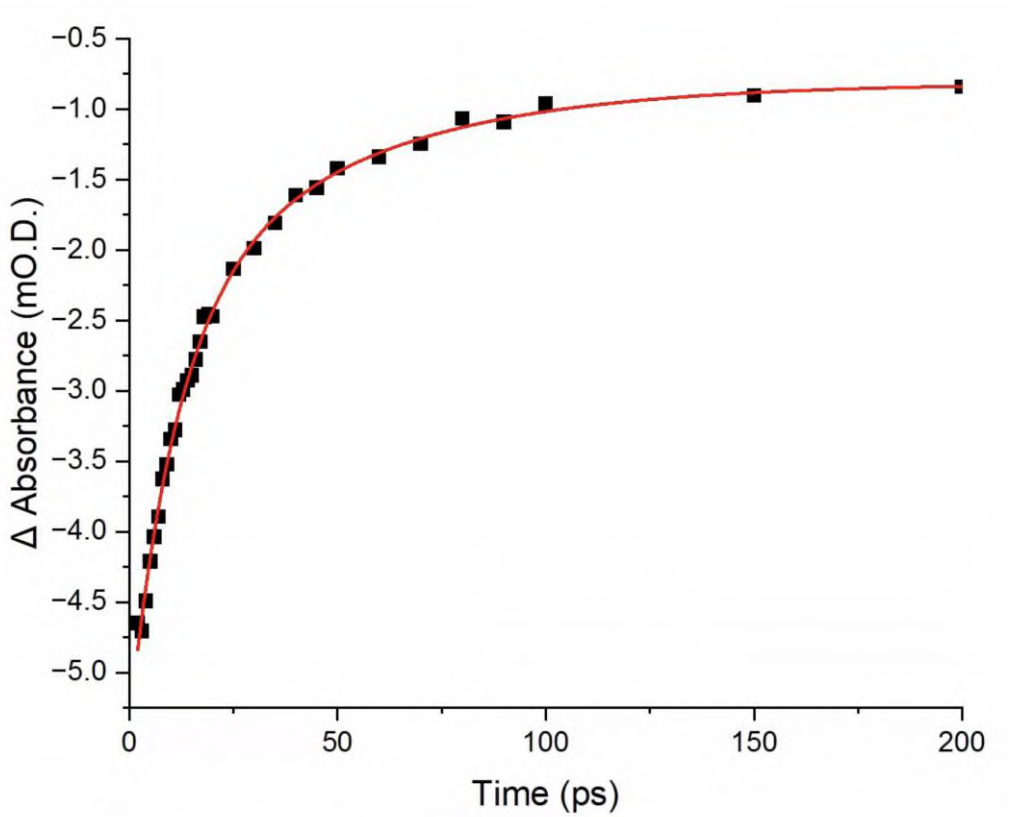

Figure 71. The change in absorbance of the bleach recovery at 2068 cm^{-1} from 2 to 200 ps. The solid red line represents a bi-exponential fit with lifetimes of 11.2 ± 1.8 ps and 45.6 ± 12.9 ps.

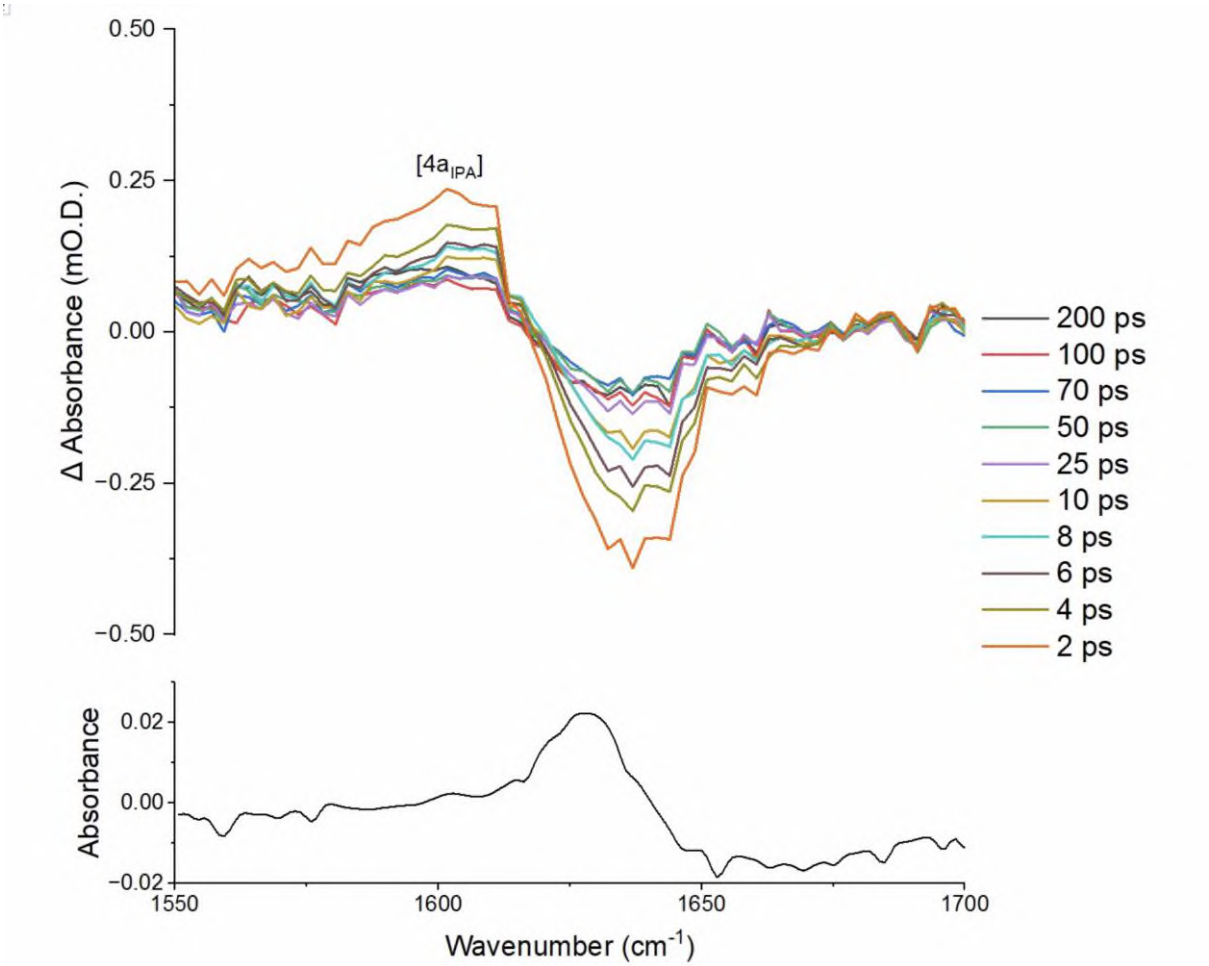

Figure 72. (Top) TRIR spectra of the 330 mm photolysis of the organic carbonyl region of [3a] at selected early pump-probe delays in IPA. The positive band of [4a$_{IPA}$] represents the solvent coordinated complex. (Bottom) Ground state IR spectrum of [3a] in IPA.

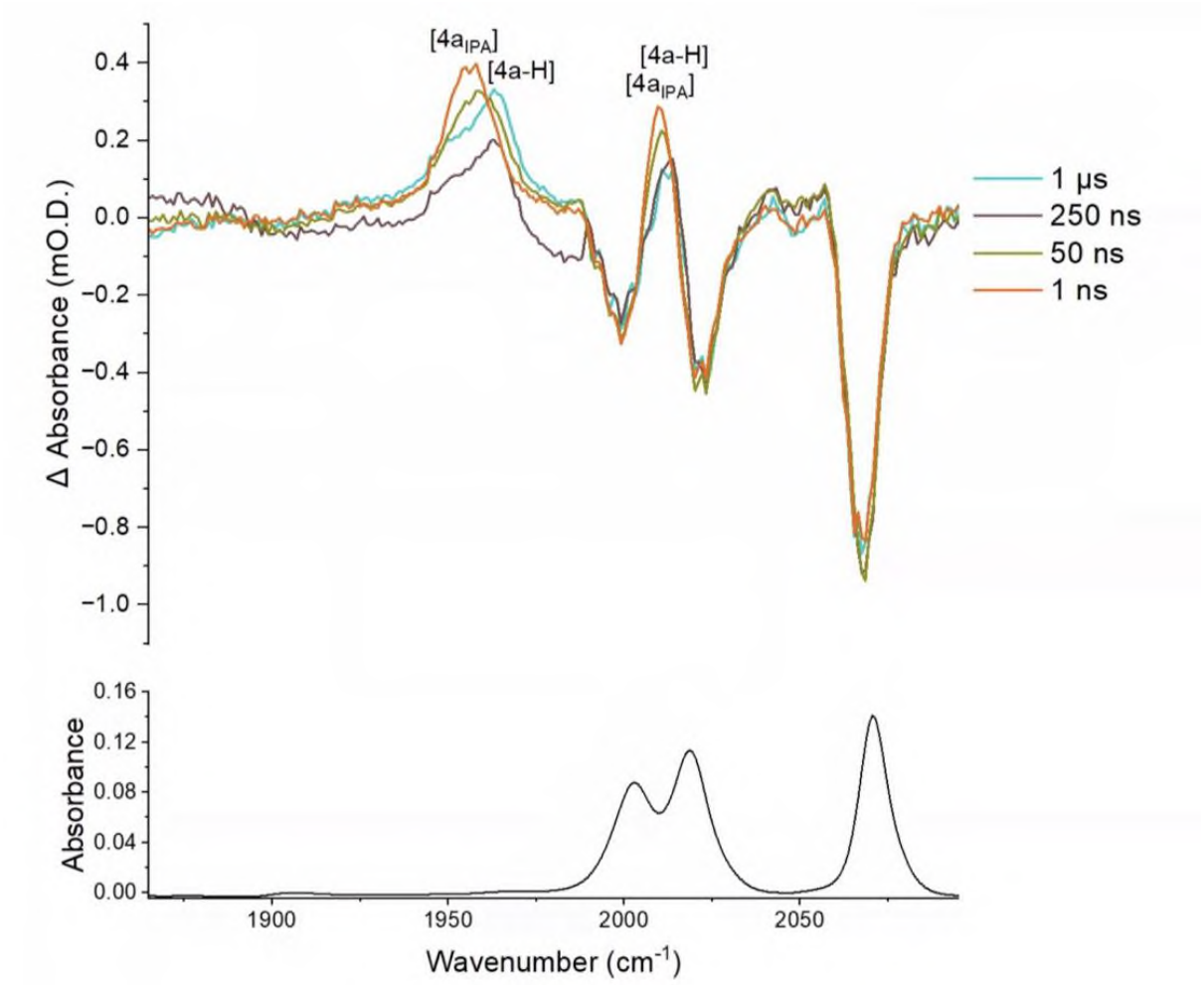

Figure 73. (Top) TRIR spectra of the 330 nm photolysis of the metal carbonyl region of [3a] at selected later pump-probe delays in IPA. The positive bands of [4a$_{IPA}$] represents the solvent coordinated complex. (Bottom) Ground state IR spectrum of [3a] in IPA.

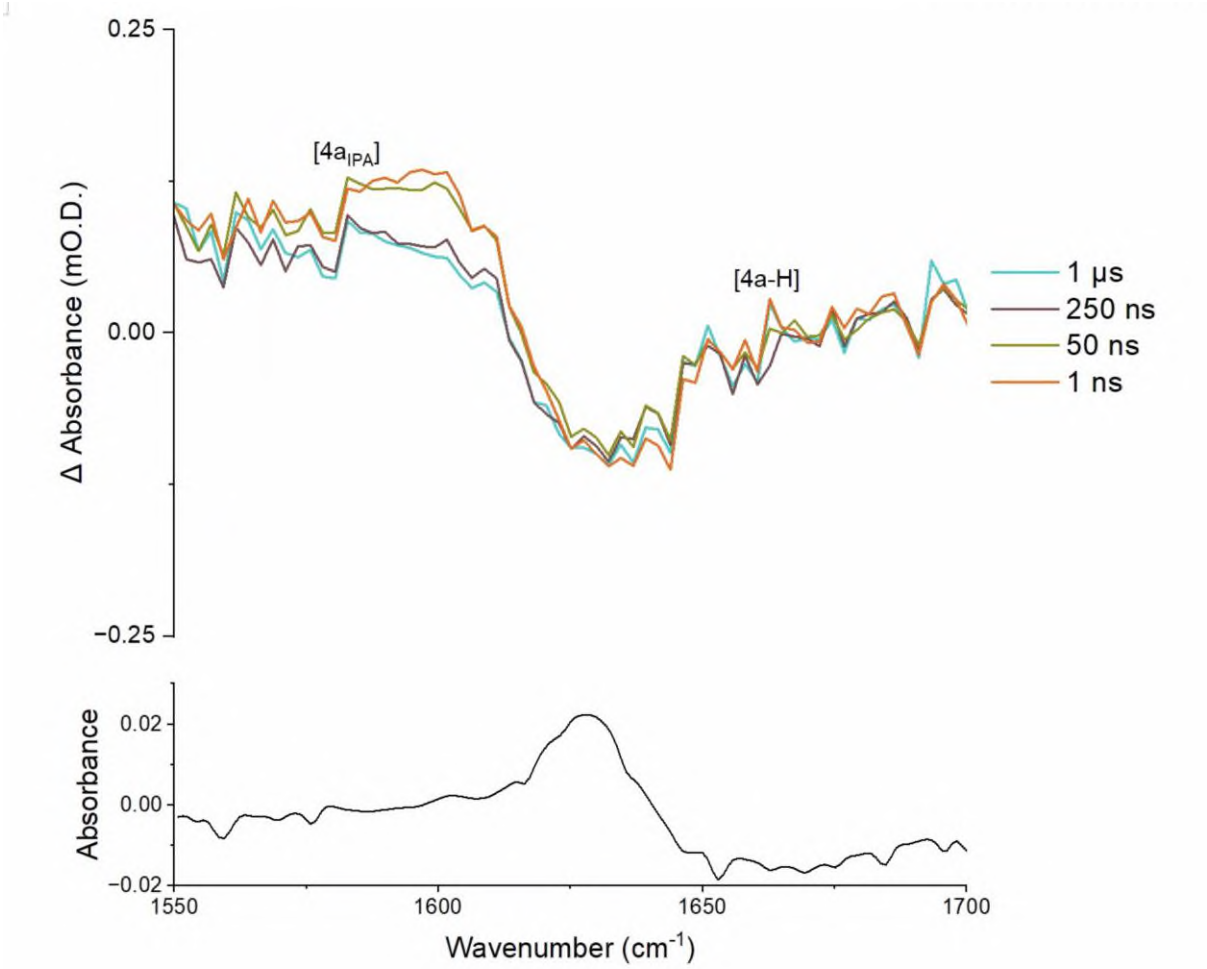

Figure 74. (Top) TRIR spectra of the 330 mm photolysis of the organic carbonyl region of [3a] at selected later pump-probe delays in IPA. The positive band of [4a$_{IPA}$] represents the solvent coordinated complex. (Bottom) Ground state IR spectrum of [3a] in IPA.

6.5 Tetrahydrofuran

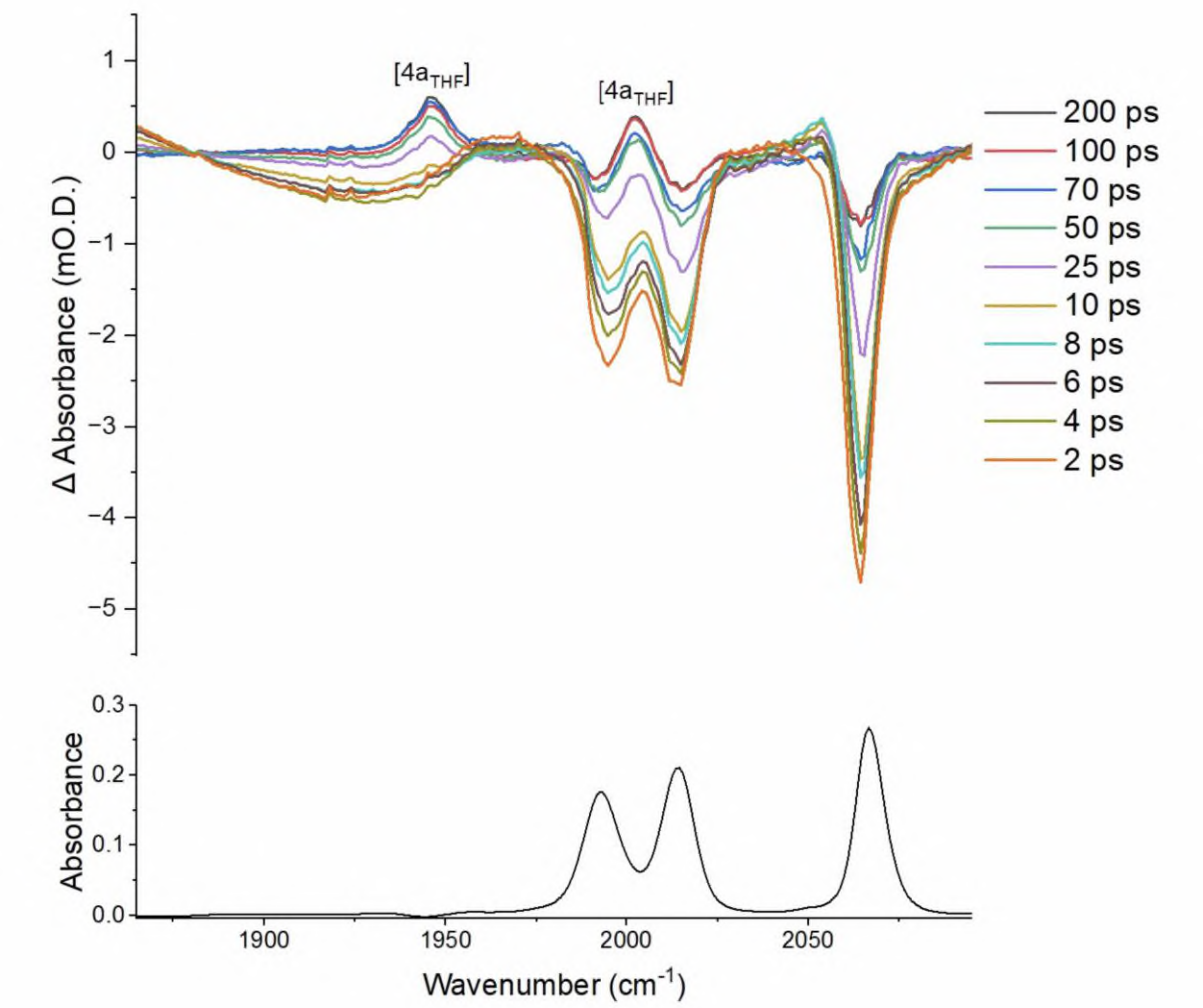

Figure 75. (Top) TRIR spectra of the 330 nm photolysis of the metal carbonyl region of [3a] at selected early pump-probe delays in THF. The positive bands of [4a$_{THF}$] represents the solvent coordinated complex. (Bottom) Ground state IR spectrum of [3a] in THF.

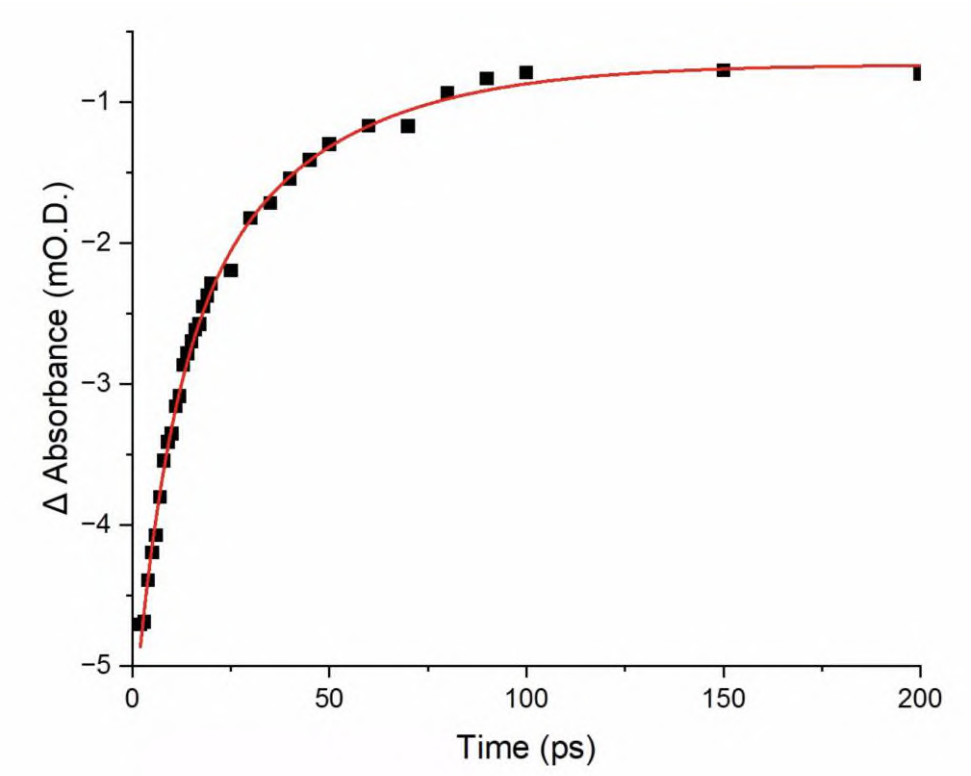

Figure 76. The change in absorbance of the bleach recovery at 2064 cm^{-1} from 2 to 200 ps. The solid red line represents a bi-exponential fit with lifetimes of 9.0 ± 1.9 ps and 35.0 ± 6.9 ps.

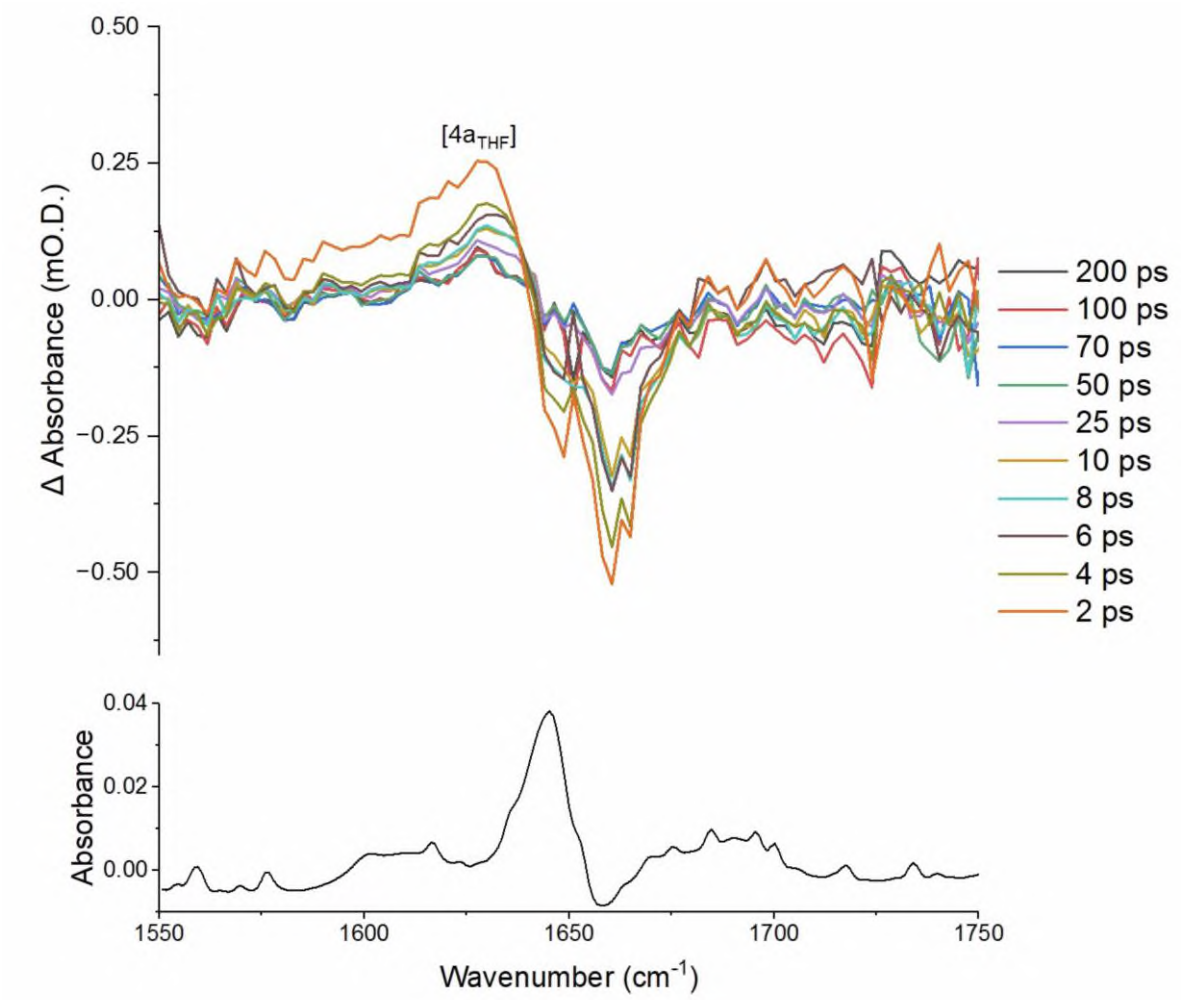

Figure 77. (Top) TRIR spectra of the 330 nm photolysis of the organic carbonyl region of [3a] at selected early pump-probe delays in THF. The positive band of [4a$_{THF}$] represents the solvent coordinated complex. (Bottom) Ground state IR spectrum of [3a] in THF.

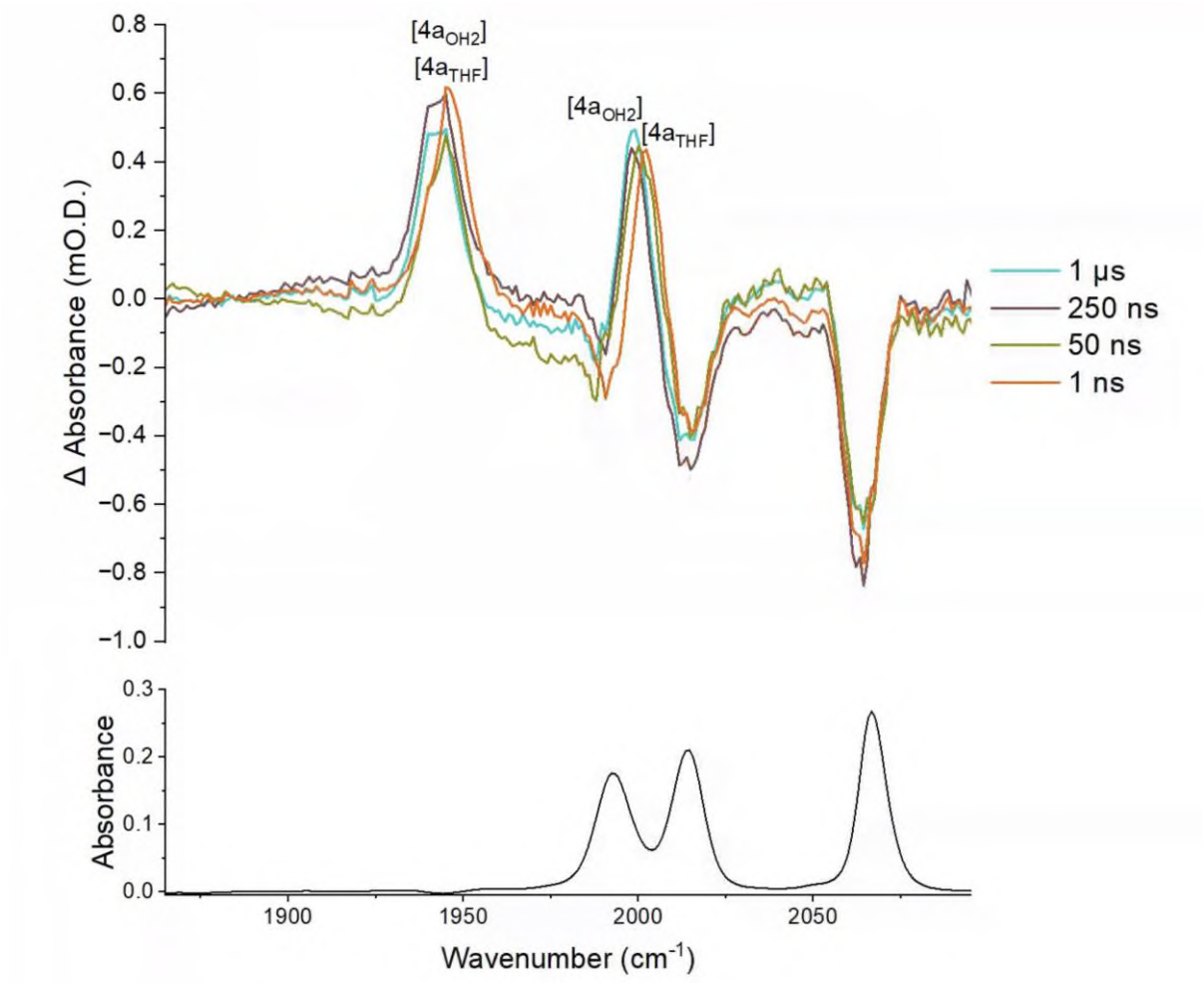

Figure 78. (Top) TRIR spectra of the 330 nm photolysis of the metal carbonyl region of [3a] at selected later pump-probe delays in THF. The positive bands of [4a$_{THF}$] represents the solvent coordinated complex. (Bottom) Ground state IR spectrum of [3a] in THF.

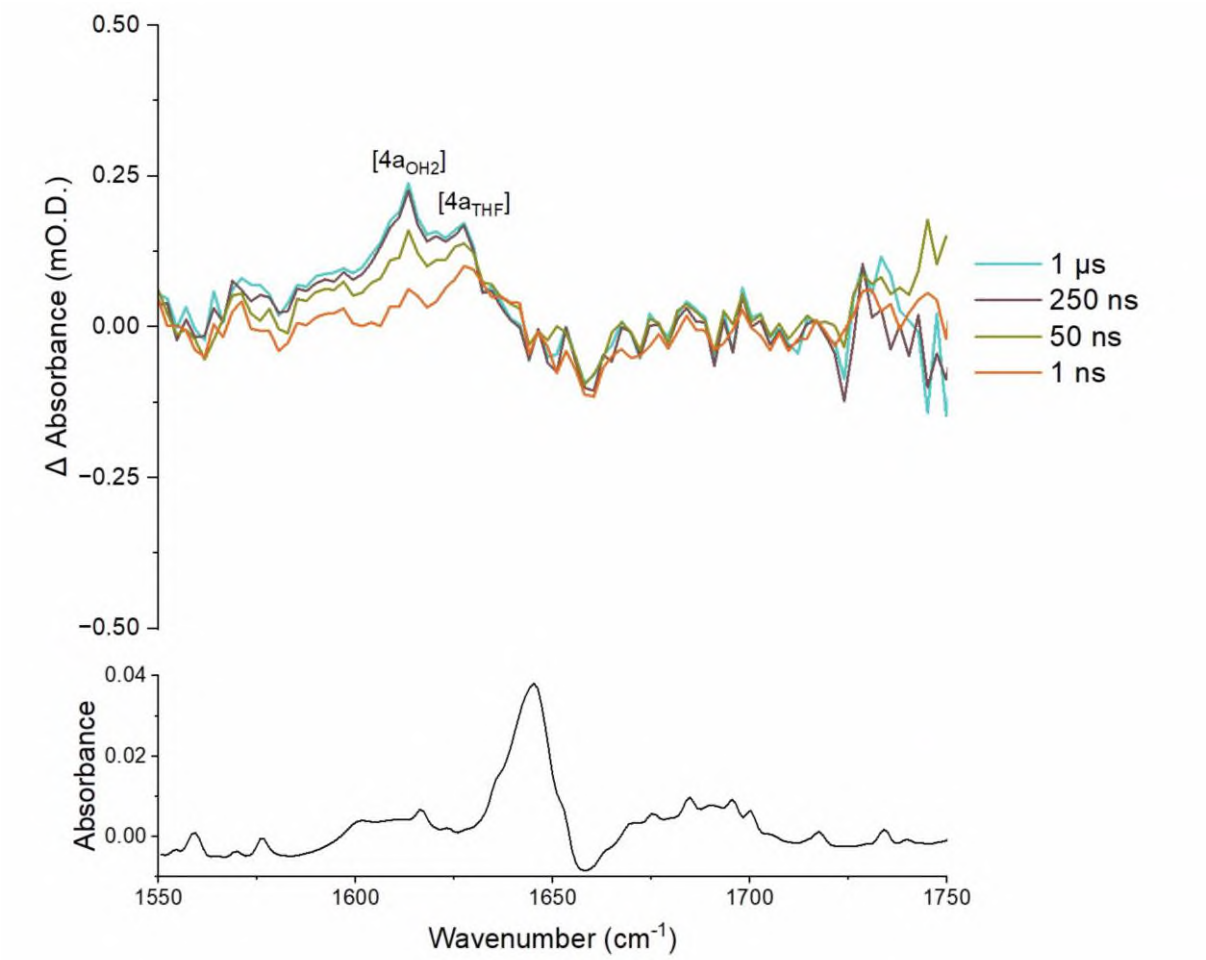

Figure 79. (Top) TRIR spectra of the 330 nm photolysis of the organic carbonyl region of [3a] at selected later pump-probe delays in THF. The positive band of [4a$_{THF}$] represents the solvent coordinated complex. (Bottom) Ground state IR spectrum of [3a] in THF.

6.6 Toluene

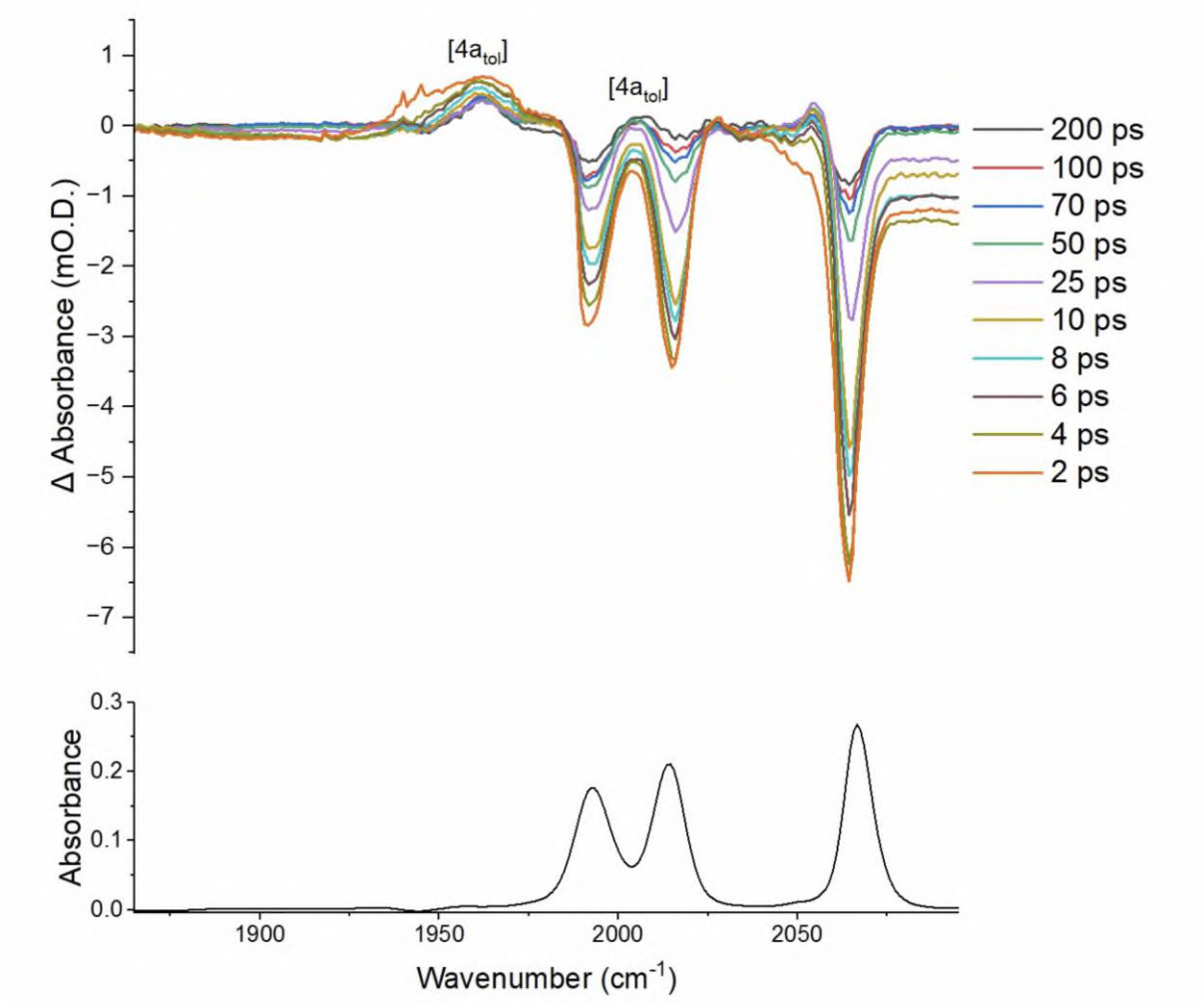

Figure 80. (Top) TRIR spectra of the 330 nm photolysis of the metal carbonyl region of [3a] at selected early pump-probe delays in toluene. The positive bands of [4a$_{tol}$] represents the solvent coordinated complex. (Bottom) Ground state IR spectrum of [3a] in toluene.

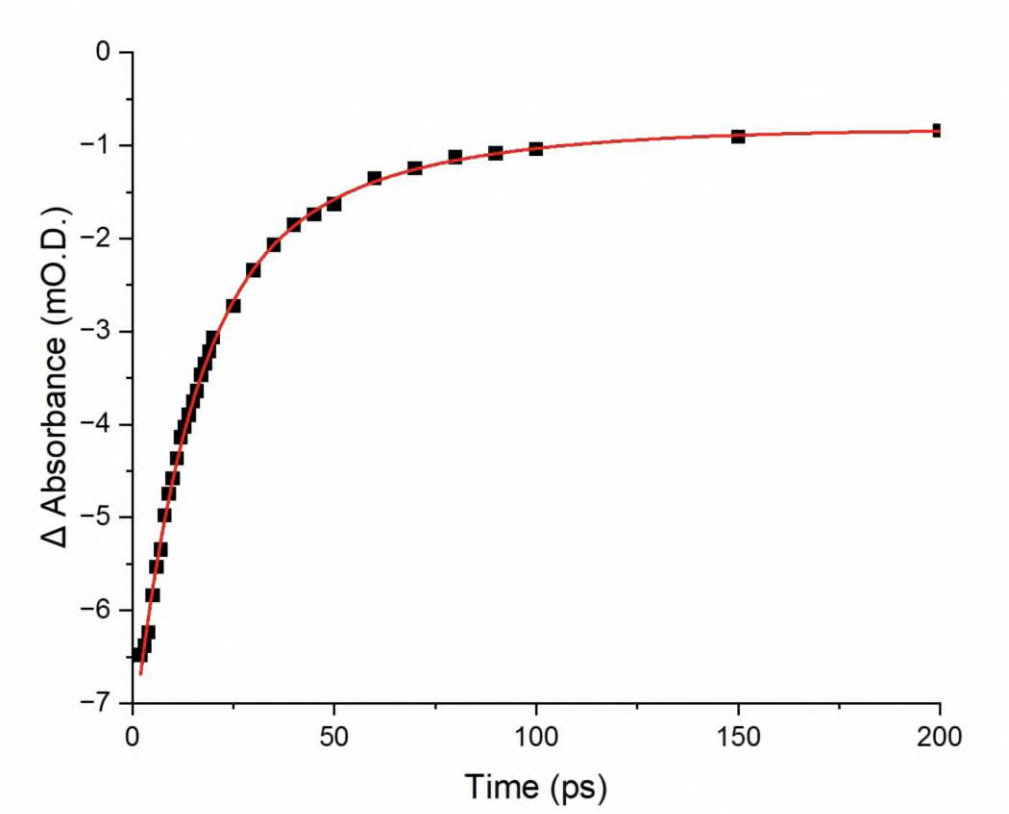

Figure 81. The change in absorbance of the bleach recovery at 2064 cm^{-1} from 2 to 200 ps. The solid red line represents a bi-exponential fit with lifetimes of 13.3 ± 1.8 ps and 43.1 ± 14.4 ps.

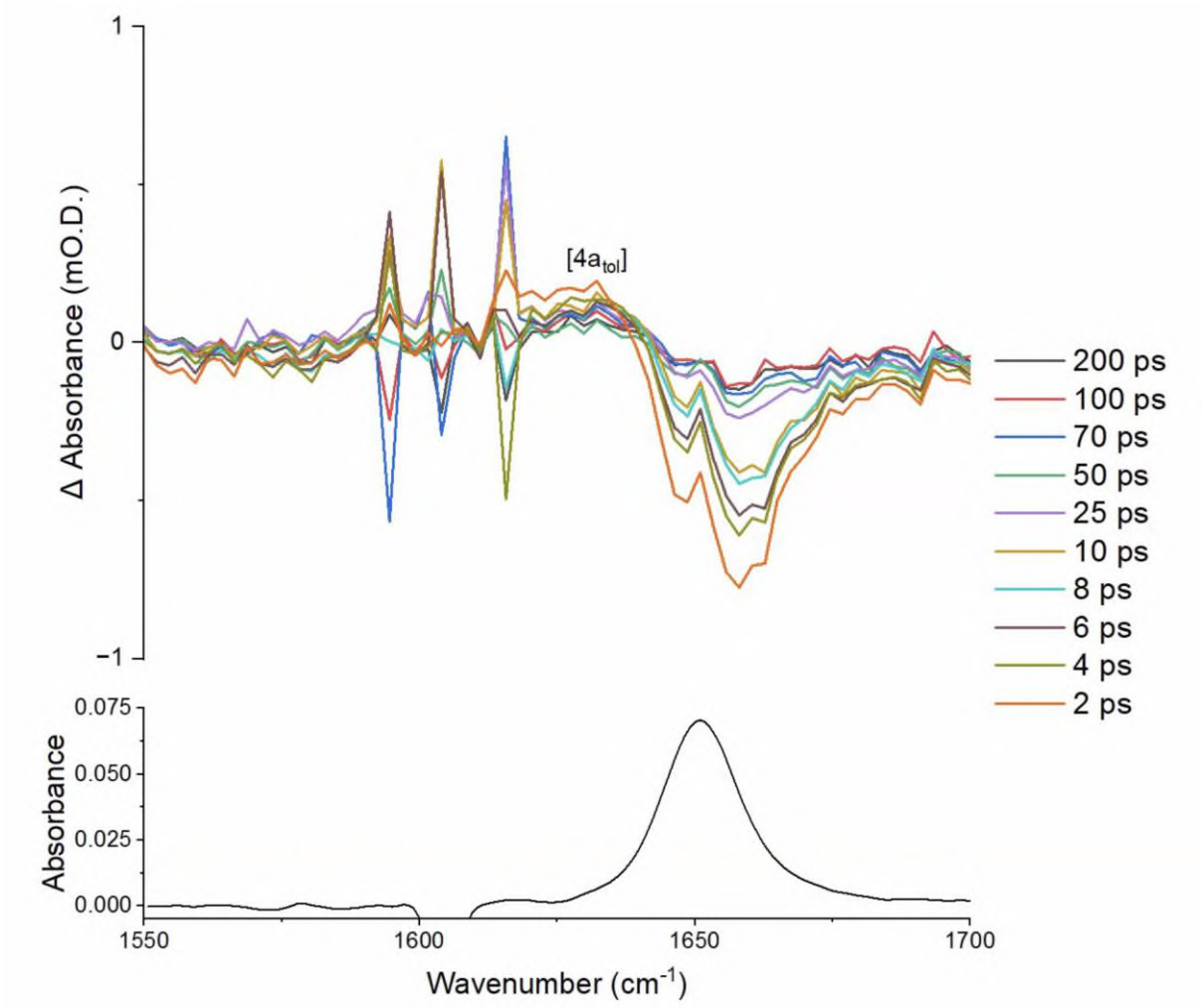

Figure 82. (Top) TRIR spectra of the 330 nm photolysis of the organic carbonyl region of [3a] at selected early pump-probe delays in toluene. The positive band of [4a$_{tol}$] represents the solvent coordinated complex. (Bottom) Ground state IR spectrum of [3a] in toluene.

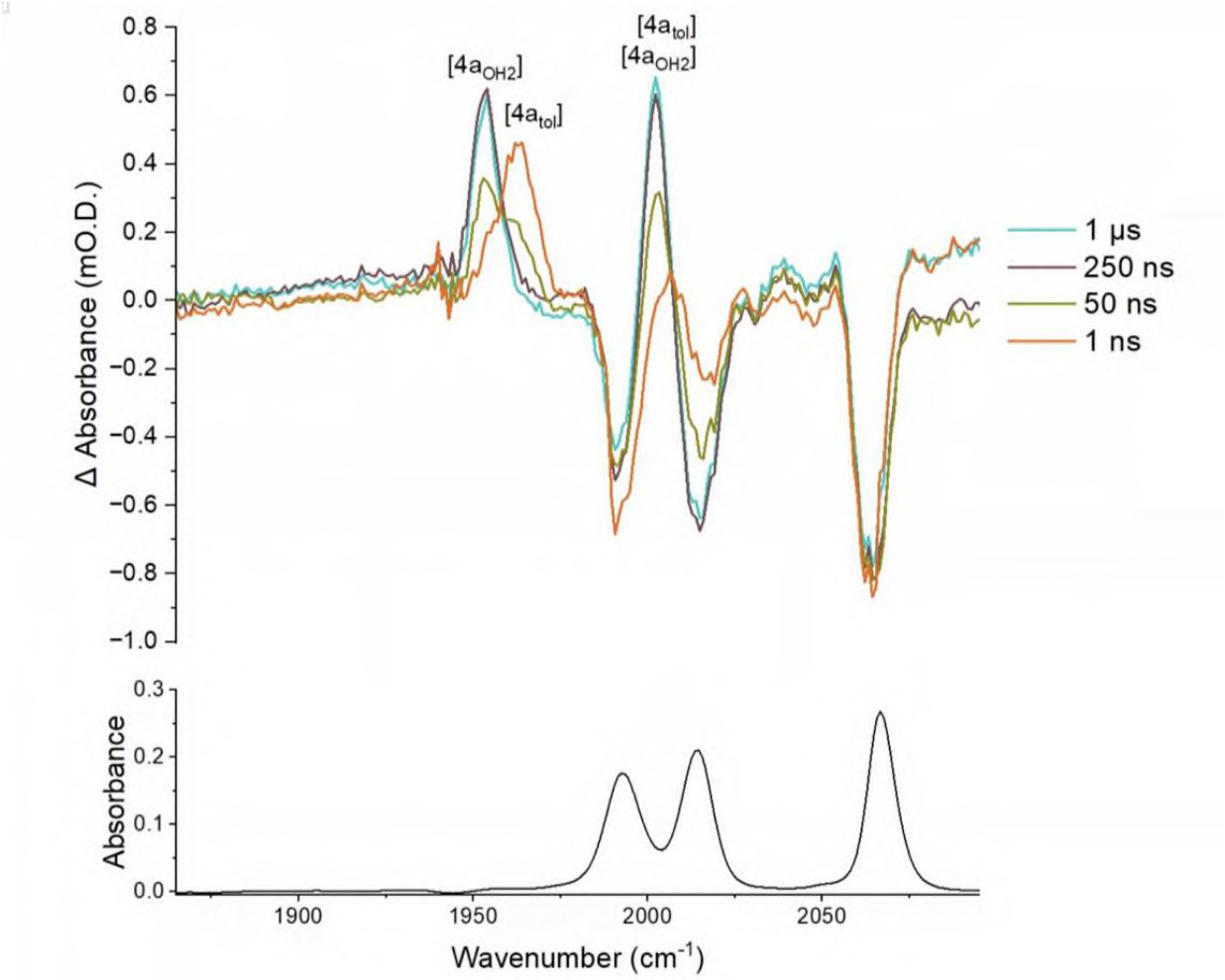

Figure 83. (Top) TRIR spectra of the 330 nm photolysis of the metal carbonyl region of [3a] at selected later pump-probe delays in toluene. The positive bands of [2a$_{tol}$] represents the toluene coordinated complex. (Bottom) Ground state IR spectrum of [3a] in toluene.

References

1. Saidi, O.; Blacker, A.J.; Lamb, G. W.; Marsden, S. P.; Taylor, J. E.; Williams, J. M. J. *O*rg*. Process Res. Dev.* **2010**, *47*, 6787-6789.
2. Fernandez, F. E.; Puerta, M. C.; Valeria, P. *Organometallics*, **2012**, *31*, 6868-6879.
3. Chelucci, G. *Cord. Chem. Rev.* **2017**, *331*, 1-36.
4. Y. Shvo, D. Czarkie, Y. Rahamim and D. F. Chodosh, *J. Am. Chem. Soc.,* **1986**, *108*, 7400-7402.
5. A. Corma, J. Nanas and M. J. Sabater, **2018**, *118*, 1410-1459.
6. Schrauzer, G. N.; **1959**, *81*, 5397-5310.
7. Shively, R. J.; Dubbert, R. A.; Pearson, A. J. *Organometallics*, **1992**, *11*, 4096-4104.
8. Shively, R. J.; Pearson, A. J. *Organometallics*, **1994**, *13*, 578-594.
9. Kim, J. B.; Pearson, A. J. *Org. Lett*., **2002**, *4*, 2837-2340.
10. Ogliaruso, M. A.; Romanelli, M. G.; Becker, E. I. *S=Chem. Rev.* **1965**, *65*, 261-367.
11. Knölker, H. J. *Synlett*, **1992**, 1002.
12. J. Watt, G. C. Bleier, M. J. Austin, S. A. Ivanov and D. L. Huber, *Royal Society of Chemistry*, **2017**, *9*, 6632-6637.
13. Coleman, M. G.; Brown, A. N.; Bolton, B. A.; Guan, H. *Adv. Synth. Catal.* **2010**, *352*, 967-970.
14. Moyer, S. A.; Funk, T. W. *Tetrahedron Lett.* **2010**, *51*, 5430-5433.
15. Johnson, T. C.; Clarkson, G. J.; Wills, M. *Organometallics*, **2011**, *30*, 1859-1868.
16. Casey, C. P.; Guan, H. *J. Am. Chem. Soc.* **2007**, *129*, 5816-5817.
17. Casey, C. P.; Guan, H. *J. Am. Chem. Soc.* **2009**, *131*, 2499-2507.
18. Tlili, A.; Shchranck, Neumann, H.; Beller, M. *Chem. Eur. J.* **2012**, *18*, 15935-15939.
19. Fleischer, S.; Werkmeister, S.; Zhou, S.; Junge, K.; Beller, M. *Chem. Eur. J.* **2012**, *18*, 9005-9010.
20. Tao, Y.; Feringa, B. L.; Barta, K. *Nature Com.* **2014**, *5*, 5602-5608.
21. Tao, Y.; Feringa, B. L.; Barta, K. *ACS Catal.* **2016**, *6*, 381-388.
22. Rawlings, A. J.; Diorazio, L. J.; Wills, M. *Org. Lett.* **2015**, *17*, 1086-1089.
23. Pan, H.; No, T. W.; Zhao, T. *Chem. Commun.* **2015**, *51*, 11907-11910.
24. K. Polidano, B. D. W. Allen, J. M.J. Williams and L. C. Merrill, *ACS Catal*., **2018**, *8*, 6440-6455.
25. K. Polidano, B. D. W. Allen, J. M.J. Williams and L. C. Merrill, *ACS Catal*., **2018**, *8*, 6440-6455.
26. Knölker, H.-J.; Goesmann, H.; Klauss, R. *Angew. Chem. Int. Ed.* **1999**, *38*, 702-705.
27. Emayavaramban, B.; Chakraborty, P.; Dahiya, P.; Sundaraju, B. *Org Lett.* **2022**, *24,* 6219-6223.

28. G. M. Greetham, P. M. Donaldson, C. Nation, I. V. Sazanovich, I. P. Clark, D. J. Shaw, A. W. Parker and M. Towrie, *Appl. Spectrosc*., **2016**, *70*, 645-653.
29. Towrie, M.; Gabrielsson, A.; Matousek, P.; Parker, A. W.; Rodriguez, A. M. B.; Vlček, A., *Appl. Spectrosc.,* **2005**, *59*, 467-473.
30. Schmidhammer, U.; Roth, S.; Riedle, E.; Tishkov, A. A.; Mayr, H., *Rev. Sci. Instrum.,* **2005**, *76*, 093111.
31. Bloembergen, N., *Reviews of Modern Physics*, **1999**, *71,* S283-S287.
32. Johnson, C. K.; Bostick, J. M.; Mounter, S. A.; Ratzlaff, K. L.; Schloemer, D. E., *Rev. Sci. Instrum.,* **1988**, *59*, 2375-2379.
33. Bredenbeck, J.; Helbing, J.; Hamm, P., *Rev. Sci. Instrum.,* **2004**, *75*, 4462-4466.
34. Yu, A.; Ye, X.; Ionascu, D.; Cao, W.; Champion, P. M., *Rev. Sci. Instrum*., **2005**, *76*, 114301.
35. Carroll, E. C. Hill, M. P.; Madsen, D.; Malley, K. R.; Larsen, D. S.; *Rev. Sci. Instrum*., **2009**, *80*, 026102.
36. Greetham, G. M.; Sole, D.; Clark, I. P.; Parker, A. W.; Pollard, M. R.; Towrie, M.; *Rev. Sci. Instrum*., **2012**, *83*, 103107.
37. B. Procacci, S. L. D. Wrathall, A. L. Farmer, D. J. Shaw, G. M. Greetham, A. W. Parker, Y. Rippers, M. Horch, J. M. Lynam and N. T. Hunt. *J. Phys. Chem.* **2024**, *128*, 1461-1472.
38. S. Hume, G. M. Greetham, P. M. Donaldson, M. Towrie, A. W. Parker, M. J. Baker and N. T. Hunt, *Anal. Chem*, **2020**, *92*, 3463-3469.
39. J. Velasquez, E. D. Pillai, P. D. Carnegie and M. A. Duncan, *The Journal of Physical Chemistry*, **2006**, *110*, 2325-2330.
40. A. D. Fortes and S. F. Parker, *Journal of the American Chemical Society*, **2022**, *144*, 17376-17386.
41. P. Portius, M. Bühl, M. W. George, F. W. Grevels and J. J. Turner, *Organometallics*, **2019**, *38*, 4288-4297.
42. Aucott, B. J., Duhme-Klair, A. K., Moulton, B. E., Clark, I. P., Sazanovich, I. V., Towrie, M., Hammarback, L. A., Fairlamb, I. J. S., & Lynam, J. M. *Organometallics,* **2019**, *38,* 11, 2391-2401.
43. E. J. Mascarenhas, M. Fondell, R. Büchner, S. Eckert, V. V. D. Cruz and A. Föhlisch, *Phys. Chem. Phys. Chem*, **2022**, *24*, 17979-17985.
44. R. M. Jay, M. R. Coates, H. Zhao, M. O. Winghart, P. Han, R. Wang, J. Harich, A. Banerjee, H. Wikmark, M. Fondle, E. T. J. Nibbering, M. Odelius, N. Huse and P. Wernet. *J. Am. Chem. Soc.* **2024**, *146*, 14000-14011.
45. Hunt, NT, Lynam, JM, Procacci, B, Fairlamb, IJS & Farmer, A. *Journal of Chemical Physics,* vol., **2025**, *162*, 174302.
46. K. Watanabe, N. Yamagiwa and Y. Torisawa, *Org. Process Res. Dev.,* **2007**, *11*, 251-258.
47. I. R. Farrell, P. Matousek, M. Towrie, A. W. Parker, D. C. Grills, M. W. George and A. Vlček, Jr, *Inorg. Chem*, **2002**, *41*, 4318-4323.
48. Eastwood, J, Hammarback, A, McRobie, M, Clark, IP, Towrie, M, Fairlamb, IJS & Lynam, JM. *Dalton Transactions*., **2020**, *49*, 5463-5470.

49. P. J. Dyson, P. G. Jessop. *Catalysis Science & Technology*, **2016**, *6*, 3302-3316.
50. W. Li, M. G. Taylor, D. Bayerl, S. Mozaffari, M. Dixit, S. Ivanov, S. Seifert, B. Lee, N. Shanaiah, Y. Lu, L. Kovarik, G. Mpourmpakis, A. M. Kari. *Nanoscale*, **2021**, *13*, 206-217.
51. R. K. Venkatraman, A. J. Orr-Ewing. *Acc. Chem. Res,* **2021**, *54*, 4383-4394.
52. B. K. Werley, X. Hou, E. P. Bertonazzi, A. R. Chianese, T. W. Funk. *Organometallics*, **2023**, *42*, 3053-3065.
53. I. A. Howard, R. Mayer, M. Meister and F. Laquai, *Journal of the American Chemical Society,* **2010**, *32*, 14866-14876.
54. H. Löslein, T. Ameri, G. J. Matt, M. Koppe, H. J. Egelhaaf, A. Troeger, V. Sgobba, D. M. Guldi and C. J. Brabec, *Macromolecular Rapid Communications*, **2013**, *34*, 1090-1097.
55. S. Karuthedath, A. Melianas, Z. Kan, V. Pranculis, M. Wohlfahrt, J. I. Khan, Gorenflot, Y. Xia, O. Inganäs, V. Gulbinas, M. Kemerink and F. Laquai, *J. Mater. Chem. A*, **2018**, *6*, 7428-7438.
56. D. W. Gehrig, I. A. Howard and F. Laquai, *The Journal of Physical Chemistry C,* **2015**, *119*, 13509-13515.